ChemPubSoc Europe

DOI: 10.1002/cmdc.201800158

CHEMMEDCHEM Communications

Optimization of Pyrazoles as Phenol Surrogates to Yield Potent Inhibitors of Macrophage Migration Inhibitory Factor

Vinay Trivedi-Parmar, Michael J. Robertson, José A. Cisneros, Stefan G. Krimmer, and William L. Jorgensen*[a]

Dedicated to Prof. E. J. Corey on the occasion of his 90th birthday.

Macrophage migration inhibitory factor (MIF) is a proinflammatory cytokine that is implicated in the regulation of inflammation, cell proliferation, and neurological disorders. MIF is also an enzyme that functions as a keto–enol tautomerase. Most potent MIF tautomerase inhibitors incorporate a phenol, which hydrogen bonds to Asn97 in the active site. Starting from a 113-μM docking hit, we report results of structure-based and computer-aided design that have provided substituted pyrazoles as phenol alternatives with potencies of 60–70 nM. Crystal structures of complexes of MIF with the pyrazoles highlight the contributions of hydrogen bonding with Lys32 and Asn97, and aryl–aryl interactions with Tyr36, Tyr95, and Phe113 to the binding.

Human macrophage migration inhibitory factor (MIF) is a proinflammatory cytokine that is implicated in the pathogenesis of numerous inflammatory diseases,[1] neurological disorders,[2] and cancer.[3] MIF is expressed in many cell types and its tissue distribution is wide-spread. Upon activation of cells such as macrophages, monocytes and T-cells, expression of MIF in turn activates release of inflammatory cytokines including interleukins, interferon, and TNFα. Complex signaling pathways are invoked when MIF binds to its membrane-bound receptors CD74 and CXCR4, leading to leukocyte chemotaxis, inflammatory response, and potential tissue damage.[3] Strong correlation is observed between MIF expression and the severity of many inflammatory and autoimmune diseases including asthma, sepsis, lupus, and rheumatoid arthritis.[4] For cancer, the AKT pathway may be activated by MIF binding causing suppression of apoptosis by inhibition of the normal action of BAD, BAX, and p53.[3] However, MIF's role in cancer is multifaceted with undesirable effects also on cell proliferation, angiogenesis, and metastasis;[3,4] MIF is over-expressed in most human cancer cells.[5]

Interestingly, MIF also shows enzymatic activity as a keto-enol tautomerase. MIF is a toroid-shaped, trimeric protein consisting of 342 amino acid residues with three identical active sites occurring at the interfaces of the monomer subunits.[6] The active sites are small, relatively cylindrical and open to the surface of the protein in the vicinity of Pro1, which serves as the catalytic base. The resultant strategy for interference with the binding of MIF to its receptor CD74 is then to find tautomerase inhibitors that change the surface characteristics of MIF.[6] Indeed, numerous studies have shown a correlation between inhibition of the enzymatic and biological activities of MIF by measuring tautomerase activity, and, for example, MIF/CD74 binding, protein phosphorylation in inflamed cells, production of interleukins, and glucocorticoid overriding ability.[6,7] Though many MIF tautomerase inhibitors have been discovered through screening of compound libraries,[6,8] lead optimization to give inhibitors with nanomolar potency has been limited. In fact we have tested the most promising compounds from the literature in a tautomerase inhibition assay[9] and only found compounds from one patent[10] and our biaryltriazole series[11] to have sub-micromolar K_i values. The results were confirmed by measurement of K_d values in a fluorescence polarization assay.[12] Exemplary potent compounds are **1** (NVS-2[10]) and **2**[11] with K_i values of ~0.03 μM, which are ~1000-fold lower than for well-known MIF inhibitors such as **3** ((*R*,*S*)-ISO-1[13]) and the chromen-4-one **4**[6a] (Figure 1).

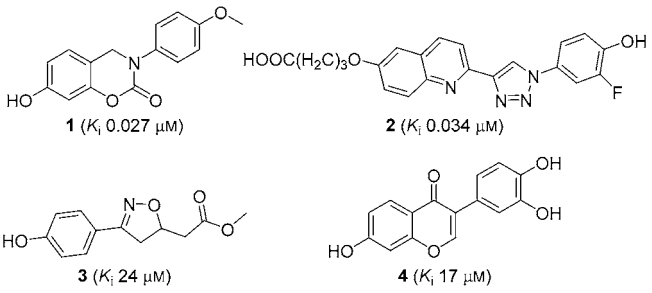

Figure 1. Examples of MIF tautomerase inhibitors with K_i data from Ref. [12].

A feature, which is addressed here, is that **1**–**4** and many other noncovalent MIF tautomerase inhibitors and substrates contain a phenol subunit, which lodges in the back of the active site and forms hydrogen bonds with the side chain of Asn97 (Figure 2).[6,11,12] Though there are more than 125 approved drugs that contain a phenolic group including, for ex-

[a] V. Trivedi-Parmar, Dr. M. J. Robertson, Dr. J. A. Cisneros, Dr. S. G. Krimmer, Prof. Dr. W. L. Jorgensen
Department of Chemistry, Yale University, New Haven, CT 06520-8107 (USA)
E-mail: william.jorgensen@yale.edu

Supporting information and the ORCID identification number(s) for the author(s) of this article can be found under https://doi.org/10.1002/cmdc.201800158.

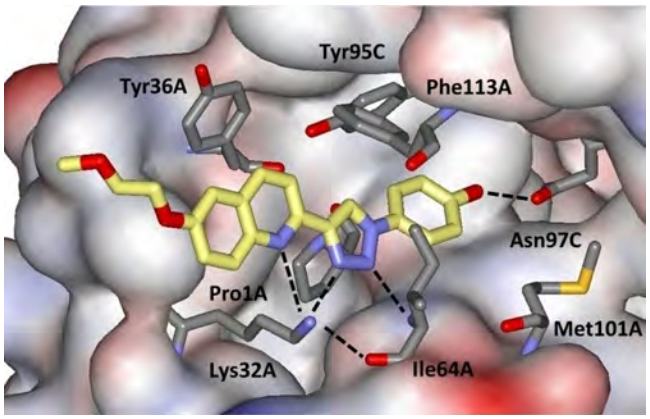

Figure 2. Rendering from a 1.8-Å crystal structure of an analogue of compound **2** bound to MIF.[11a] Carbon atoms of the inhibitor are colored yellow. Hydrogen bonds are indicated with dashed lines.

ample, acetaminophen, albuterol, amoxicillin, raloxifene, and doxycycline, the oral bioavailability of phenols is well-known to often be unacceptably low owing to metabolic glucoronidation[14] and/or sulfation.[15] Thus, we set out to find a phenol-free series of MIF tautomerase inhibitors with low-nanomolar potencies.

Success in the past has come from exchange of the phenol for a 6:5 fused heteroaromatic incorporating a pyrrole or pyrazole that retains the hydrogen-bond donating character of phenol.[16] However, the MIF active site is too constricted near Asn97 for this approach to be viable; addition of a methyl group *ortho* to the hydroxy group for the compound in Figure 2 leads to a ~100-fold loss in activity.[11a] Instead, our interest has focused on replacement of the phenol by a pyrazole. Owing to the geometrical differences, this requires exploration of new series with a pyrazole core. Fortunately, in the initial virtual screening study[8a] 11 compounds were found to be active in an assay that measured interference of binding between MIF and immobilized CD74 ectodomain; and, one contained a pyrazole with the expected hydrogen bonds to Asn97 in the docked structure. This compound, **5** (Figure 3), gave an IC_{50} of 15 μM in the binding assay; however, it showed little activity in a tautomerase assay using 4-hydroxyphenylpyruvate (HPP) as the substrate, with a maximum of 30% inhibition at 50 μM.[8a] Thus, we pursued alternative series from the virtual screening and from de novo design, which provided the biaryltriazoles including **2**.[11] However, our interest in **5** was renewed because in another phenol-containing inhibitor series[7b] rapid metabolic glucoronidation and sulfation were observed. It was decided to retest **5** in an HPP tautomerase assay using optimized protocols in our laboratory.[9] Though the K_i for **5** from this assay was only 113 μM, in view of its low molecular weight and possibilities for substitution in the phenyl ring, we were encouraged to perform structure-based, computer-aided lead optimization.[17] As detailed here, this has been successful in providing pyrazole derivatives with ~2000-fold greater potency.

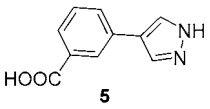

5

Figure 3. Docking hit **5**.[8a]

In working with **5**, it was noted that it had high solubility in polar media. This motivated successful pursuit of a crystal structure with MIF in spite of the modest K_i (Figure 4). There are two copies of **5** in each MIF trimer. The expected hydrogen bonds with Asn97 have average N–O and N–N lengths of 3.0 and 3.1 Å, while Lys32 has hydrogen bonds with the carboxylate group of **5** (3.0 and 2.7 Å) and the oxygen atom of Ile64 (2.7 Å). The NH of Ile64 also forms one with the carboxylate (2.9 Å), and the phenyl ring of **5** is well packed between Pro1, Tyr95, and Phe113. From this structure and model building with the BOMB program,[17b] substitution *para* to the pyrazolyl group seemed likely to yield beneficial interactions with Tyr36 and possibly Phe113. Thus, constructs **6**–**8** were pursued where R^1 was mostly an aryl group (Figure 5).

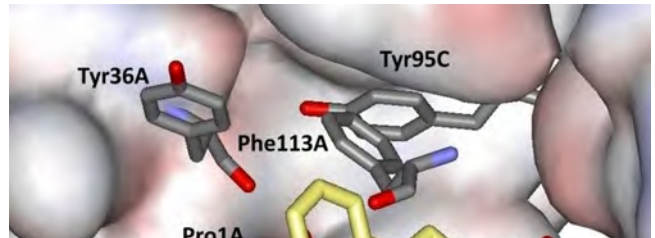

Figure 4. Rendering from the 2.0-Å crystal structure of compound **5** bound to MIF. Details as in Figure 2.

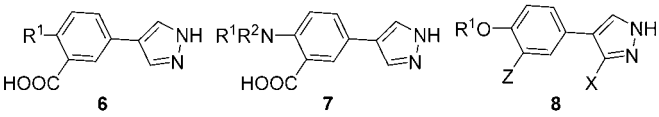

Figure 5. Designs for pyrazole-based MIF inhibitors.

The syntheses of **6**–**8** are detailed in the Supporting Information. As summarized in Scheme 1, the key steps started from the commercially available phenyl iodide **9**, which underwent Pd- or Cu-mediated coupling to yield phenylaryl, arylanilinyl, or biaryl ether derivatives **10**–**12**. Installation of the pyrazole was then achieved by a Suzuki coupling to yield esters **13**–**15**, which were hydrolyzed under mild conditions to provide the desired carboxylic acids.

The compounds reported here are listed in Table 1 along with the results from the tautomerase assay. The identity of assayed compounds was confirmed by ^1H and ^{13}C NMR and

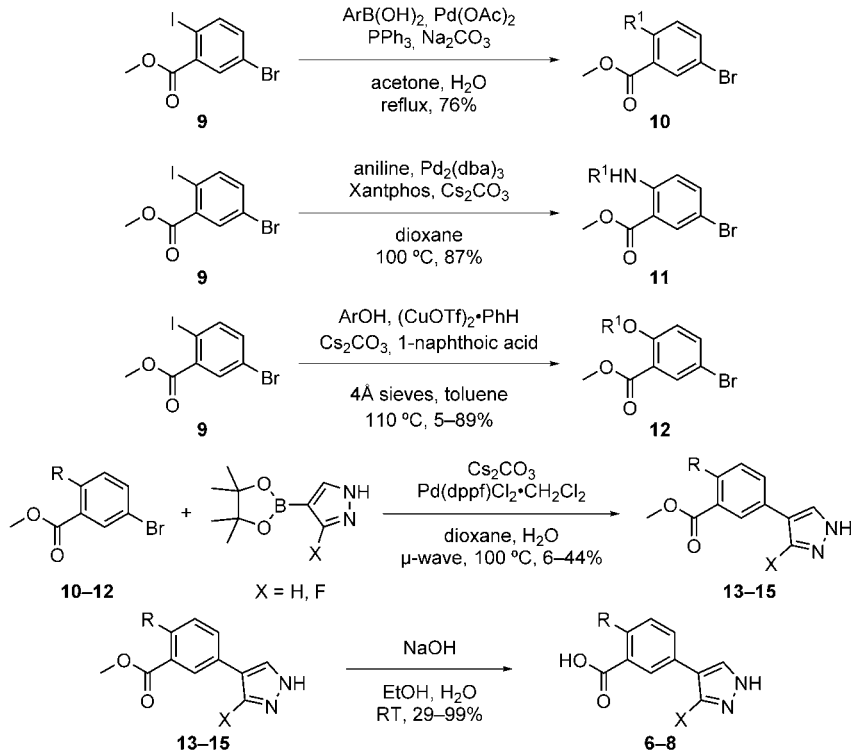

Scheme 1. Synthesis of pyrazole-based MIF inhibitors.

Table 1. Experimental inhibition constants.

Compd	R[1][a]	R[2]	Z	X	K_i [μM]
5	H	–	–	–	113
6a	Ph	–	–	–	20.6
6b	1-Np	–	–	–	19.5
6c	2-Np	–	–	–	5.4
7a	Ph	H	–	–	12.7
7b	2-Np	Me	–	–	4.2
8a	Ph	–	COOH	H	6.8
8b	*o*-MePh	–	COOH	H	4.3
8c	*m*-MePh	–	COOH	H	3.8
8d	*p*-MePh	–	COOH	H	7.0
8e	*m*-FPh	–	COOH	H	1.7
8f	*p*-FPh	–	COOH	H	4.6
8g	2-Np	–	COOH	H	4.3
8h	2-Np	–	SO_2Me	H	6.4
8i	2-Np	–	SO_2NH_2	H	5.6
8j	9-phenanthryl	–	COOH	H	2.3
8k	2-adamantyl	–	COOH	H	2.6
8l	4-Acen	–	COOH	H	1.1
8m	1-Np	–	COOH	F	0.48
8n	2-Np	–	COOH	F	0.51
8o	4-Et-2-Np	–	COOH	F	0.15
8p	5-Et-2-Np	–	COOH	F	0.17
8q	7-Et-2-Np	–	COOH	F	0.14
8r	4-*c*Pr-2-Np	–	COOH	F	0.11
8s	4-*c*Pr,7-Et-2-Np	–	COOH	F	0.066
8t	*p*-Bp	–	COOH	F	0.35
8u	*m*-Bp	–	COOH	F	0.13
8v	3,5-diMe-*m*-Bp	–	COOH	F	0.24
8w	4-OEt-*m*-Bp	–	COOH	F	0.075
8x	4-MrPrO-*m*-Bp	–	COOH	F	0.067

[a] Np = naphthyl; Acen = 1,2-dihydroacenaphthyl; *c*Pr = cyclopropyl; Bp = biphenyl; MrPrO = *N*-morpholinylpropoxy.

high-resolution mass spectrometry; HPLC analyses established purity as >95%. As in prior studies, the inhibition constants K_i were determined using HPP as the substrate.[9,11] Inhibitory activity is measured from formation of the borate complex of the enol product at 305 nm using a plate reader. Absorbance is measured in triplicate on two occasions. The average K_i results are reported; the standard error is typically 10–20% of the K_i value. In addition, the aqueous solubilities of several compounds were determined with a shake-flask procedure.[11,12,18] Saturated solutions are filtered and analyzed by UV-vis spectroscopy.

Consistent with the modeling, addition of an aryl group in **6** did provide a significant boost over **5**, bringing the K_i values down to ~20 μM for a phenyl or 1-naphthyl group and to 5 μM for 2-naphthyl (**6c**). The analogous anilinyl and phenoxy compounds, **7a** and **8a**, were prepared, and the greater activity and pharmacological desirability of diaryl ethers placed the subsequent focus on the latter series. A 2.3-Å crystal structure for the complex of **8a** with MIF was also obtained (Figure 6), which does show aryl–aryl contacts between the phenoxy phenyl group and both Tyr36 and Phe113. A basic SAR (structure–activity relationship) study was then carried out with **8b**–**8f**, which revealed a small activity range for addition of a methyl or fluoro substituent, with *para*-substitution the least favored. Consistent with this guidance, the 2-naphthyl analogue **8g** was found to show good activity at 4.3 μM; the BOMB modeling indicated increased contact with Phe113 projecting to the right in Figure 6. Modeling further indicated that still larger hydrophobic groups could be accommodated in this region at the entrance of the MIF active site. This was

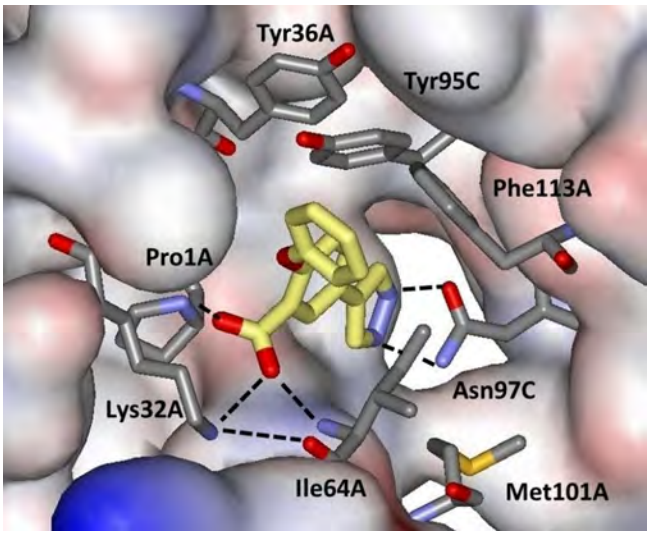

Figure 6. Rendering from the 2.3-Å crystal structure of compound **8a** bound to MIF. Details as in Figure 2.

borne out by K_i values of 1–3 μM obtained for phenanthryl, adamantyl, and acenaphthyl analogues, **8j**–**8l** (Figure 7). However, the project seemed stalled at this point without reaching the desired low-nanomolar range and with increasing concerns about solubility.

For the biaryltriazoles series, it was recalled that placement of a fluorine adjacent to the hydroxy group in compounds like **2** provided a ~3-fold increase in activity.[11] The effect was attributed to enhancing the acidity of the phenol, which increases the strength of the hydrogen bond with Asn97, and also to hydrophobic contact of the fluorine with the side chain of Met 101 (Figure 2). For the pyrazoles, the enhanced hydrogen bonding could be envisioned for a fluorine at the 3-position; however, the fluorine would project more toward the side chain of Ile64 rather than Met101 with uncertain outcome (Figure 4). Still, a potential additional benefit might arise from the influence of the fluorine on the tautomeric equilibrium for the pyrazole. Reliable quantum mechanical calculations (MP2/6-311++G**) show that the N1-H tautomer is favored by 3.6 kcal mol^{-1} over the N2-H tautomer with a fluorine in the 3-position (Figure 8).[19] From the present crystal structures the hydrogen bonds are expected to be more linear for the N1-H tautomer as implied by the alignment of the side-chain oxygen atom of Asn97 and N1 in Figures 4 and 6.

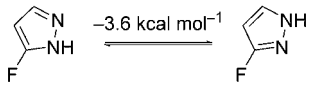

Figure 8. Shift in the tautomeric equilibrium with a fluorine atom.[19]

Preparation of the fluorinated pyrazole for the Suzuki coupling in Scheme 1 proved difficult. Multiple routes were attempted, but success was only achieved using a SEM [2-(trimethylsilyl)ethoxymethyl] protecting group; the yield was still low, but sufficient to proceed (Scheme 2).

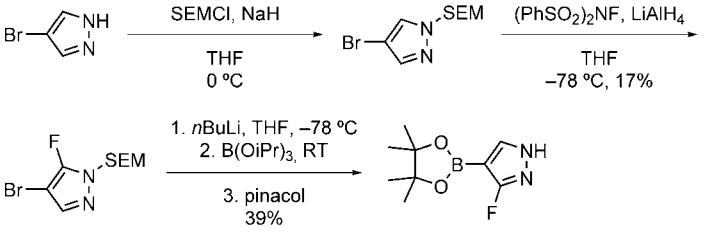

Scheme 2. Synthesis of fluorinated pyrazoles.

The effort was highly fruitful yielding a nearly 10-fold increase in potency in progressing from the parent 2-naphthyl inhibitor **8g** (4.3 μM) to its fluorinated analogue **8n** (0.51 μM). It was also possible to obtain a crystal structure for this compound in complex with MIF at 2.0-Å resolution (Figure 9). The structure confirmed the positioning of the fluorine between the side chains of Ile64 and Met101. There is one copy of the inhibitor in each MIF trimer in this case; the N–O and N–N hydrogen bond lengths with Asn97 are 2.87 and 3.12 Å. There are also close-packed aryl–aryl interactions between the naphthyl group of **8n** and Tyr36 and Phe113.

Though the exact positioning of the naphthyl group may be influenced by crystal packing, the structure and BOMB modeling indicated that additional gains in activity could arise from alkyl-substitution at the 4-, and 5-positions of the naphthyl group to achieve further contact with Phe113 or at the 7-position for contact with Ile64. This was shown to be correct with the ethyl analogues **8o**, **8p**, and **8q**, which each provided a 3-fold lowering of the K_i relative to **8n**. Addition of a cyclopropyl group at the 4-position also appeared promising for interaction with the front edge of Phe113; this was realized with **8r** bringing the K_i to 0.11 μM. Combining this with the 7-ethyl substitution provided the very potent **8s** with a K_i of 0.066 μM.

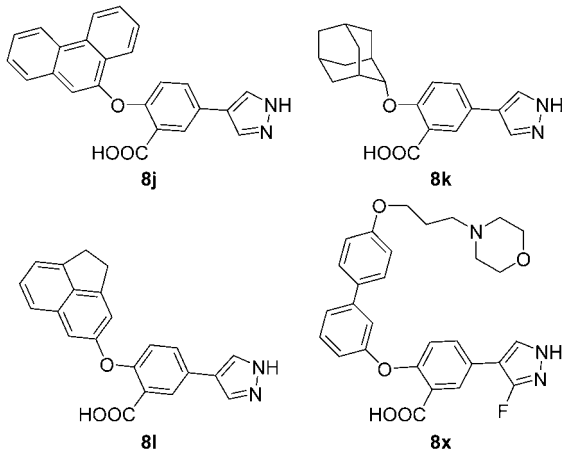

Figure 7. Some pyrazole-based MIF inhibitors reported herein.

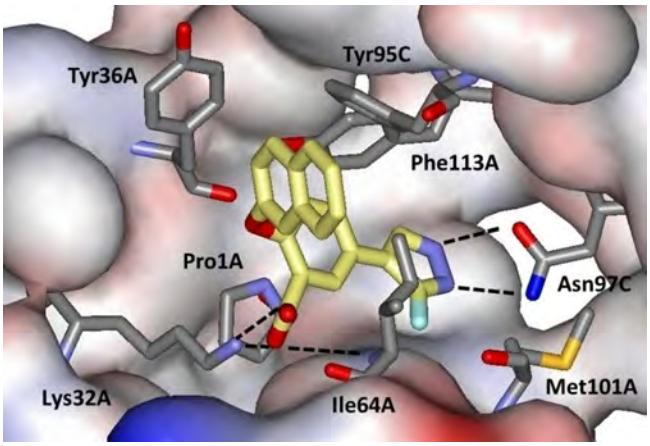

Figure 9. Rendering from the 2.0-Å crystal structure of compound **8n** bound to MIF. Details as in Figure 2.

From the structures for **8a** and **8n** (Figures 6 and 9) and modeling, it was also clear that it should be possible to expand to a biphenyl at either the *para* or *meta* position of **8a**. Thus, **8t** and **8u** were synthesized and provided significantly lower K_i values (0.35 and 0.13 μM) than the unsubstituted naphthyl analogues, **8m** and **8n**. Substantial activity gains could be expected by judicious substitution for the biphenyls; however, only a few derivatives were prepared with **8w** and **8x** (Figure 7) demonstrating ~0.07 μM potency and that large groups can be extended into the solvent from the terminal 4-position.

Two additional items are worth noting. First, the results for **8g**, **8h**, and **8i** show that the carboxylic acid group may be replaced by a methylsulfone or sulfonamide with little impact on potency. This is relevant if one wished to explore these compounds as potential neurological agents,[2] as sulfones are expected to exhibit better penetration of the blood–brain barrier than carboxylic acids or sulfonamides.[20] Secondly, it is always important to monitor aqueous solubilities for compounds of interest for oral administration.[11,17,21] Most oral drugs are observed to have aqueous solubilities of 4 to 4000 $\mu g\,mL^{-1}$, which translates to 10 μM to 10 mM for a drug with a molecular weight of 400.[21] The solubilities of several of the present compounds were measured in Britton-Robinson buffer at pH 6.5.[18] As noted, the solubility of the starting compound **5** is very high ($927 \pm 88\ \mu g\,mL^{-1}$). The solubility of the parent 2-naphthyl analogue **8g** is also high ($739 \pm 32\ \mu g\,mL^{-1}$); it is affected little by addition of the fluorine in **8n** ($681 \pm 59\ \mu g\,mL^{-1}$), while switch to the sulfonamide **8i** yields a significant decrease ($55.2 \pm 4.8\ \mu g\,mL^{-1}$). Given these results, it was surprising to find in the biphenyl series that the solubility of **8w** is only $1.7 \pm 0.7\ \mu g\,mL^{-1}$. However, this is readily remedied by attachment of solvent-exposed, solubilizing groups[11b] as in **8x** ($34.6 \pm 4.8\ \mu g\,mL^{-1}$, or 67 μM).

To facilitate further study of the in vitro and in vivo biology of MIF, series of potent MIF tautomerase inhibitors have been pursued. Starting from a 113-μM docking hit, a novel series, which features a pyrazole instead of a phenol, was optimized to yield compounds with K_i values as low as 60–70 nM. The optimization was greatly facilitated by molecular modeling and the ability to obtain multiple high-resolution crystal structures, which guided the effective selection and placement of substituents. Recognition of the potential benefit of addition of a fluorine in the pyrazole ring also provided an essential boost along with a synthetic challenge. Current efforts are being directed at testing the influence of the inhibitors on suppressing MIF-stimulated cell proliferation and at preclinical studies for off-target activity and metabolism.

Experimental Section

Recombinant expression and purification of human MIF was carried out as previously reported.[11] Crystallization of MIF in complex with **5** and **8g** was achieved by soaking with apo-MIF crystals, while for the complexes of **8a** and **8n**, co-crystallization was performed via sitting drop vapor diffusion at 20 °C. The structures were determined in-house using a Rigaku 007 HF+ diffractometer and Saturn 944+ CCD detector at $T = 100$ K. The crystal structures have been deposited in the RSCB Protein Data Bank with PDB IDs 6CBG (**5**), 6CBF (**8a**), 6CB5 (**8g**), and 6CBH (**8n**). The Supporting Information contains the synthetic procedures, NMR and HRMS spectral data for all new compounds, and details for the crystallography and solubility measurements (72 pages).

Acknowledgements

Gratitude is expressed to the US National Institutes of Health (NIH grant number GM32136) for research support, to the US National Science Foundation for a fellowship for M.J.R. (grant number DGE-1122492), and to Drs. Thomas Steitz, Michael Strickler, and Yong Xiong for assistance at the Yale Richards Center.

Conflict of interest

The authors declare no conflict of interest.

Keywords: MIF inhibitors · phenol bioisosteres · protein crystallography · pyrazoles · tautomerase

[1] a) E. Lolis, R. Bucala, *Expert Opin. Ther. Targets* **2003**, *7*, 153–164; b) J. Garai, T. Lóránd, *Curr. Med. Chem.* **2009**, *16*, 1091–1114; c) D. Greven, L. Leng, R. Bucala, *Expert Opin. Ther. Targets* **2010**, *14*, 253–264; d) Y. Asare, M. Schmitt, J. Bernhagen, *Thromb. Haemostasis* **2013**, *109*, 391–398.

[2] a) N. E. Savaskan, G. Fingerle-Rowson, M. Buchfelder, I. Y. Eyüpoglu, *Int. J. Cell Biol.* **2012**, *2012*, 139573; b) M. F. Leyton-Jaimes, J. Kahn, A. Israelson, *Exp. Neurol.* **2018**, *301B*, 83–91.

[3] a) C. Bifulco, K. McDaniel, L. Leng, R. Bucala, *Curr. Pharm. Des.* **2008**, *14*, 3790–3801; b) H. Conroy, L. Mawhinney, S. C. Donnelly, *Q. J. Med.* **2010**, *103*, 831–836; c) L. Pawig, C. Klasen, C. Weber, J. Bernhagen, H. Noels, *Front. Immunol.* **2015**, *6*, 429; d) N. Kindt, F. Journe, G. Laurent, S. Saussez, *Oncol. Lett.* **2016**, *12*, 2247–2253; e) C. C. G. Nobre, J. M. Galvão de Araújo, T. A. A. M. Fernandes, R. N. O. Cobucci, D. C. F. Lanza, V. S. Andrade, J. V. Fernandes, *Pathol. Oncol. Res.* **2017**, *23*, 235–244.

[4] C. O'Reilly, M. Doroudian, L. Mawhinney, S. C. Donnelly, *Med. Res. Rev.* **2016**, *36*, 440–460.

[5] S. N. Babu, G. Chetal, S. Kumar, *Asian Pac. J. Cancer Prev.* **2012**, *13*, 1737–1744.

[6] a) M. Orita, S. Yamamoto, N. Katayama, S. Fujita, *Curr. Pharm. Des.* **2002**, *8*, 1297–1317; b) J. Garai, T. Lóránd, *Curr. Med. Chem.* **2009**, *16*, 1091–

1114; c) J. Bloom, S. Sun, Y. Al-Abed, *Expert Opin. Ther. Targets* **2016**, *20*, 1463 – 1475.
[7] a) P. D. Senter, Y. Al-Abed, C. N. Metz, F. Benigni, R. A. Mitchell, J. Chesney, J. Han, C. G. Gartner, S. D. Nelson, G. J. Todaro, R. Bucala, *Proc. Natl. Acad. Sci. USA* **2002**, *99*, 144 – 149; b) A. A. Hare, L. Leng, S. Gandavadi, X. Du, Z. Cournia, R. Bucala, W. L. Jorgensen, *Bioorg. Med. Chem. Lett.* **2010**, *20*, 5811 – 5814.
[8] a) Z. Cournia, L. Leng, S. Gandavadi, X. Du, R. Bucala, W. L. Jorgensen, *J. Med. Chem.* **2009**, *52*, 416 – 424; b) H. Ouertatani-Sakouhi, F. El-Turk, B. Fauvet, M.-K. Cho, D. P. Karpinar, D. Le Roy, M. Dewor, T. Roger, J. Bernhagen, T. Calandra, M. Zweckstetter, H. A. Lashuel, *J. Biol. Chem.* **2010**, *285*, 26581 – 26598; c) L. Xu, Y. Zhang, L. Zheng, C. Qiao, Y. Li, D. Li, X. Zhen, T. Hou, *J. Med. Chem.* **2014**, *57*, 3737 – 3745; d) L.-T. Tsai, T.-H. Lin, *J. Biomol. Screening* **2014**, *19*, 1116 – 1123; e) M. C. Zapatero, P. Pérez, M. J. Vázquez, G. Colmenarejo, M. de los Frailes, F. Ramón, *J. Biomol. Screening* **2016**, *21*, 446 – 458.
[9] J. A. Cisneros, M. J. Robertson, M. Valhondo, W. L. Jorgensen, *Bioorg. Med. Chem. Lett.* **2016**, *26*, 2764 – 2767.
[10] A. Billich, P. Lehr, H. Gstach (Novartis AG, Novartis Pharma GmbH), Int. PCT Pub. No. WO2006045505 A1, **2006**.
[11] a) P. Dziedzic, J. A. Cisneros, M. J. Robertson, A. A. Hare, N. E. Danford, R. H. Baxter, W. L. Jorgensen, *J. Am. Chem. Soc.* **2015**, *137*, 2996 – 3003; b) J. A. Cisneros, M. J. Robertson, B. Q. Mercado, W. L. Jorgensen, *ACS Med. Chem. Lett.* **2017**, *8*, 124 – 127.
[12] J. A. Cisneros, M. J. Robertson, M. Valhondo, W. L. Jorgensen, *J. Am. Chem. Soc.* **2016**, *138*, 8630 – 8638.
[13] Y. Al-Abed, D. Dabideen, B. Aljabari, A. Valster, D. Messmer, M. Ochani, M. Tanovic, K. Ochani, M. Bacher, F. Nicoletti, C. Metz, V. A. Pavlov, E. J. Miller, K. J. Tracey, *J. Biol. Chem.* **2005**, *280*, 36541 – 36544.
[14] a) B. Wu, K. Kulkarni, S. Basu, S. Zhang, M. Hu, *J. Pharm. Sci.* **2011**, *100*, 3655 – 3681; b) A. Rowland, J. O. Miners, P. I. Mackenzie, *Int. J. Biochem. Cell Biol.* **2013**, *45*, 1121 – 1132.
[15] a) E. Chapman, M. D. Best, S. R. Hanson, C.-H. Wong, *Angew. Chem. Int. Ed.* **2004**, *43*, 3526 – 3548; *Angew. Chem.* **2004**, *116*, 3610 – 3632; b) C. Rakers, F. Schumacher, W. Meinl, H. Glatt, B. Kleuser, G. Wolber, *J. Biol. Chem.* **2016**, *291*, 58 – 71.
[16] a) J. L. Wright, T. F. Gregory, S. R. Kesten, P. A. Boxer, K. A. Serpa, L. T. Meltzer, L. D. Wise, *J. Med. Chem.* **2000**, *43*, 3408 – 3419; b) R. R. Wilkening, R. W. Ratcliffe, A. K. Fried, D. Meng, W. Sun, L. Colwell, S, Lambert, M. Greenlee, S. Nilsson, A. Thorsell, M. Mojena, C. Tudela, K. Frisch, W. Chan, E. T. Birzin, S. P. Rohrer, M. L. Hammond, *Bioorg. Med. Chem. Lett.* **2006**, *16*, 3896 – 3901.
[17] a) H. Gohlke, G. Klebe, *Angew. Chem. Int. Ed.* **2002**, *41*, 2644 – 2676; *Angew. Chem.* **2002**, *114*, 2764 – 2798; b) W. L. Jorgensen, *Acc. Chem. Res.* **2009**, *42*, 724 – 733; c) P. Schneider, G. Schneider, *J. Med. Chem.* **2016**, *59*, 4077 – 4086; d) W. L. Jorgensen, *Bioorg. Med. Chem.* **2016**, *24*, 4768 – 4778.
[18] E. Baka, J. E. A. Comer, K. Takács-Novák, *J. Pharm. Biomed. Anal.* **2008**, *46*, 335 – 341.
[19] M. Jarończyk, J. C. Dobrowolski, A. P. Maruzek, *THEOCHEM* **2004**, *673*, 17 – 28.
[20] a) S. A. Hitchcock, L. D. Pennington, *J. Med. Chem.* **2006**, *49*, 7559 – 7583; b) J. M. Meinig, S. J. Ferrara, T. Banerji, T. Banerji, H. S. Sanford-Crane, D. Bourdette, T. S. Scanlan, *ACS Chem. Neurosci.* **2017**, *8*, 2468 – 2476.
[21] W. L. Jorgensen, E. M. Duffy, *Adv. Drug Delivery Rev.* **2002**, *54*, 355 – 366.

Manuscript received: March 11, 2018
Accepted manuscript online: March 25, 2018
Version of record online: April 23, 2018

JACS
JOURNAL OF THE AMERICAN CHEMICAL SOCIETY

Article

pubs.acs.org/JACS

A Fluorescence Polarization Assay for Binding to Macrophage Migration Inhibitory Factor and Crystal Structures for Complexes of Two Potent Inhibitors

José A. Cisneros, Michael J. Robertson, Margarita Valhondo, and William L Jorgensen*

Department of Chemistry, Yale University, New Haven, Connecticut 06520-8107, United States

Supporting Information

ABSTRACT: Human macrophage migration inhibitory factor (MIF) is both a keto−enol tautomerase and a cytokine associated with numerous inflammatory diseases and cancer. Consistent with observed correlations between inhibition of the enzymatic and biological activities, discovery of MIF inhibitors has focused on monitoring the tautomerase activity using L-dopachrome methyl ester or 4-hydroxyphenyl pyruvic acid as substrates. The accuracy of these assays is compromised by several issues including substrate instability, spectral interference, and short linear periods for product formation. In this work, we report the syntheses of fluorescently labeled MIF inhibitors and their use in the first fluorescence polarization-based assay to measure the direct binding of inhibitors to the active site. The assay allows the accurate and efficient identification of competitive, noncompetitive, and covalent inhibitors of MIF in a manner that can be scaled for high-throughput screening. The results for 22 compounds show that the most potent MIF inhibitors bind with K_d values of ca. 50 nM; two are from our laboratory, and the other is a compound from the patent literature. X-ray crystal structures for two of the most potent compounds bound to MIF are also reported here. Striking combinations of protein−ligand hydrogen bonding, aryl−aryl, and cation−π interactions are responsible for the high affinities. A new chemical series was then designed using this knowledge to yield two more strong MIF inhibitors/binders.

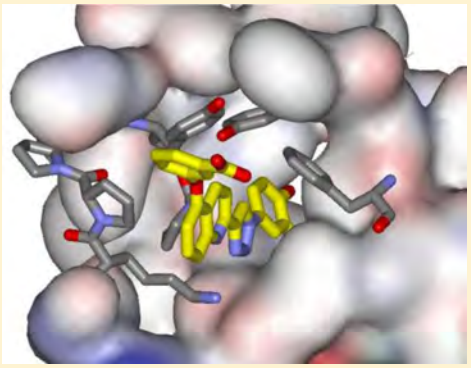

INTRODUCTION

Macrophage migration inhibitory factor (MIF) is a proinflammatory cytokine that is involved in numerous inflammatory and autoimmune diseases including rheumatoid arthritis, diabetes, sepsis, and acute respiratory distress syndrome.[1−4] Release of MIF from activated cells such as macrophages and T-cells in turn promotes release of other inflammatory cytokines. MIF is also overexpressed in many cancer cells where it enhances cell proliferation by inhibiting accumulation of the tumor suppressor p53.[5] The complex biological activities of MIF as a cytokine are modulated by its binding to the cell-surface receptors CD74, CXCR2, and CXCR4. MIF is a homotrimeric protein with 342 residues, which also displays enzymatic activity as a keto−enol tautomerase. There are three identical active sites at the interfaces of the monomer subunits. The enzymatic activity appears to be vestigial in humans; however, nonphysiological substrates including D-dopachrome methyl ester (DOPA) and hydroxyphenyl pyruvic acid (HPP) have been identified and form the bases for the most common assays.[6,7] Although inhibition of the tautomerase activity does not guarantee inhibition of biological function, many studies have supported a correlation.[8,9] A recent report has further strengthened the view that MIF-CD74 binding occurs near the tautomerase sites and that the protrusion of inhibitors outside the active sites leads to reduced biological activity.[10]

Most studies to identify MIF inhibitors have screened compound libraries using the DOPA or HPP tautomerase assays.[4,9,11−14] IC_{50} or K_i values are reported for inhibition of the tautomerization of these substrates. As discussed previously,[15] execution of these assays is complicated by multiple factors including the light sensitivity of DOPA, the slow rate of tautomerization of HPP, spectral interference of inhibitors and products, choice of protein concentration, and short times for the linear range of product formation in both cases. There has been limited report on activities of consensus reference compounds in the screening studies except for the isoxazoline (*R*)-ISO-1.[16] The IC_{50} results for it, which range from 7 μM to >100 μM, reflect the difficulties in obtaining consistency.[9,16,17] We also reinvestigated the chromenone Orita-13, which had been the most active compound in the journal literature with a reported K_i of 0.038 μM in the DOPA assay.[11] However, while K_i results should be independent of the substrate, repeated testing in our HPP assay yielded modest K_i values of 13−22 μM.[15] Extension of the comparisons to additional compounds from the literature has revealed a pattern of substantial inconsistencies in reports of activities from MIF tautomerase assays.[18] Therefore, we decided to pursue development of a direct binding assay that can overcome the

Received: May 12, 2016
Published: June 14, 2016

DOI: 10.1021/jacs.6b04910
J. Am. Chem. Soc. 2016, 138, 8630−8638

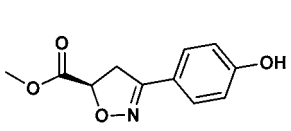

(*R*)-ISO-1

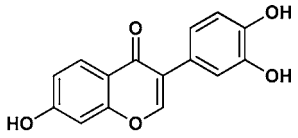

Orita-13

problems with the tautomerase assays. Based on our recent finding of biaryltriazoles as potent MIF tautomerase inhibitors, we were able to design and synthesize fluorescent ligands that can be used as effective tracers in a fluorescence polarization (FP) assay.[19] Displacement of a ligand by a fluorescent probe yields a readily quantified increase in fluorescent polarization that reflects the fraction of bound ligand. The usual advantages of FP assays apply including use of standard microplate readers, direct determination of K_d values with no need for substrates or radiolabeled reagents, and the ability to reanalyse the assay plates.[19] In contrast, for the tautomerase assays, the measurements of product formation can only be made once in the first seconds after the addition of the substrates. Furthermore, since the present tracers have low-nanomolar affinity for MIF, only small amounts of the protein are required. In the course of this work, we also determined the crystal structures of the complexes for two MIF ligands with particularly high affinities. The results reveal common structural features for achieving strong binding with MIF.

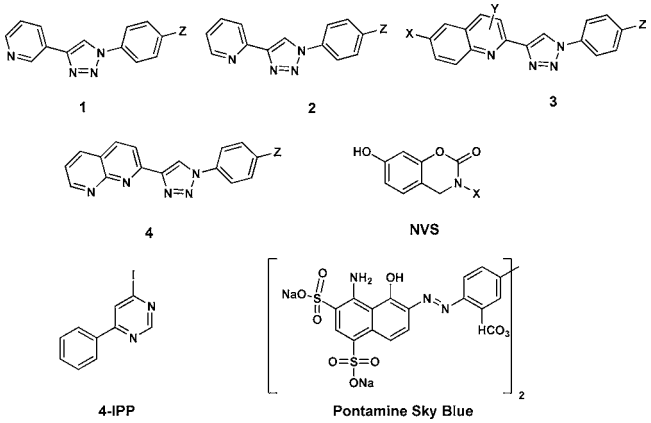

EXPERIMENTAL SECTION

Chemistry. We previously reported biaryltriazoles with the general structures **1**–**4** as MIF tautomerase inhibitors with K_i values as low as 0.057 μM in the HPP assay.[15] X-ray crystal structures for complexes of the parent quinoline **3a** (X = Y = H, Z = OH) and its analogue with X = MOEO (methoxyethoxy) were also reported and confirmed the expected binding in the MIF active sites with the X group on C6 of the quinoline protruding into the solvent.[15] The analogues of **1**–**4** utilized here were reported previously with the exception of **3j**;[15] their syntheses feature a 1,3-dipolar cycloaddition of a phenylazide with a substituted ethynylheterocycle obtained via a Sonogashira coupling. We have also examined the journal and patent literature for other potential strong binders. Compounds reported in a patent from workers at Novartis appeared particularly promising.[20] Twenty two benzoxazinones were exemplified, and it was stated that they had activities of 20 nM–20 μM in an HPP tautomerase assay. The second example, which we refer to as NVS-2 (X = *p*-methoxyphenyl), was singled out as having an IC_{50} of 20 nM. We resynthesized it along with examples 1 and 6, NVS-1 (X = cyclohexyl), and NVS-6 (X = *p*-hydroxyphenyl). As described in the Supporting Information, the general procedure from the patent was followed; however, the details on the protection of the 7-hydroxy group were unclear. It was found that a *tert*-butyldimethylsilyloxy group worked well (Scheme 1). NVS-6 was obtained from 4-methoxy-2-hydroxybenzaldehyde and 4-methoxyaniline upon treatment with sodium borohydride, followed by demethylation of both methoxy groups using pyridinium hydrochloride. Additional reference compounds, ISO-1, Orita-13, 4-IPP, and Pontamine Sky Blue (PSB), were obtained from commercial sources (Alfa-Aesar, Tocris, Santa Cruz Biotechnology). Compound identity was confirmed by NMR and mass spectrometry, and >95% purity of all assayed compounds was established by HPLC.

Biology. The expression and purification of human MIF followed the previous procedures.[15] The protein has been prepared on two occasions and stored at −80 °C. Aliquots are thawed for the assaying and crystal growth, and never refrozen. Activities were shown to be consistent for different samples using multiple control compounds. The HPP tautomerase assay was carried out as described before.[15] Inhibitory activity is monitored by measuring formation of the borate complex of the enol product at 305 nm using a Tecan Infinite F500 plate reader. Details for the FP assay are described below and in the Supporting Information.

Crystallography. X-ray crystal structures at 1.8-Å resolution were obtained for complexes of NVS-2 and 3-((2-(1-(3-fluoro-4-hydroxyphenyl)-1*H*-1,2,3-triazol-4-yl)quinolin-5-yl)oxy)benzoic acid (**3i**) with human MIF. Crystals of apo MIF were obtained by the hanging drop method. Subsequently, 2 μL drops containing the apo MIF crystals were treated with 10 mM suspensions of the ligands in DMSO. In both cases, after several weeks, the initial protein crystals cracked and dissolved, and new crystals formed (Figure S1). The crystals were cryoprotected, and data collection was performed on a Rigaku 007HF + X-ray source with a Saturn 944+ CCD detector at Yale. Data processing, phasing, model building, and refinement were carried out as described previously.[15] Crystals of NVS-2 were found to occupy the $P3_121$ space group, while those of **3i** were $I222$. Full details are provided in the Supporting Information. The structures have been deposited with the RCSB Protein Data Bank with PDP IDs 5HVT and 5HVS, respectively.

RESULTS AND DISCUSSION

Design of Fluorescent Ligands. The fluorescent ligands were designed based on the biaryltriazoles previously reported by our group.[15] As summarized in Scheme 2, starting with **3b**, which has a K_i of 0.77 μM in the HPP assay, a fluorine was added adjacent to the hydroxyl group to yield **3c** and a K_i of 0.33 μM. The improvement can be attributed to the fluorine enhancing the acidity of the hydroxyl group, which forms a hydrogen bond with Asn97, and/or filling a small hydrophobic space contacting Met101. Compound **3c** also bears an amino group that was reacted with the isothiocyanate derivative of fluorescein (FITC) to yield the fluorescent analogue **A**, which was subsequently found in saturation experiments described below to have a K_d of 0.181 μM. Exploration to further improve

Scheme 1. Synthesis of NVS-2

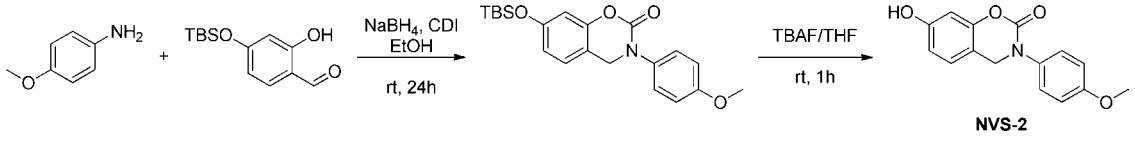

DOI: 10.1021/jacs.6b04910
J. Am. Chem. Soc. 2016, 138, 8630–8638

Scheme 2. Design of Fluorescent Ligands A and B

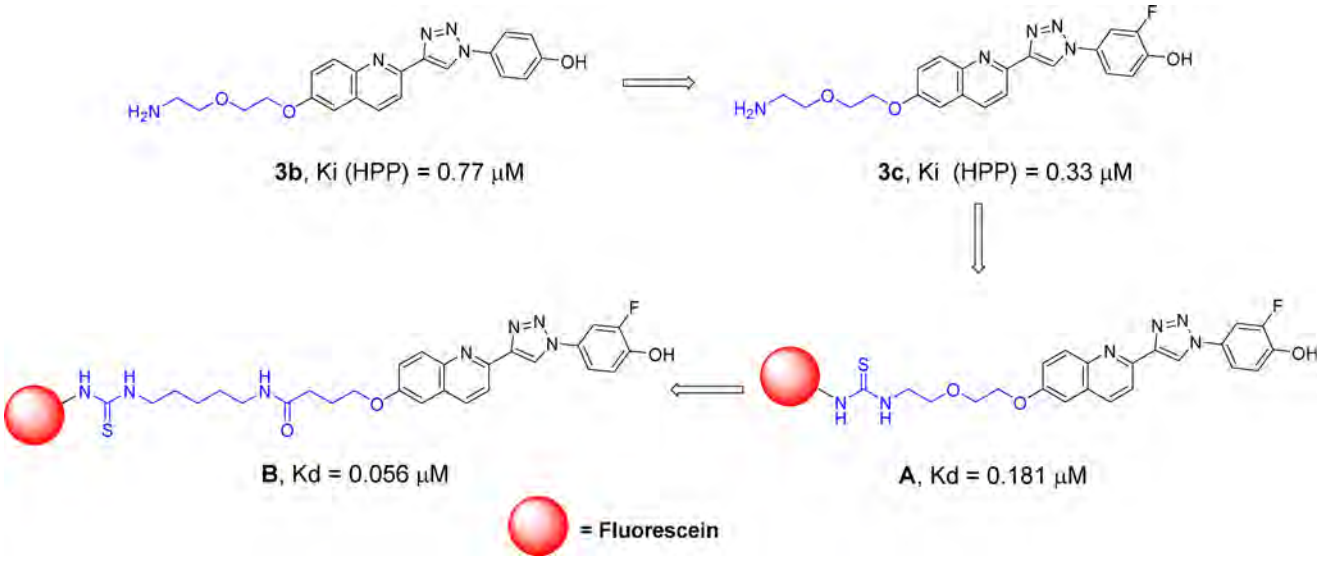

Scheme 3. Complete Structure of Fluorescent MIF Ligand B Used in the FP Assays

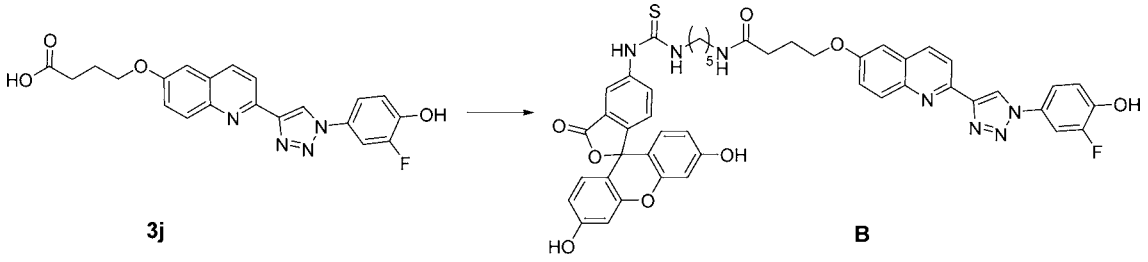

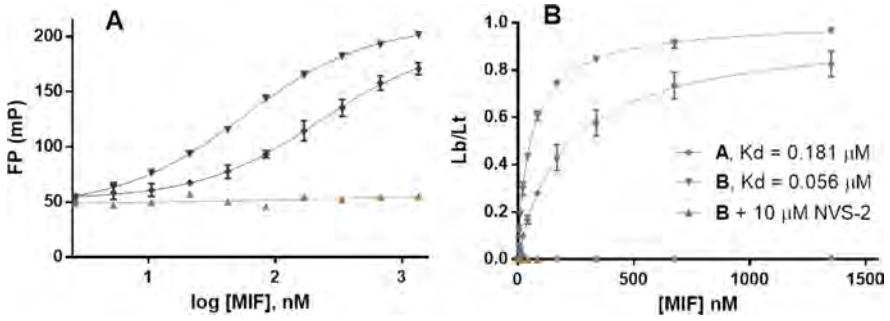

Figure 1. Determination of binding affinity of tracers **A** and **B** through saturation experiments. (A) Variation of FP values for both tracers as a function of MIF concentration. Bottom curve indicates the high specificity of ligand **B** toward the active site of MIF. (B) K_d determination for ligands **A** and **B**. L_b/L_t = ratio of ligand bound to the total. Data shown from quadruplicate experiments in three independent assays. Mean ± SEM plotted for all data.

the affinity of the fluorescent ligand included expansion of the spacer between the quinoline ring and the fluorophore. This led to the fluorescent ligand **B**, which has a K_d of 0.056 μM and was prepared from the carboxylic acid **3j** (Scheme 3). The increased potency is beneficial in allowing use of a lower protein concentration in the FP assay. Based on the previous[15] and current crystallographic results and the consistent structure–activity data (SAR), it is fully expected that these fluorescent ligands, derived from competitive inhibitors, bind to the active sites of MIF. Therefore, they can be used to identify not only compounds that competitively bind to the tautomerase sites but also compounds that can bind to allosteric sites that may disrupt or block the active site and keep the tracer from binding.

FP Assay Development. The assay was developed in a 96-well format. To determine if the fluorescent ligands bind to the protein and their affinity, binding saturation experiments were carried out. After determination of the lowest concentration of the tracer that gives a consistent FP value, this concentration (0.004 μM) was fixed and increasing amounts of MIF (0 to 1.35 μM) were added, which caused an increase in the FP values by around 4-fold (Figure 1A). In order to determine if any nonspecific binding occurs, the assay was also carried out in the presence of a high concentration of a high-affinity ligand (NVS-2), which binds to the active site based on the crystal structure presented below. Ligand **B** shows very high specificity since there is no variation in the FP value from that of the free tracer in the presence of 10 μM NVS-2 (Figure 1A, bottom

DOI: 10.1021/jacs.6b04910
J. Am. Chem. Soc. 2016, 138, 8630–8638

Table 1. Results for Tautomerase Inhibition (K_i) from the HPP Assay and for Binding (K_d) from the Fluorescence Polarization Assay[a]

compd	X	Y	Z	K_i (μM)	K_d (μM)[b]
1a	–	–	OH	37	30% (25 μM)
2a	–	–	OH	8.8	1.75
3a	H	H	OH	0.59	0.260
3b	AEOEO	H	OH	0.77	0.348
3c	AEOEO	H	3-F,4-OH	0.33	0.163
3d	MOEO	H	F	8.9	(>1.5)
3e	MOEO	H	OMe	NA	NA
3f	MrEOEO	H	OH	0.41	0.211
3g	MrEOEO	H	3-F,4-OH	0.15	0.152
3h	H	5-*p*-COOH-OPh	3-F,4-OH	0.11	0.110
3i	H	5-*m*-COOH-OPh	3-F,4-OH	0.057	0.071
3j	$O(CH_2)_3COOH$	H	3-F,4-OH	0.034	0.063
4a	H	H	OH	1.48	0.347
5a	OCH_3	–	–	1.90	1.71
5b	COOH	–	–	1.70	1.15
Orita-13	–	–	–	17	20% (100 μM)
(*R*)-ISO-1	–	–	–	24	24
NVS-1	cyclohexyl	–	–	0.569	0.456
NVS-2	*p*-OMe-Ph	–	–	0.027	0.055
NVS-6	*p*-OH-Ph	–	–	0.185	0.159
4-IPP	–	–	–	(4.5)[c,d]	(0.446)[c]
PSB	–	–	–	ND	49% (200 μM)

[a]MOEO = methoxyethoxy; AEOEO = aminoethoxyethoxy; Mr = *N*-morpholinyl. NA = not active. [b]K_d or % bound at indicated concentration in parentheses. [c]Covalent inhibitor: result is time-dependent. [d]IC_{50} from ref 9.

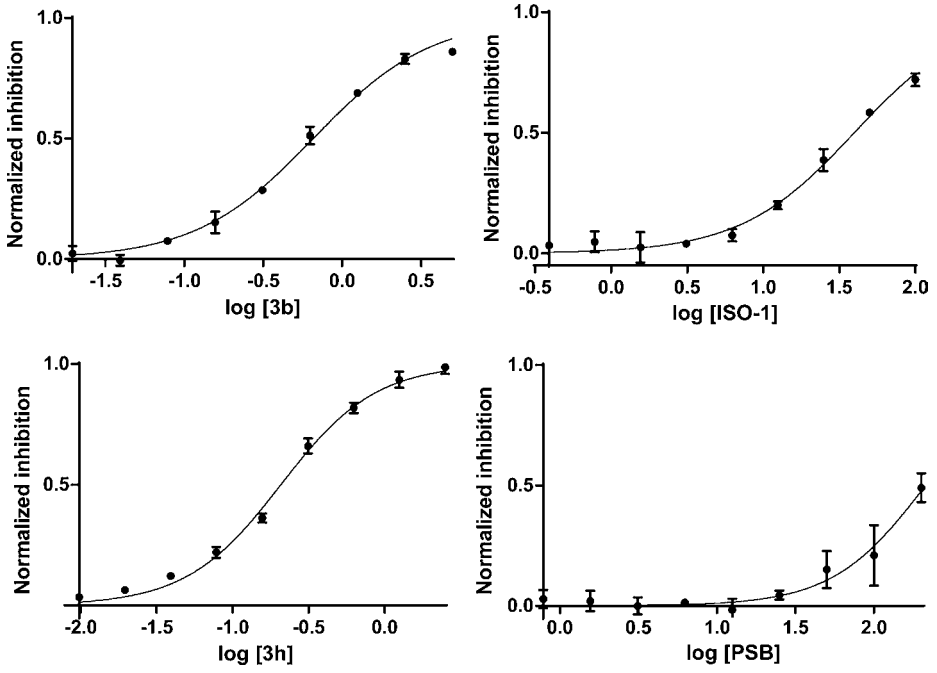

Figure 2. Determination of IC_{50} for representative compounds. Plotted data from quadruplicate experiments in three independent assays, mean ± SEM.

curve). At high MIF and NVS-2 concentrations there is no indication that the tracer participates in any binding that would be signaled by an increase in the FP value. Thus, the fluorescent ligand binds to the tautomerase sites, and the fraction of ligand bound to ligand total can be calculated with the highest and lowest FP values obtained in the saturation experiments. Using GraphPad Prism 6, K_d values are readily determined by plotting this fraction vs the concentration of the protein and fitting the results to the Hill equation. From Figure 1B, tracer **B** has greater affinity (K_d = 0.056 ± 0.002 μM) than tracer **A** (K_d = 0.181 ± 0.034 μM).

Competition Assays. In order to develop a competitive FP assay to determine the affinities of unlabeled compounds, tracer **B** was selected since its higher affinity allows use of a smaller amount of protein to give a sufficient difference in FP values. At 0.056 μM MIF, the ΔmP between positive and negative

DOI: 10.1021/jacs.6b04910
J. Am. Chem. Soc. 2016, 138, 8630−8638

controls is ca. 80 mP. Thus, we settled on standard assay conditions of 0.004 μM tracer **B** and 0.056 μM MIF.

The compounds listed in Table 1 were assayed. Most are known noncovalent tautomerase inhibitors of MIF including 11 biaryltriazoles,[15] (*R*)-ISO-1,[16] and Orita-13.[11] In addition, we added an inactive analogue **3e**, where the 4-methoxy group disrupts the characteristic hydrogen bond with Asn-97,[15] **3j**, and the three NVS compounds.[20] We also assayed 4-IPP, a well-known covalent MIF inhibitor,[21] and the azo dye pontamine sky blue (PSB), which is reported to bind on the surface of MIF and inhibit both the tautomerase activity of MIF and its binding to CD74 (IC_{50} = 0.81 μM).[22]

For the FP assay, compounds were incubated at room temperature with human MIF for 20 min, followed by the addition of tracer **B**. This order of addition is preferred because of the high affinity of the tracer; otherwise, it takes modest inhibitors such as ISO-1 1−2 h to reach equilibrium for displacing the bound tracer. A standard buffer solution was used composed of 20 mM HEPES, 150 mM NaCl, and 0.01% Tween-20 with a pH of 7.4. Fluorescence polarization was monitored for 1 h with λ_{exc} = 485 ± 20 nm and λ_{em} = 535 ± 25 nm. The IC_{50} of each compound for reducing the fluorescence polarization was determined by fitting the data to a nonlinear regression for log concentration vs response (Figure 2). The IC_{50} is then transformed into the corresponding K_d via eq 1,[23] where K_d^t is the K_d of the tracer (0.056 μM), L_t and L_b are the total and bound concentrations of the tracer, and P_t is the total MIF concentration. Full experimental details are provided in the Supporting Information.

$$K_d = \frac{L_b IC_{50} K_d^t}{P_t L_t + L_b(P_t - L_t + L_b - K_d^t)} \quad (1)$$

The results from the HPP and FP assays are recorded in Table 1. In principle, the K_i and K_d values for a noncovalent inhibitor that binds to the tautomerase sites should be the same under identical assay conditions. However, variations can arise from multiple sources. For example, allosteric binding might or might not lead to tautomerase inhibition and/or displacement of the fluorescent ligand. In addition, the assay conditions are not identical. An important consideration is the pH. The tautomerase assays with both HPP and DOPA are carried out at pH 6−6.1, the optimal conditions for the substrates, while we have performed the FP assay at physiological pH, 7.4. The pH affects the protonation of functional groups in fluorophores and, therefore, the amount of fluorescence. In general, an acidic pH is worse than an alkaline pH for fluorescence assays. pH 7.4 keeps the fluorescecent properties of fluorescein in an optimal range and enhances the biological relevance.[24] There is also influence of the pH on the protein−ligand binding, which we examined for tracer **A** (Figure 3). As shown, increasing the pH from 5.1 to 7.4 clearly enhances the binding of **A**, and presumably the other biaryltriazoles, to MIF; the effect is likely associated with progressive deprotonation of the catalytic Pro1, which has a pK_a of ca. 5.6.[25]

Another issue in FP assays is possible alteration of the fluorescence by test compounds. The fluorescent properties of the tracer in the presence of the compounds, but in the absence of protein, should be checked before assaying. In the present cases, some compounds have no effect on FP values even at high concentrations, e.g., ISO-1 and PSB. However, other compounds, specifically **1a**, **3d**, and Orita-13, did yield effects. In general, the undesirable effects decrease with the concentration such that concentrations of test compounds below 1−3 μM do not cause interference. However, this modulation of the fluorescence does not allow determination of the affinity of those compounds for which the limiting concentration is lower than their K_d values. Another issue that can affect fluorescence is aggregation. Compounds that form aggregates or precipitates can yield misleading FP values. Overall, the high concentrations needed to determine the affinity of weak ligands can be problematic due to potential nonspecific binding of the ligand to the tracer.[24] The use of detergents in the FP buffers such as Tween-20 helps to avoid aggregation; however, at high concentrations, this issue may still arise. Other assays including the tautomerase one are also prone to aggregation problems at high concentrations.[26]

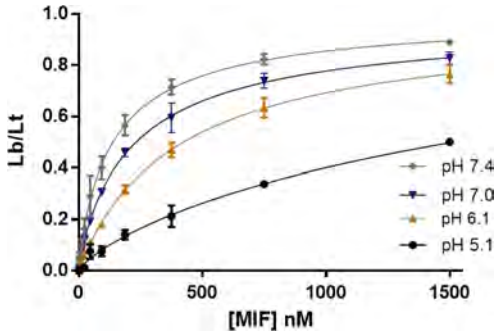

Figure 3. Influence of the pH in the binding of tracer **A** to MIF. Lb/Lt = ratio of ligand bound to the total. Data shown from quadruplicate experiments in two independent assays. Mean ± SEM plotted for all data.

In spite of the caveats, we do observe similar results with our tautomerase and FP assays for the compounds in Table 1. This is especially true for the most potent compounds including **3g**−**3j** and the three NVS compounds, and the order of activities is well preserved. The consistency between the present K_i and K_d results supports the accuracy of both assays and contrasts the inconsistencies in prior reports for the tautomerase activities of reference compounds.[18] Progression from **1a** (3-pyridinyl) to **2a** (2-pyridinyl) to **3a** (2-quinolinyl) increases tautomerase inhibition in parallel with binding to MIF. The effects of substituents for the quinoline series, **3a**−**3i**, are also in good accord. The replacement of the phenolic hydroxyl group by a methoxy group in **3e** abolishes the binding and tautomerse inhibition, while the addition of a fluorine next to the hydroxyl group improves the K_i and K_d values by a factor of 2 for **3b**/**3c** and **3f**/**3g**. For compound **3d** the phenolic OH is replaced by F leading to weaker inhibition, again due to loss of hydrogen bonding with Asn97.[15] In this case for the FP assay, no inhibition is evident up to 1.5 μM. Above this point, there is interference with the fluorescence, so a K_d value could not be determined. The two assays also agree essentially quantitatively that the most potent triazole derivatives, **3i** and **3j**, incorporate an oxybenzoic acid substituent at the 5-position in the quinoline ring or an oxybutanoic acid substituent at the 6-position yielding K_i and K_d values of 0.034−0.071 μM. Insights on the structural origins of this effect are provided below.

Turning to the reference compounds, as noted above, Orita-13 with a K_i of 17 μM is much less active in our HPP assay[15] than expected from the original report of 0.038 μM in the DOPA assay.[11] The modest activity is supported by the present FP results in which only 20% binding is found at 100 μM. (*R*)-ISO-1 is unequivocally more active in the FP assay with an

DOI: 10.1021/jacs.6b04910
J. Am. Chem. Soc. 2016, 138, 8630−8638

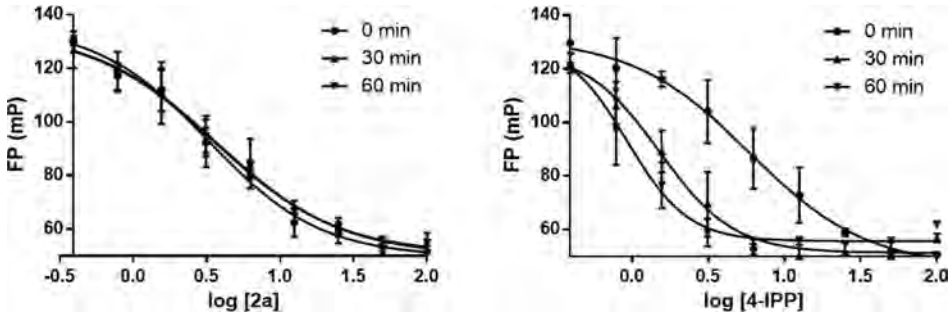

Figure 4. Contrasting FP results for a noncovalent inhibitor **2a** (left) and a covalent one, 4-IPP (right). The results for the covalent inhibitor depend on the detection time showing increasing amounts of unbound tracer with increasing time. Mean ± SEM plotted for all data.

average K_d of 24 μM, from three separate measurements of 21, 22, and 30 μM. Our group and others have assayed (*R*)-ISO-1 multiple times yielding IC_{50} and K_i values ranging from 7 to >100 μM. In three separate measurements with the present protocols, we obtained K_i values of 21, 24, and 28 μM for (*R*)-ISO-1, also averaging 24 μM. These two cases reflect that significant variations are more probable for reports of activities of less potent compounds, likely for the pH, aggregation, and spectral interference issues noted above.

In view of the previous inconsistencies with published results,[15,18] it was gratifying to find that, in our HPP assay, the NVS compounds are indeed potent tautomerase inhibitors with K_i values of 0.569, 0.027, and 0.185 μM for NVS-1, NVS-2, and NVS-6, respectively. The activities of NVS-2 and **3j** are essentially identical at 0.03 μM, which establishes them as the most potent tautomerase inhibitors to our knowledge. The K_i of 0.027 μM for NVS-2 is very similar to the previously reported IC_{50} of 0.020 μM (20 nM).[20] In addition, the K_d values from the FP assay are quantitatively similar to the K_i results. NVS-2, **3i**, and **3j** with K_d values of 0.055−0.071 μM bind the most strongly to MIF among the compounds studied here.

Covalent and Allosteric Inhibition. The FP assay also allows discrimination of covalent and noncovalent inhibitors. The formation of a covalent bond between an inhibitor and a residue in a binding site is expected to occur more slowly than establishment of a noncovalent complex. Consequently, the activity of the covalent binder will appear to increase with increasing time. We monitored the FP for 1 h after the 20 min incubation period with a noncovalent inhibitor (**2a**) and the covalent inhibitor 4-IPP.[21] As seen in Figure 4, there is a clear difference between the results. The noncovalent interactions of **2a** are formed quickly, and the equilibrium between the bound and unbound tracer is time independent. On the other hand, in the case of 4-IPP the FP results are time dependent showing the expected decrease in fluorescence polarization (increase in unbound tracer) with increasing time.

Finally, PSB has been reported as an allosteric inhibitor of MIF tautomerase activity as well as an agent able to block the binding of MIF to CD74 with an IC_{50} value of 0.81 μM.[22] Crystallographic results show PSB bound to the interface between two MIF trimers.[22] According to our FP results, the affinity of this compound is low with 49% binding of PSB at 200 μM.

However, concern can be expressed that the compound is aggregating at such concentrations; when the amount of Tween-20 was reduced below 0.01%, the FP signal was lost. Though PSB does not bind in the active site, in some multimeric form it may cover the active site and cause partial exclusion of the tracer.

Assay Quality. In order to provide a measure of the quality of HTS assays, Zhang et al. introduced the Z' factor, which is calculated from the mean signals of the positive and negative controls (μ_{c+} and μ_{c-}) and their standard deviations (σ_{c+} and σ_{c-}) using the formula $Z' = 1 - [3(\sigma_{c+} + \sigma_{c-})/|\mu_{c+} - \mu_{c-}|]$.[27] As the signal range increases and the variations decrease, Z' tends to the ideal limit of 1, while Z' values above 0.5 are considered "excellent".[27] From four independent measurements of the positive (tracer B plus MIF) and negative (tracer B alone) controls for the present FP assay, the Z' factor is 0.69.

Crystal Structures. X-ray structures were obtained for crystals of two of the most potent inhibitors identified here with human MIF. A close-up of the structure in the vicinity of the tautomerase site is shown for **3i** in Figure 5. The general

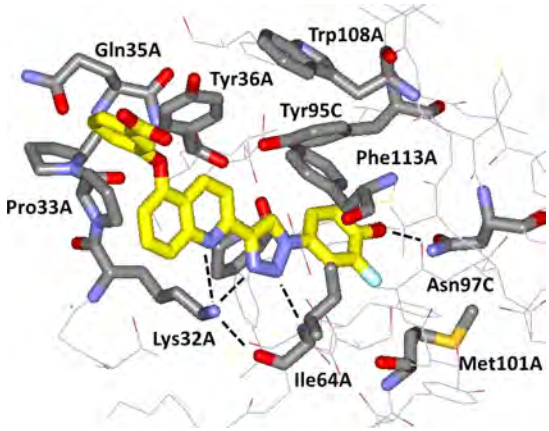

Figure 5. Rendering from the 1.8-Å X-ray crystal structure of **3i** bound to human MIF. Residues near the active site are illustrated with carbon atoms of **3i** in yellow. Dashed lines indicate hydrogen bonds. The PDB code is 5HVS.

features are as expected from the prior reports for **3a** and its analogue with an MOEO group at C6 of the quinoline ring.[15] The protein−ligand complexation features multiple hydrogen bonds and aryl−aryl interactions. All three tautomerase sites of the MIF trimer are occupied by **3i**. The ammonium group of Lys32 is coordinated by the quinoline nitrogen, N3 of the triazole, and the carbonyl oxygen of Ile64 at distances of 3.14, 3.97, and 2.79 Å, respectively. N2 of the triazole is also in a hydrogen bond with the backbone nitrogen of Ile64 (2.93 Å), and the phenolic oxygen is 2.59 Å from the side chain nitrogen or oxygen atom of Asn97. The new feature is the accommodation of the phenoxy group on C5 of the quinoline

DOI: 10.1021/jacs.6b04910
J. Am. Chem. Soc. 2016, 138, 8630−8638

ring. It is partially tucked into the pocket between Pro33 and Tyr36. The added van der Waals contacts can account to some extent for the increased potency of **3i** over **3c** and **3g**, whose substituents at C6 of the quinoline are solvent-exposed. There is also an electrostatic benefit of the negative carboxylate group on the phenoxy ring in view of its proximity to Lys32. Decreases in potency of 2- to 10-fold are found when the carboxylate group is replaced by neutral or positively charged alternatives.[15] Another new feature is that the fluorine atom adjacent to the phenolic hydroxyl group is oriented down between Ile64 and Asn97, making closest contact with C_γ of Met101 (3.07 Å). This was expected from molecular modeling studies,[15] but the ligands in the previous crystal structures lacked the fluorine atom. As noted above, the 2-fold increases in potency obtained by addition of the fluorine atom may be attributed to inductive enhancement of the hydrogen bond between the hydroxyl group and Asn-97 and/or the hydrophobic contact with Met101.

The corresponding structure for NVS-2 is illustrated in Figure 6. The interaction themes are similar to the case for **3i**

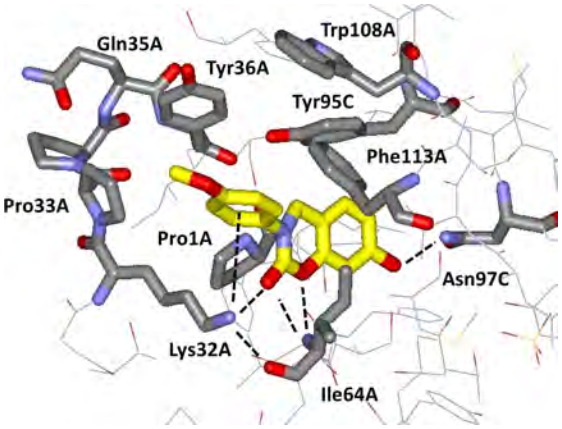

Figure 6. Rendering from the 1.8-Å X-ray crystal structure of **NVS-2** bound to human MIF. The PDB code is 5HVT.

with coordination of the Lys32 ammonium group by the carbonyl groups of NVS-2 (2.80 Å) and Ile64 (2.86 Å), a bifurcated hydrogen bond between the backbone NH of Ile64 and the NVS-2 carbonyl (3.20 Å) and ring oxygen (3.12 Å) atoms, and a hydrogen bond between the hydroxyl group of NVS-2 and Asn97 (2.62 Å). A striking additional feature is a cation−π interaction between the anisyl group of NVS-2 and Lys32; the ammonium group is positioned below the ring center with distances of 4.5−5.5 Å to all six carbon atoms, typical of cation−π interactions.[28,29] As for **3i**, there are also multiple aryl−aryl interactions between the inhibitors and Tyr36, Tyr95, and Phe113. The complementarity between NVS-2 and the MIF tautomerase site appears almost ideal with the remarkable multidentate coordination of Lys32, satisfaction of the hydrogen-bonding demands of Ile64 and Asn97, and the aryl−aryl interactions for Tyr36, Tyr95, and Phe113. The only part of the ligand that appears to not be engaged in beneficial interactions is the terminal methoxy group, though its electron-donating character may enhance the hydrogen-bond accepting character of the carbonyl group in the oxazinone ring. This notion is consistent with the 3-fold stronger binding for NVS-2 than for NVS-6 in which the solvent-exposed methoxy group is replaced by hydroxy. The ca. 10-fold weaker binding for the cyclohexyl analogue NVS-1 clearly results from loss of the cation−π interaction with Lys-32. In view of its small size with a heavy atom count (HAC) of only 20, the ligand efficiency for NVS-2 is high at 0.50 ($(-2.3RT/\mathrm{HAC})\ \log K_d$).[30] For the much larger **3i**, the ligand efficiency is 0.30.

It should also be noted that, as in the case of **3i**, all three tautomerase sites are occupied by copies of NVS-2. This may reflect the strength of the interactions, or it may be regulated by protein−protein packing. In the crystal structure for **3a** bound to MIF (PDB ID: 4WR8),[15] there is only one tautomerase site occupied per MIF trimer; however, the protein−protein interface has tight contact between the quinoline rings of the inhibitors protruding from the surfaces of pairs of MIF trimers. For the present cases, **3i** extends much farther than NVS-2 from the active site (Figure 7), so it is likely that MIF signaling via binding to cell-surface receptors including CD74 will be more impaired in the presence of **3i**.[22] Thus, higher ligand efficiency may not be desirable in this case. We have also used the substituents at C5 and C6 of the quinoline to enhance the solubility of the biaryltriazoles.[15]

Combined Design. In view of the striking cation−π interaction for NVS-2 in Figure 6, a new molecular design was sought to merge this feature with the triazolylphenol core of **3**. Structure building with the BOMB program[31] suggested that

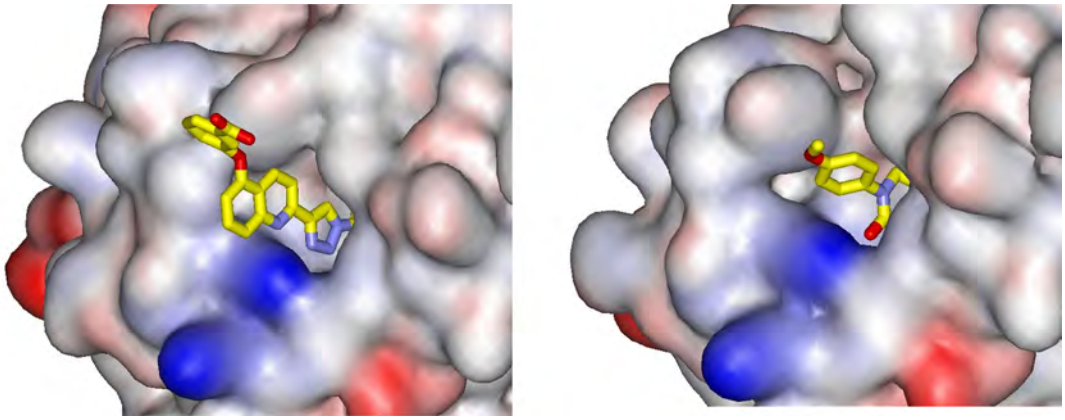

Figure 7. Renderings from the crystal structures for **3i** (left) and NVS-2 (right) illustrating the difference in protrusion from the MIF binding site. The protein is shown as a space-filling surface. The orientation of the terminal methoxy group of NVS-2 varies depending on the binding site of the MIF trimer.

DOI: 10.1021/jacs.6b04910
J. Am. Chem. Soc. 2016, 138, 8630−8638

replacement of the quinolinyl group of **3** with a phenoxy group as in **5** would be appropriate (Figure 8). It is expected that the

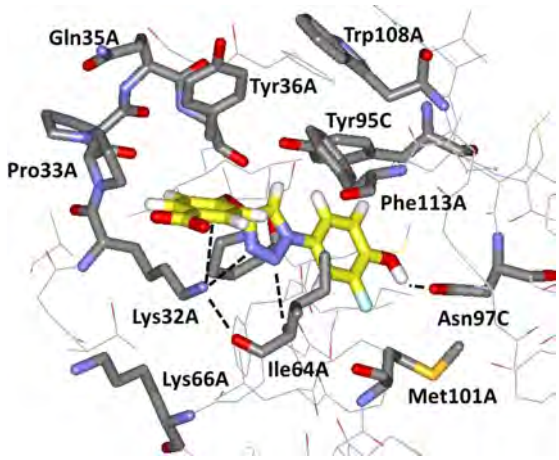

Figure 8. Computed structure for the complex of MIF and **5b** as modeled with the BOMB program. Anticipated hydrogen bonds and the cation−π interaction are indicated with dashed lines.

cation−π interaction is enhanced by substituents that would further increase the electron-richness of the phenoxy group. Thus, we had interest in preparing the 4-methoxy (**5a**) and carboxylic acid (**5b**) derivatives. **5b** is expected to be ionized to the carboxylate above pH 5.

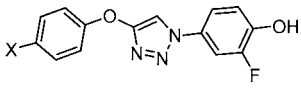

5a (X = OMe) **5b** (X = COOH)

The synthesis of compounds **5** is outlined in Scheme 4; full details are in the Supporting Information. Treatment of 4-

Scheme 4. Synthesis of Compounds 5a and 5b

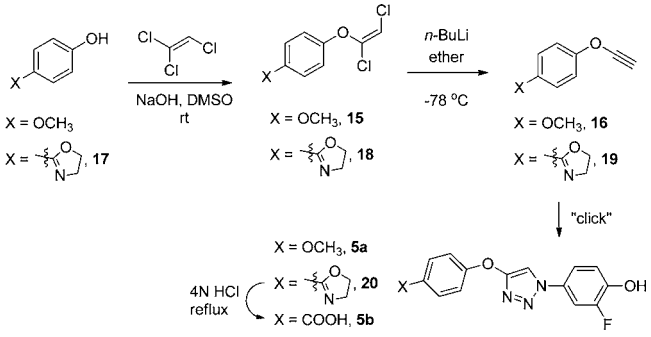

methoxyphenol with trichloroethylene and base, followed by dehydrohalogenation with *n*-butyl lithium, yielded the ethynyl ether,[32] which was converted to **5a** by a one-pot Cu(I)-catalyzed "click" reaction using 4-azido-2-fluorophenol generated *in situ*.[15] However, synthesis of **5b** required an oxazoline protecting group[33] in view of the step using *n*-butyl lithium. The two compounds were then assayed and show good potency with K_i and K_d values of 1−2 μM (Table 1). They are significantly more potent than (*R*)-ISO-1 and the parent 2-pyridyl analogue **2a**. The small difference in the K_i values for the acid (**5b**) and ether (**5a**) derivatives is consistent with what was observed for **3i** (0.057 μM) and its methoxyethoxy analogue (0.082 μM).[15] Thus, the quinolinyl and phenoxy motifs of **3** and **5** provide interesting polydentate alternatives for accommodation of Lys32 by incorporating azine coordination or a cation−π interaction (Figures 5 and 8).

CONCLUSION

In this work, a fluorescence polarization assay was developed by designing and synthesizing two fluorescein-labeled inhibitors of MIF. The high affinity of tracer **B** permits use of low concentrations of both the tracer (0.004 μM) and the protein (0.056 μM) in the FP assay. The FP assay shows multiple advantages over the traditional HPP and DOPA tautomerase assays used for discovery of molecules that bind to MIF including ease of use and detection, stability of reagents, and ready expansion to HTS formats. Both the HPP and FP assays were applied to 22 compounds including known noncovalent, covalent, and allosteric inhibitors of MIF. The results for the noncovalent inhibitors show excellent accord between the measured K_i and K_d values giving confidence in the viability of the present protocols for both assays. We also synthesized a particularly interesting compound from the patent literature, NVS-2; it and **3j** are the most potent inhibitors/binders in our assays. With K_i values of 0.03 μM, they are roughly 1000-fold more potent than the prototypical MIF inhibitor (*R*)-ISO-1.

Furthermore, the FP assay was shown to perform well for the covalent inhibitor 4-IPP, which demonstrated the expected time-dependence for its binding results. The weak allosteric inhibitor PSB also yielded a response in the FP assay showing some interference with binding of the tracer at high concentrations. The assay results were much enhanced by obtaining X-ray crystal structures at 1.8-Å resolution for two of the most potent MIF inhibitors/binders, **3i** and NVS-2. The structures confirmed that the anticipated binding of these molecules and the closely related tracers occurs in the MIF tautomerase active sites. The structures also illustrate the exquisite binding of these potent compounds to MIF featuring extensive hydrogen-bonding and aryl−aryl interactions along with a cation−π interaction for the anisyl group of NVS-2. A new chemical series was then designed merging the triazolylphenol core of **3** with the cation−π feature of NVS-2 to yield additional strong MIF inhibitors/binders, **5a** and **5b**. The present structural and activity results along with the availability of the FP assay place further work on seeking regulators of the activity of MIF on a firm foundation.

ASSOCIATED CONTENT

Supporting Information

The Supporting Information is available free of charge on the ACS Publications website at DOI: 10.1021/jacs.6b04910.

Full synthetic procedures and spectral characterization data for all intermediates and final compounds; crystallographic data; experimental details of the HPP and FP assays (PDF)

AUTHOR INFORMATION

Corresponding Author

*william.jorgensen@yale.edu

Notes

The authors declare no competing financial interest.

DOI: 10.1021/jacs.6b04910
J. Am. Chem. Soc. 2016, 138, 8630−8638

■ ACKNOWLEDGMENTS

Gratitude is expressed to the National Institutes of Health (GM32136) for research support and to the National Science Foundation (DGE-1122492) for a fellowship to M.J.R. The authors also thank Dr. Julian Tirado-Rives and Prof. Richard H. G. Baxter for technical advice.

■ REFERENCES

(1) Morand, E. F.; Leech, M.; Bernhagen, J. *Nat. Rev. Drug Discovery* **2006**, *5*, 399−411.
(2) Garai, J.; Lorand, T. *Curr. Med. Chem.* **2009**, *16*, 1091−1114.
(3) Asare, Y.; Schmitt, M.; Bernhagen, J. *Thromb. Haemostasis* **2013**, *109*, 391−398.
(4) Xu, L.; Li, Y.; Sun, H.; Zhen, X.; Qiao, C.; Tian, S.; Hou, T. *Drug Discovery Today* **2013**, *18*, 592−600.
(5) Conroy, H.; Mawhinney, L.; Donnelly, S. C. *QJM* **2010**, *103*, 831−836.
(6) Rosengren, E.; Bucala, R.; Aman, P.; Jacobsson, L.; Odh, G.; Metz, C. N.; Rorsman, H. *Mol. Med.* **1996**, *2*, 143−149.
(7) Rosengren, E.; Aman, P.; Thelin, S.; Hansson, C.; Ahlfors, S.; Björk, P.; Jacobsson, L.; Rorsman, H. *FEBS Lett.* **1997**, *417*, 85−88.
(8) Senter, P. D.; Al-Abed, Y.; Metz, C. N.; Benigni, F.; Mitchell, R. A.; Chesney, J.; Han, J.; Gartner, C. G.; Nelson, S. D.; Todaro, G. J.; Bucala, R. *Proc. Natl. Acad. Sci. U. S. A.* **2002**, *99*, 144−149.
(9) Cournia, Z.; Leng, L.; Gandavadi, S.; Du, X.; Bucala, R.; Jorgensen, W. L. *J. Med. Chem.* **2009**, *52*, 416−424.
(10) Pantouris, G.; Syed, M. A.; Fan, C.; Rajasekaran, D.; Cho, T. Y.; Rosenberg, E. M., Jr; Bucala, R.; Bhandari, V.; Lolis, E. J. *Chem. Biol.* **2015**, *22*, 1197−1205.
(11) Orita, M.; Yamamoto, S.; Katayama, N.; Aoki, M.; Takayama, K.; Yamagiwa, Y.; Seki, N.; Suzuki, H.; Kurihara, H.; Sakashita, H.; Takeuchi, M.; Fujita, S.; Yamada, T.; Tanaka, A. *J. Med. Chem.* **2001**, *44*, 540−547.
(12) Ouertatani-Sakouhi, H.; El-Turk, F.; Fauvet, B.; Cho, M.-K.; Karpinar, D. P.; Le Roy, D.; Dewor, M.; Roger, T.; Bernhagen, J.; Calandra, T.; Zweckstetter, M.; Lashuel, H. A. *J. Biol. Chem.* **2010**, *285*, 26581−26598.
(13) Xu, L.; Zhang, Y.; Zheng, L.; Qiao, C.; Li, Y.; Li, D.; Zhen, X.; Hou, T. *J. Med. Chem.* **2014**, *57*, 3737−3745.
(14) Tsai, L.-T.; Lin, T.-H. *J. Biomol. Screening* **2014**, *19*, 1116−1123.
(15) Dziedzic, P.; Cisneros, J. A.; Robertson, M. J.; Hare, A. A.; Danford, N. E.; Baxter, R. H.; Jorgensen, W. L. *J. Am. Chem. Soc.* **2015**, *137*, 2996−3003.
(16) Al-Abed, Y.; Dabideen, D.; Aljabari, B.; Valster, A.; Messmer, D.; Ochani, M.; Tanovic, M.; Ochani, K.; Bacher, M.; Nicoletti, F.; Metz, C.; Pavlov, V. A.; Miller, E. J.; Tracey, K. J. *J. Biol. Chem.* **2005**, *280*, 36541−36544.
(17) Balachandran, S.; Rodge, A.; Gadekar, P. K.; Yadav, V. N.; Kamath, D.; Chetrapal-Kunwar, A.; Bhatt, P.; Srinivasan, S.; Sharma, S.; Vishwakarma, R. A.; Dagia, N. M. *Bioorg. Med. Chem. Lett.* **2009**, *19*, 4773−4776.
(18) Cisneros, J. A.; Robertson, M. J.; Valhondo, M.; Jorgensen, W. L. *Bioorg. Med. Chem. Lett.* **2016**, *26*, 2764−2767.
(19) For a review, see: Lea, W. A.; Simeonov, A. *Expert Opin. Drug Discovery* **2011**, *6*, 17−32.
(20) Billich, A.; Lehr, P.; Gstach, H. PCT/EP2005/011233, WO2006/045505 A1, 2006.
(21) Winner, M.; Meier, J.; Zierow, S.; Rendon, B. E.; Crichlow, G. V.; Riggs, R.; Bucala, R.; Leng, L.; Smith, N.; Lolis, E.; Trent, J. O.; Mitchell, R. A. *Cancer Res.* **2008**, *68*, 7253−7257.
(22) Bai, F.; Asojo, O. A.; Cirillo, P.; Ciustea, M.; Ledizet, M.; Aristoff, P. A.; Leng, L.; Koski, R. A.; Powell, T. J.; Bucala, R.; Anthony, K. G. *J. Biol. Chem.* **2012**, *287*, 30653−30663.
(23) Rossi, A. M.; Taylor, C. W. *Nat. Protoc.* **2011**, *6*, 365−87.
(24) Smart, P. L.; Laidlaw, I. M. S. *Water Resour. Res.* **1977**, *13*, 15−33.
(25) Stamps, S. L.; Fitzgerald, M. C.; Whitman, C. P. *Biochemistry* **1998**, *37*, 10195−10202.
(26) Seidler, J.; McGovern, S. L.; Doman, T. N.; Shoichet, B. K. *J. Med. Chem.* **2003**, *46*, 4477−4486.
(27) Zhang, J. H.; Chung, T. D.; Oldenburg, K. R. *J. Biomol. Screening* **1999**, *4*, 67−73.
(28) Burley, S. K.; Petsko, G. A. *FEBS Lett.* **1986**, *203*, 139−143.
(29) Ma, J. C.; Dougherty, D. A. *Chem. Rev.* **1997**, *97*, 1303−1324.
(30) Hopkins, A. L.; Groom, C. R.; Alex, A. *Drug Discovery Today* **2004**, *9*, 430−431.
(31) Barreiro, G.; Kim, J. T.; Guimarães, C. R. W.; Bailey, C. M.; Domaoal, R. A.; Wang, L.; Anderson, K. S.; Jorgensen, W. L. *J. Med. Chem.* **2007**, *50*, 5324−5329.
(32) (a) Moyano, A.; Charbonnier, F.; Greene, A. E. *J. Org. Chem.* **1987**, *52*, 2919−2922. (b) Graf, K.; Rühl, C. L.; Rudolph, M.; Rominger, F.; Hashmi, A. S. *Angew. Chem., Int. Ed.* **2013**, *52*, 12727−12731.
(33) Meyers, A. I.; Mihelich, E. D. *Angew. Chem., Int. Ed. Engl.* **1976**, *15*, 270−281.

DOI: 10.1021/jacs.6b04910
J. Am. Chem. Soc. 2016, 138, 8630−8638

ACS Medicinal Chemistry Letters

Letter

pubs.acs.org/acsmedchemlett

Systematic Study of Effects of Structural Modifications on the Aqueous Solubility of Drug-like Molecules

José A. Cisneros, Michael J. Robertson, Brandon Q. Mercado, and William L. Jorgensen*

Department of Chemistry, Yale University, New Haven, Connecticut 06520-8107, United States

Supporting Information

ABSTRACT: Aqueous solubilities and activities have been measured for 17 members of the quinolinyltriazole series of inhibitors of human macrophage migration inhibitory factor (MIF). Systematic variation of a solvent-exposed substituent provided increases in solubility from 2 μg/mL for the parent compound **3a** up to 867 μg/mL. The low solubility of **3a** results from its near-planar structure and an intermolecular hydrogen bond, as revealed in a small-molecule X-ray structure. Removal of the hydrogen bond yields a 3-fold increase in solubility, but a 7-fold drop in activity. **5b** emerges as the most potent MIF inhibitor with a K_i of 14 nM and good solubility, 47 μg/mL, while **4e** has both high potency and solubility.

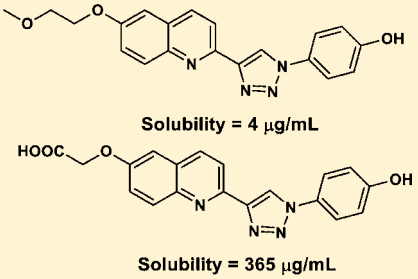

KEYWORDS: *Aqueous solubility, MIF inhibitors, crystallography*

Aqueous solubility is well-known as a critical property in the development of drugs.[1−5] Poor solubility is associated with difficulties in the reliable performance of assays, in obtaining oral formulations for *in vivo* administration, and in bioavailability. On the other hand, high solubility may lead to poor cell permeability and rapid excretion. The optimal range for the aqueous solubility S of drugs intended for oral delivery is ca. 10 μM to 10 mM or, equivalently, 4−4000 μg/mL for a compound with a molecular weight of 400.[2] Oral drugs with solubilities below 1 μM are very rare.

Poor solubility is a common issue in drug discovery efforts, since hydrophobic compounds bind well to target proteins for the same reasons that proteins fold to shield their hydrophobic groups from the aqueous environment. The problems may arise early from poorly soluble compounds that are obtained as hits in high-throughput screening. They often become aggravated during lead optimization, since the most reliable way to increase potency is to add hydrophobic substituents that fill hydrophobic regions in the target's binding site. Consistently, target proteins with highly hydrophobic binding sites are particularly prone to inhibitor designs with poor solubility. A classic example is non-nucleoside inhibitors of HIV-1 reverse transcriptase, NNRTIs.[6] The binding site in this case features a cluster of residues with aliphatic and aromatic side chains, and poor solubility has characterized many classes of NNRTIs. This is especially true for diaminopyrimidines, including the FDA-approved drugs etravirine and rilpivirine (**1**). In comparison to **1**, we were able to increase the solubility ca. 700-fold to 14 μg/mL for the triazine analogue with a morpholinylpropoxy substituent (**2**) while retaining excellent potency in infected T-cell assays.[7] This illustrates the basic principle for improving solubility without loss of potency: add conformationally flexible substituents with polar groups to a site in the inhibitor that is solvent-exposed in the complex with the protein. The benefit of flexibility includes the entropic gain from populating more conformers in solution than in the crystal. A corollary is to reduce planarity for inhibitors with multiple aromatic rings, which also leads to less tight packing in the crystalline state.[8] However, the addition of polar groups comes with uncertainties, since they may also form stabilizing hydrogen bonds in the crystal.

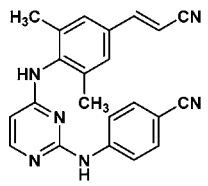

1

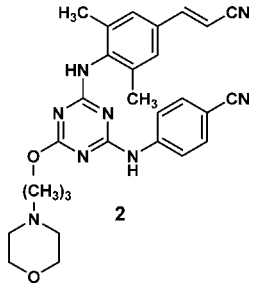

2

More recently, solubility has become an issue in our development of inhibitors of the tautomerase activity of the human macrophage migration inhibitory factor (MIF).[9] Specifically, surprisingly low solubility of 2.2 μg/mL was found for the parent quinolinyltriazole **3a** (R = H), which arose from *de novo* design. However, modeling indicated that substituents at the 6- and 7-positions of the quinoline ring should be solvent exposed. This expectation was confirmed by obtaining X-ray

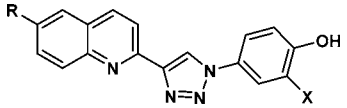

3 (X = H), **4** (X = F)

Received: November 8, 2016
Accepted: December 1, 2016
Published: December 1, 2016

DOI: 10.1021/acsmedchemlett.6b00451
ACS Med. Chem. Lett. 2017, 8, 124−127

crystal structures for **3a** and the R = methoxyethoxy (MOEO) analogue **3d** (Figure 1). The binding site is again seen to include

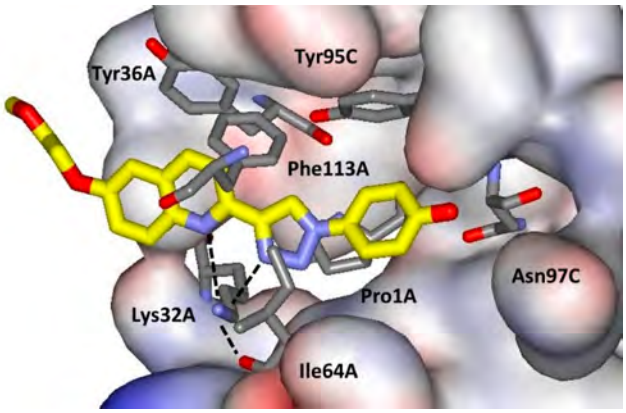

Figure 1. Rendering from the 1.8-Å crystal structure of **3d** bound to MIF (PDB ID: 4WRB).[9] Carbon atoms of **3d** are colored yellow. Some residues in front of the ligand have been removed for clarity. Coordination of Lys32A is highlighted with dashed lines; the methoxyethoxy group on C6 of the quinoline is solvent-exposed.

multiple residues with aromatic and aliphatic side chains. The poor solubility of **3a** in spite of its four nitrogen atoms and hydroxyl group can be attributed to its expected near planarity,[10] which has now been confirmed by a small molecule crystal structure.[11] As illustrated in Figure 2, the nearly planar monomers are well-stacked in the crystal structure and there are also intermolecular hydrogen bonds between the quinoline nitrogen atoms and phenolic hydroxyl groups (2.73 Å) in adjacent molecules (Figure 3). As expected, **3a** in isolation or in the crystal adopts a conformation with the quinoline nitrogen atom *anti* to N3 of the triazole ring to minimize lone-pair repulsion, while the conformation is *syn* in the complex with MIF to provide optimal coordination of the ammonium group of Lys32A (Figure 1).

Under the circumstances, it was decided to explore the solubility range that could be obtained by systematic variation of the substituent R in the 6-position of **3** and **4**. Two analogues of **5**[9] were also considered along with the deshydroxy compound **6**. Disruption of planarity by, e.g., addition of a substituent at C3 of

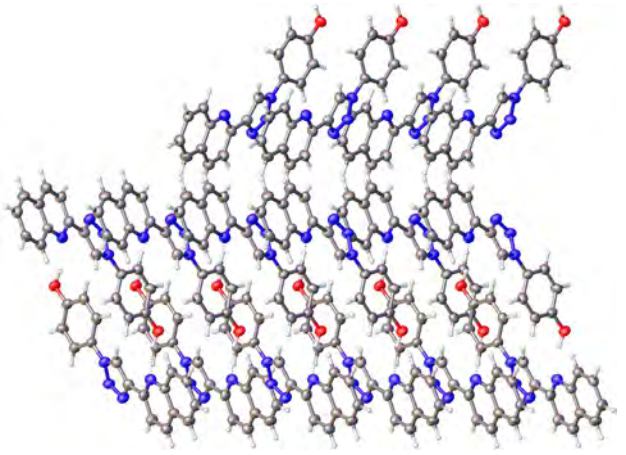

Figure 2. Illustration of the packing in the 0.84-Å crystal structure of **3a**. The space group is $Pca2_1$. The thermal ellipsoids are depicted at the 50% probability level. The CCDC ID is 1514977.

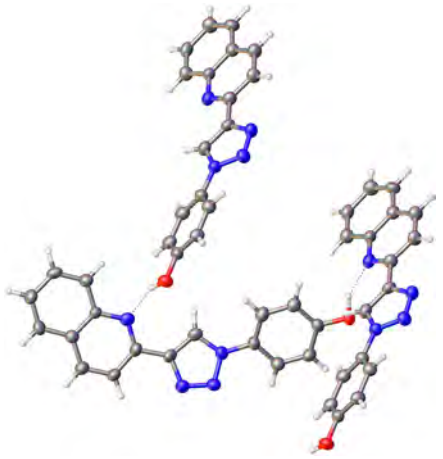

Figure 3. Close-up of the intermolecular hydrogen bonding in the crystal structure of **3a**.

the quinoline is not viable, as it is accompanied by large decreases in potency in view of the slot-like binding site (Figure 1) and coordination of Lys32.[9] In all, aqueous solubilities and inhibition constants K_i were determined for 17 analogues with 11 different substituents, as reported in Table 1. The aqueous solubilities were measured with a standard shake-flask procedure.[6,9,12] Saturated solutions are obtained by stirring for 2 days in Britton–Robinson buffer (pH 6.5), followed by filtration (Acrodisc syringe, 0.2 μm pore) and UV–vis analysis (Agilent 8453). Piroxicam has been used as a control more than 10 times, yielding $S = 6.5 \pm 1.7$ μg/mL, which is consistent with a reference value of 6.36 ± 0.04 μg/mL.[12] The inhibition constants were also determined as before using 4-hydroxyphenylpyruvic acid (HPP) as the substrate.[9,13,14] Inhibitory activity is monitored by measuring formation of the borate complex of the enol product at 305 nm using a Tecan Infinite F500 plate reader. Nine of the 17 inhibitors have been reported previously;[9,13] the synthetic and spectroscopic details for the new compounds (**3b**, **3c**, **3e**, **3f**, **3i**, **4c**, **4e**, **6**) are provided in the Supporting Information.

As reflected in Table 1, to improve solubility, we favor substituents that contain alkyleneoxy linkages with hydroxy, amino, and carboxylic acid termini. Amide and ester components are viewed as less desirable for drug prospects, owing to their potential decomposition by proteolytic enzymes. All compounds showed solubility gains over the parent **3a**. Among the smallest substituents, the benefits for the hydroxyethoxy and amino-ethoxy analogues **3b** and **3c** were modest, while the carboxymethoxy analogue **3i** provided a striking solubility boost to 365 μg/mL.

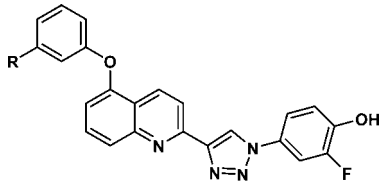

5

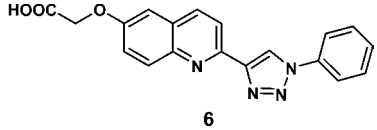

6

Though it worked well in the present cases, in general, the impact of addition of substituents with a carboxylic acid is uncertain,

DOI: 10.1021/acsmedchemlett.6b00451
ACS Med. Chem. Lett. 2017, 8, 124–127

Table 1. Computed Octanol/Water log P's, Experimental Aqueous Solubility at pH 6.5 (S in μg/mL), and K_i (μM)

Cp	R	ClogP	QP[a]	S	K_i
3a	H	3.80	3.32	2.2	0.23
3b	$HOCH_2CH_2O$	3.22	2.88	2.6	0.53
3c[b]	$H_2NCH_2CH_2O$	3.29	2.12	3.7	0.26
3d	$H_3COCH_2CH_2O$	3.98	3.49	3.6	0.20
3e	$H_3CO(CH_2CH_2O)_2$	3.85	3.81	2.4	0.147
3f	2-THP-CH_2O	4.89	4.07	3.4	0.27
3g[b]	$H_2N(CH_2CH_2O)_2$	3.36	2.43	13.9	0.36
3h[c]	4-Mr$(CH_2CH_2O)_2$	4.24	2.82	48.5	0.161
3i	$HOOCCH_2O$	3.04	2.64	365	0.20
4a[b]	$H_2N(CH_2CH_2O)_2$	3.35	2.77	9.1	0.144
4b	4-Mr$(CH_2CH_2O)_2$	4.24	3.16	27.2	0.074
4c	$HOOCCH_2O$	3.38	2.98	37.0	0.048
4d	$HOOC(CH_2)_3O$	4.06	3.90	19.2	0.039
4e	$HOOCCH_2OCH_2CH_2O$	3.63	3.30	867	0.037
5a	$H_3COCH_2CH_2O$	5.70	5.54	6.1	0.024
5b	HOOC	5.64	4.70	47.2	0.014
6[d]	$HOOCCH_2O$	2.48	3.32	1046	1.37
7[e]					27.3

[a]QPlogP. [b]TFA salt. [c]Mr = morpholinyl. [d]des-Hydroxy analogue of **3i**. [e](*R*)-ISO-1.

since carboxylic acids often form hydrogen-bonded dimers in their crystals.[4,15] The purely ether-containing substituents in **3d**, **3e**, and **3f** also just gave modest improvements for the solubility, and it is notable that addition of a second ethyleneoxy unit in going from **3d** to **3e** was not helpful. However, significant gains were found with amino-containing substituents in **3g** and **3h**.[16] It is well-known that introduction of morpholine and related heterocycles is normally successful in improving aqueous solubility.[5,7] The groups are expected to be protonated at physiological pH, which benefits hydration, and their saturated, nonplanar character eschews tight crystal packing.

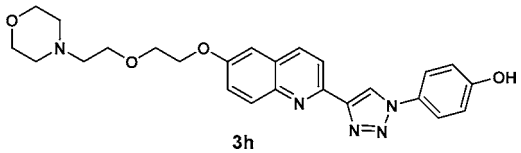

3h

Turning to **4a**–**4e**, addition of the fluorine atom adjacent to the phenolic hydroxyl group reduces solubility by factors of ca. 2–10 for the matched pairs **4a** and **3g**, **4b** and **3h**, and **4c** and **3i**. This is the typical direction in view of the increase in hydrophobicity, except in special cases where the fluorine is 2 or 3 carbon atoms removed from an oxygen.[5,17] Lengthening the linker by two methylene units in going from **4c** to **4d** reduced the solubility from 37 to 19 μg/mL; however, addition of an ethyleneoxy group in progressing to **4e** was very beneficial, yielding a 23-fold boost to 867 μg/mL. For **5a** and **5b**, the improvements with a carboxylic acid group are again apparent. Then, with **6**, removal of the intermolecular hydrogen bond in the crystal was tested; the result of 1046 μg/mL reflects a 3-fold increase over the solubility of **3i**.

In Table 1, computed octanol/water partition coefficients, ClogP and QPlogP, have been included as determined by ChemDraw and QikProp.[18,19] These are of interest as a measure of hydrophobicity and since log P and log S values are known to be correlated. The solubility equation of Yalkowsky estimates log S = 0.5 − log P − 0.01(t_m −25), where t_m is the melting point,[2,5,20] and a simpler relationship is log S = −log P − 0.2 with an rms error of 1.0 log unit.[9] Thus, log S does decrease linearly with increasing hydrophobicity, as represented by log P, but much quantitative uncertainty is associated with the crystalline state, as reflected in t_m and other terms that have been introduced to represent it in predictive methods.[2] The log P predictions with the present methods are in generally good accord with an average difference of 0.62, though the discrepancies for **3c**, **3h**, and **4b** are greater than 1 log unit. Presently, log P is not found to be a good predictor of log S. For **3a**–**3e**, the log P values would suggest solubilities in the 10^{-3} to 10^{-4} M range, while the observed values are closer to 10^{-5} M, owing presumably to the π-stacking in the crystals (Figure 2). Differences in log P are also not a good gauge of differences in log S for the present compounds. For example, **5a** might be expected to be 100-fold less soluble than **3d** based on log P, but it is more soluble; similarly, the enhanced solubility of **4e** is not reflected in its log P.

Concerning the Yalkowsky equation, routine measurement of melting points is not common today in drug discovery settings. However, we did measure the melting points of several of the compounds. They are 200–205 °C for **3d**, 268–270 °C for **4d**, and 230–235 °C for **4e**. Application of the Yalkowsky equation using the average of the two log P values in Table 1 then yields predicted log S values of −5.0, −5.9, and −5.0 for the three compounds, respectively, which translate to 3.5, 0.5, and 3.9 μg/mL. Thus, compared to the experimental solubilities in Table 1, the prediction for **3d** is accurate, but the enhanced solubilities for **4d** and **4e** are completely missed. Even differences in solubility are difficult to predict, and, if solubility is an important issue, there is no alternative but to measure it.

Finally, for the K_i results, the tautomerase assay was repeated for all of the listed compounds in this report in order to limit variations from the protein preparation, incubation times, and spectrometer.[13] For **3a**–**3i**, the activities are mostly in a narrow range of 0.2–0.4 μM, which is expected since the structural variations are only for the solvent-exposed substituent; additional modulation may come from interactions with residues on the surface of MIF. For example, the greater potency for **3e** may result from the $CH_3O(CH_2CH_2O)_2$ appendage curling back and making hydrophobic contacts with the rings of Pro33 and Pro34, which are in the gray area above Lys32 in Figure 1. The present K_i results for **3a**, **3g**, and **3h** also agree well with K_d values that we reported recently for these compounds from a fluorescence polarization assay.[14] As found previously,[9,14] addition of the fluorine in going from **3** to **4**, e.g., **3g** to **4a** or **3h** to **4b**, enhances the activities ca. 3-fold, owing to contact with Met101 and enhancement of the hydrogen bond between the phenolic hydroxyl group and Asn97. Modeling also suggested introduction of the phenoxy group at C5 of the quinoline fragment to pick up contacts with Tyr36,[9,14] which has yielded the most potent compounds, **5a** and **5b**. In addition, the importance of the hydrogen bond between the phenolic OH and Asn97 was confirmed by the increase in K_i to 1.37 μM for **6** from 0.20 μM for **3i**. As an additional control, the reference MIF inhibitor (*R*)-ISO-1 (**7**)[21] was also assayed; the observed K_i of 27.3 μM is similar to the prior average value of 24 μM from multiple measurements.[14]

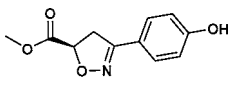

7

The principal purpose of this study was to explore systematically the effects of variations of a solvent-exposed substituent on

DOI: 10.1021/acsmedchemlett.6b00451
ACS Med. Chem. Lett. 2017, 8, 124–127

aqueous solubility in a drug-like series. The related work in the literature is largely scattered and less extensive, though the matched pair study of Zhang et al.[4] and the study of polyether and alcohol substituents by Zhu et al.[22] are particularly notable. The sequence of substituents in Table 1 may be of use to others who are faced with a similar challenge, though the quantitative outcomes will undoubtedly be different for other molecular series. However, the present and earlier results[5,7] do point to the utility of the addition of polyether chains terminated with a morpholine ring or surrogates for improving aqueous solubility. In the present case, addition of polyether chains with a carboxylic acid was also highly effective.

■ ASSOCIATED CONTENT

Supporting Information

The Supporting Information is available free of charge on the ACS Publications website at DOI: 10.1021/acsmedchemlett.6b00451.

Synthetic procedures, NMR and HRMS spectral data for all new compounds, and crystallographic details for **3a** (PDF)

Crystallographic data for **3a** (CIF)

■ AUTHOR INFORMATION

Corresponding Author

*E-mail: william.jorgensen@yale.edu.

ORCID

William L. Jorgensen: 0000-0002-3993-9520

Notes

The authors declare no competing financial interest.

■ ACKNOWLEDGMENTS

Gratitude is expressed to the National Institutes of Health (GM32136) for research support and to the National Science Foundation for a fellowship for M.J.R. (DGE-1122492).

■ ABBREVIATIONS

DCM, dichloromethane; THP, tetrahydropyran; TFA, trifluoroacetic acid

■ REFERENCES

(1) Lipinski, C. A.; Lombardo, F.; Dominy, B. W.; Feeney, P. J. Experimental and computational approaches to estimate solubility and permeability in drug discovery and development settings. *Adv. Drug Delivery Rev.* **1997**, *23*, 3−25.

(2) Jorgensen, W. L.; Duffy, E. M. Prediction of drug solubility from structure. *Adv. Drug Delivery Rev.* **2002**, *54*, 355−366.

(3) Stegemann, S.; Leveiller, F.; Franchi, D.; de Jong, H.; Lindén, H. When poor solubility becomes an issue: From early stage to proof of concept. *Eur. J. Pharm. Sci.* **2007**, *31*, 249−261.

(4) Zhang, L.; Zhu, H.; Mathiowetz, A.; Gao, H. Deep understanding of structure-solubility relationship for a diverse set of organic compounds using matched molecular pairs. *Bioorg. Med. Chem.* **2011**, *19*, 5763−5770.

(5) Walker, M. A. Improving Solubility by Structural Modification. *Top. Med. Chem.* **2013**, *9*, 69−106.

(6) Jorgensen, W. L. Computer-aided discovery of anti-HIV agents. *Bioorg. Med. Chem.* **2016**, *24*, 4768−4778.

(7) Bollini, M.; Cisneros, J. A.; Spasov, K. A.; Anderson, K. S.; Jorgensen, W. L. Optimization of diarylazines as anti-HIV agents with dramatically enhanced solubility. *Bioorg. Med. Chem. Lett.* **2013**, *23*, 5213−5216.

(8) Ishikawa, M.; Hashimoto, Y. Improvement in Aqueous Solubility in Small Molecule Drug Discovery Programs by Disruption of Molecular Planarity and Symmetry. *J. Med. Chem.* **2011**, *54*, 1539.

(9) Dziedzic, P.; Cisneros, J. A.; Robertson, M. J.; Hare, A. A.; Danford, N. E.; Baxter, R. H.; Jorgensen, W. L. Design, Synthesis, and Protein Crystallography of Biaryltriazoles as Potent Tautomerase Inhibitors of Macrophage Migration Inhibitory Factor. *J. Am. Chem. Soc.* **2015**, *137*, 2996−3003.

(10) Dahlgren, M. K.; Schyman, P.; Tirado-Rives, J.; Jorgensen, W. L. Characterization of Biaryl Torsional Energetics and its Treatment in OPLS All-Atom Force Fields. *J. Chem. Inf. Model.* **2013**, *53*, 1191−1199.

(11) Crystals of **3a** were grown via vapor diffusion with DMSO and water. A resulting crystal was diffracted under a cold nitrogen stream on a Rigaku MicroMax 007HF+ equipped with a Saturn 944+ CCD detector with Cu Kα. The structure was solved with direct methods. Heavy atoms were refined anisotropically, and hydrogen atoms were refined using a riding model. The hydrogen atom isotropic displacement parameters were fixed to the U values of the atoms to which they are linked, multiplied by 1.2. The molecules pack well with a pseudoslipped stacked morphology. The median plane formed by the triazole ring creates angles of 8.0(3)° and 23.9(4)° with the quinoline and phenol groups, respectively.

(12) Baka, E.; Comer, J. E. A; Takács-Novák, K. Study of equilibrium solubility measurement by saturation shake-flask method using hydrochlorothiazide as model compound. *J. Pharm. Biomed. Anal.* **2008**, *46*, 335−341.

(13) Cisneros, J. A.; Robertson, M. J.; Valhondo, M.; Jorgensen, W. L. Irregularities in enzyme assays: The case of macrophage migration inhibitory factor. *Bioorg. Med. Chem. Lett.* **2016**, *26*, 2764−2767.

(14) Cisneros, J. A.; Robertson, M. J.; Valhondo, M.; Jorgensen, W. L. A Fluorescence Polarization Assay for Binding to Macrophage Migration Inhibitory Factor and Crystal Structures for Two Potent Inhibitors. *J. Am. Chem. Soc.* **2016**, *138*, 8630−8638.

(15) Etter, M. C. Encoding and decoding hydrogen-bond patterns of organic compounds. *Acc. Chem. Res.* **1990**, *23*, 120−126.

(16) The primary amines **3c**, **3g**, and **4a** were prepared as their TFA salts. This resulted from use of trityl protecting groups that are removed with TFA, yielding the salts. Attempted isolation of the free amines by treatment with $NaHCO_3$ and extraction with DCM or ethyl acetate gave poor yields, owing to low solubility of the amines.

(17) Lee, W.-G.; Chan, A. H.; Spasov, K. A.; Anderson, K. S.; Jorgensen, W. L. Design, Conformation, and Crystallography of 2-Naphthyl Phenyl Ethers as Potent Anti-HIV Agents. *ACS Med. Chem. Lett.* **2016**, *7*, 0000−0000.

(18) *ChemBioDraw 12.0.2*; CambridgeSoft Inc.: Cambridge, MA, 2014.

(19) *QikProp 4.0*; Schrödinger Inc.: New York, NY, 2014.

(20) Ran, Y.; He, Y.; Yang, G.; Johnson, J. L. H.; Laskowski, S. H. Estimation of aqueous solubility of organic compounds using the general solubility equation. *Chemosphere* **2002**, *48*, 487−509.

(21) Lubetsky, J. B.; Dios, A.; Han, J.; Aljabari, B.; Ruzsicska, B.; Mitchell, R.; Lolis, E.; Al-Abed, Y. The tautomerase active site of macrophage migration inhibitory factor is a potential target for discovery of novel anti-inflammatory agents. *J. Biol. Chem.* **2002**, *277*, 24976−24982.

(22) Zhu, G.-D.; Arendsen, D. L.; Gunawardana, I. W.; Boyd, S. A.; Stewart, A. O.; Fry, D. G.; Cool, B. L.; Kifle, L.; Schaefer, V.; Meuth, J.; Marsh, K. C.; Kempf-Grote, A. J.; Kilgannon, P.; Gallatin, W. M.; Okasinski, G. F. Selective Inhibition of ICAM-1 and E-Selectin Expression in Human Endothelial Cells. 2. Aryl Modifications of 4-(Aryloxy)thieno[2,3-c]pyridines with Fine-Tuning at C-2 Substituents. *J. Med. Chem.* **2001**, *44*, 3469−3487.

DOI: 10.1021/acsmedchemlett.6b00451
ACS Med. Chem. Lett. 2017, 8, 124−127

Pathol. Oncol. Res. (2017) 23:235–244
DOI 10.1007/s12253-016-0138-6

REVIEW

Macrophage Migration Inhibitory Factor (MIF): Biological Activities and Relation with Cancer

Camila Cristina Guimarães Nobre[1] · Josélio Maria Galvão de Araújo[1] · Thales Allyrio Araújo de Medeiros Fernandes[2,3] · Ricardo Ney Oliveira Cobucci[1,4] · Daniel Carlos Ferreira Lanza[5] · Vânia Sousa Andrade[1] · José Veríssimo Fernandes[1]

Received: 1 September 2016 / Accepted: 13 October 2016 / Published online: 23 October 2016

Abstract Macrophage migration inhibitory factor (MIF) emerged in recent years as an important inflammation mediator, playing a prominent role in the pathogenesis of various types of malignant neoplasm. MIF is a glycoprotein that presents a wide spectrum of biological activities and exerts a complex interaction with various cellular signaling pathways, causing imbalance of homeostasis. Experimental and clinical studies show that high levels of MIF are found in almost all types of human cancers and are implicated in seemingly all stages of development of the tumors. The production of MIF is triggered through an autocrine signal emitted by tumor cells, and stimulates the production of cytokines, chemokines, and growth as well as angiogenic factors that lead to growth of the tumor, increasing its aggressiveness and metastatic potential. MIF is produced by virtually all types of human body cells, in response to stress caused by different factors, leading to pathological conditions such as chronic inflammation and immunomodulation with suppression of immune surveillance and of immune response against tumors, angiogenesis, and carcinogenesis. In this review, we present recent advances on the biological activity of MIF, the signaling pathways with which it is involved and their role in tumorigenesis.

Keywords Macrophage migration inhibitory factor · Neoplasms · Tumorigenesis · Inflammation

✉ Thales Allyrio Araújo de Medeiros Fernandes
thalesallyrio@yahoo.com.br

✉ José Veríssimo Fernandes
veris@cb.ufrn.br

[1] Postgraduate Program in Parasite Biology, Department of Microbiology and Parasitology, Federal University of Rio Grande do Norte, CEP, Natal, RN 59072-970, Brazil

[2] Department of Biomedical Sciences, University of Rio Grande do Norte State, CEP, Mossoró, RN 59607-360, Brazil

[3] Postgraduate Program in Health and Society, University of Rio Grande do Norte Stat, Mossoró, RN, Brazil

[4] Department of Gynecology and Obstetrics, University Potiguar, CEP, Natal, RN 59056-00, Brazil

[5] Department of Biochemisty, Federal University of Rio Grande do Norte, CEP, Natal, RN 59072-970, Brazil

Introduction

Macrophage migration inhibitory factor (MIF) was originally identified as a product isolated from the supernatants of activated T lymphocyte culture and was characterized as a cytokine capable of inhibiting the random migration of macrophages, being one of the first to be described [1]. Currently, MIF is considered a multifunctional molecule that activates the production of inflammatory cytokines such as tumor necrosis factor-α (TNF-α), interleukin-1β (IL-1β), interleukin-6 (IL-6), and interferon (IFN-γ). Also, it acts as an immunomodulator hormone produced by the pituitary gland, induced by glucocorticoids [2–4].

MIF is constitutively expressed in a variety of cells, its tissue distribution is almost ubiquitous, and its release into the circulation seems to occur from preformed stocks and stored in the intracellular environment [5–7].

MIF may exert its biological effects on cells through different cell signaling pathways (Fig. 1).

The binding of MIF to its CD74 receptor, in the presence of a signaling complex consisting of CD44, and a tyrosine kinase, Src, mediates a cascade of events leading to phosphorylation of ERK-1/2 [8], activating various effector proteins involved in the inflammatory response [9]. MIF is also a noncognate binder of the chemokine receptors CXCR that

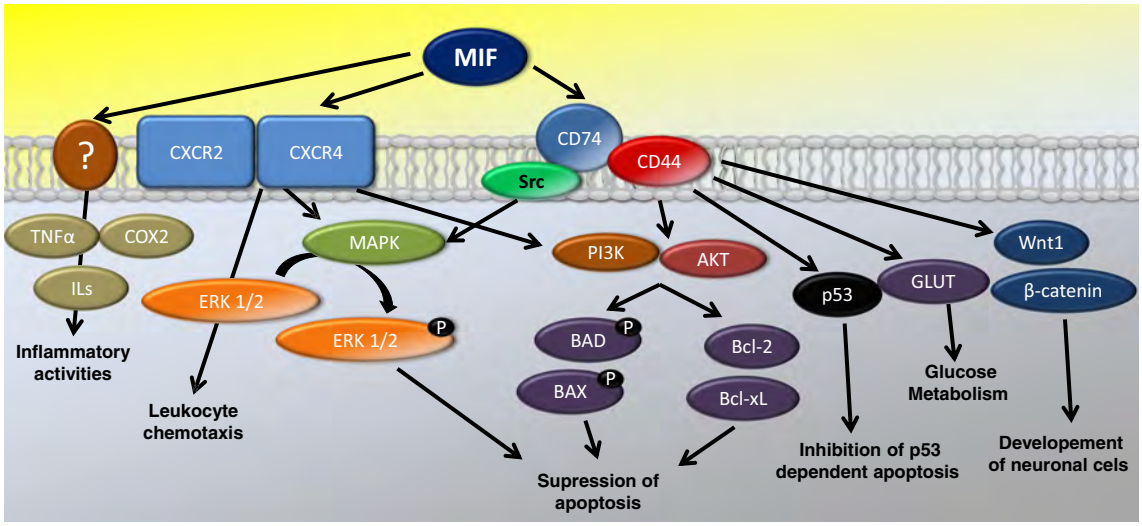

Fig. 1 Signaling patways regulated by the Macrophague Migration Inhibitory Factor (MIF). The arrows indicate the described relationships between MIF and the schematized intracellular pathways

directly binds them both, CXCR2 and CXCR4, and formation of the signaling complexes involving CXCR2 and CD74, that induces internalization of the receptors and stimulates leukocyte chemotaxis [10].

The binding of MIF to its receptor, CD74, also leads to activation of the AKT pathway through the mediation of kinases SRC and PI3K [11]. This activation leads to numerous cellular responses but, more importantly, AKT activation provides a signal, allowing the crucial cells to be capable of resisting apoptosis, due to phosphorylation and inactivation of the pro-apoptotic proteins BAD and BAX [11]. In lymphoid cells, activation of AKT induced by MIF is associated with increased NF-kB function, leading to increased expression of proteins Bcl-xL and Bcl-2 and suppression of apoptosis [12].

Previous research found that MIF is capable of activating cells of the immune system by acting directly on them or acting indirectly by generating other stimuli to the immune system. Thus, MIF is important in the activation of innate and adaptive immune responses, but also activates specific mechanisms which cause damage to the tissues. Due to its action on the immune-inflammatory response, MIF has the potential to trigger inflammatory and autoimmune diseases that affect multiple organs [13, 14].

The human MIF gene is located on chromosome 22q11.2 and encodes a highly conserved protein containing 115 amino acids. It is produced by a variety of cell types in response to stress [15], being considered a key regulator of the immune and inflammatory responses [16]. The gene expression is regulated by two polymorphic sites located in the promoter region. The first consists of a repetition CATT in −794 positions, which is represented 5–8 times, and the second is a single nucleotide polymorphism -173G/C [9]. The presence of more than 5 repeat of CATT, and of allele -173C, has been associated with increased susceptibility to and severity of a variety of inflammatory and autoimmune diseases [17–19]. It has also been associated with increased risk for prostate cancer [20] and gastric cancer [21].

MIF is also associated with the development of various types of inflammatory, lymphoproliferative, and autoimmune disorders [22] and is expressed in almost all stages of development of a wide variety of human cancers [23]. Furthermore, it may have a multifunctional role in human cancer since it exerts auto- and paracrine effects on cancer cells, promoting cell proliferation, growth, progression, and immune escape of tumor; inducing angiogenesis and migration of cells; and suppressing apoptosis and autophagy in tumor cells [24, 25].

The present review presents recent advances about biological activities of MIF and its participation in the activation of several cell signaling pathways, including its role in the promotion, progression, and invasion of several types of human cancers.

Biological Activities of MIF

MIF is a pluripotent and pleiotropic cytokine, which plays critical roles in inflammatory and immune responses, as well as in the development of tumors. It assists macrophages in carrying out functions such as phagocytosis, adherence, motility, and transendothelial migration. Besides, it is implicated in almost all stages of the development of neoplasia and its presence in high levels expression is a common feature of most types human cancer [23].

MIF is constitutively expressed in a variety of immune and non-immune cells such as eosinophils, neutrophils, granulocytes, and monocytes/macrophages, B and T lymphocytes, and endocrine, endothelial, epithelial, and neuronal

cells of different histogenetic origin, in response to the stress situations [7], being considered a key regulator of the immune and inflammatory responses [16]. In the nervous system, MIF is constitutively expressed in neurons within the hypothalamus, cortex, and hippocampus and has been implicated in different roles, including the modulation of nitric oxide and prostaglandin production, a stimulatory role in catecholamine metabolism, and the regulation of neuronal sensitivity to glucocorticoids [26].

MIF plays a central role in the etiology of various types of inflammatory and autoimmune disorders. It is found in high levels of expression in all stages of almost all types of human cancers, being strongly associated with the development of tumors [22]. The production of MIF, through autocrine signaling of tumor cells, stimulates the production of cytokines, chemokines (including MIF itself), and angiogenic and growth factors, whose expression is associated with inhibition of the induction of p53-dependent apoptosis and of the antitumor immune response [27, 28] . Thus, MIF contributes to cancer cell proliferation, for growth and progression of the tumor, increasing its aggressiveness and metastatic potential [23].

In addition to its role as a cytokine and chemokine, MIF also functions as a hormone, being secreted alongside ACTH, by the pituitary gland in response to stressors such as endotoxinaemia, and acts by regulating the anti-inflammatory and immunosuppressive activities of glucocorticoids, enabling the activation of the inflammatory and immune responses. Under conditions of stress, such as hypoxia and redox potential, MIF causes many changes to take place in the increased expression of genes such as those of the erythropoietin (EPO), glucose transporters (GLUT), vascular endothelial growth factor (VEGF), and matrix metalloproteinase (MMPs). All these changes are caused by up-regulation of hypoxia-inducible factor 1 (HIF-1) [9]. MIF is also implicated with an increase of expression of gene encoders of nitric oxide and cyclooxygenase-2 (COX-2) [29].

MIF also exhibits enzymatic thiol protein oxidoreductase and phenylpyruvate tautomerase activities [30]. Furthermore, it induces the production of derived myeloid cells (MDSCs) with suppressive action of T and NK cells [31], which together with tumor-associated macrophages (TAMs) lead to a strong suppression of the functions of these cells [32].

To perform its functions, MIF needs to interact with a wide variety of chemical mediators and other molecules, through a complex network of events that involve the activation of several cell signaling pathways, showing their great diversity of biological activities. Described below are some of the biological activities of MIF, which are also presented in summary form in Table 1.

Inflammatory Activities

The physiological role of MIF is to act to counterbalance the profound inhibitory effects of steroids on the inflammatory and immune responses [33]. MIF is a cytokine inducing inflammation that, when produced, stimulates the release of other cytokines, such as TNF-α, IFN-γ, IL-1β, IL-6, IL-8, and IL-12, from macrophages triggering a strong inflammatory response [3]. Glucocorticoids are endogenous anti-inflammatory steroids that are synthesized in response to stress or injury, in part to regulate inflammation. MIF has glucocorticoid-antagonist action and acts as a pituitary hormone to counteract the anti-inflammatory and immunosuppressive activity of glucocorticoids produced by the adrenal

Table 1 Biological activities of MIF and their mechanisms of action

MIF activities	Mechanisms of action
1. Inflammatory cytokine	Modulates the expression of activators of inflammation such as nitric oxide COX-2, PGE2 and TLR4, with recruitment of inflammatory cells.
2. Chemotactic chemokine	Induces rolling, adhesion of leukocytes to vessel wall, and transendothelial migration of these cells.
3. Hormone activity	Acts as a glucocorticoid-antagonist, by suppressing its anti-inflammatory effects, to regulate inflammatory and immune responses.
4. Enzymatic activity	Converts D-dopachrome in 5,6-dihydroxy-2-carboxylic acid and acts as a phenylpyruvate tautomerase, using phenylpyruvate and p-hydroxyphenylpyruvate as substrates.
5. Deregulation of the cell cycle	Prepares the cell to bypass the cell cycle arrest and the death induction by apoptosis mediated by p53.
6. Immune suppression	Suppresses the antitumor immune surveillance by inhibition of cytotoxicity of NK cells and CD8 + lymphocytes.
7. Growth and differentiation of neuronal cells	Acts by activating the signaling pathway Wnt/β-catenin, increasing the activity β-galactosidase and by promoting NSPC differentiation.
8. Tumorigenic activity	Stimulates proliferation of tumor cells and tumor growth by activation of various signaling pathways, inhibits apoptosis and immune response, and increases VEGF.
9. Angiogenesis induction	Induces secretion of pro-angiogenic factors bFGF and VEGF favoring formation of blood vessel
10. Contribution to metastasis formation	Reduces the expression of E-cadherin and increased expression of matrix metalloproteinases, favoring metastasis.

glands, which results in the activation of the inflammatory and immune response [4, 34].

MIF also acts in modulating the expression of several other pro-inflammatory molecules, including MIF itself, nitric oxide, and cyclooxygenase 2 (COX-2) [29], thus creating an inflammatory environment, which leads to a significant increase in COX-2 production, which in turn increases production of prostaglandin 2 (PGE2), which also has inflammatory activity, generating positive feedback to the inflammatory response [35]. Moreover, MIF plays a critical role in the regulation of the innate immune response, through the pattern recognition receptor modulation, such as TLR4. Activation of TLR4 results in the production of pro-inflammatory mediators, including MIF, which induces the recruitment of inflammatory cells, among them neutrophils [36].

Chemotactic Activities

Although MIF was first identified as an inhibitor of macrophage migration, subsequent studies revealed that in the presence of inflammatory mediators, it is also capable of inducing leukocyte rolling, adherence, and transmigration of these cells [36]. MIF may exert a chemokine-like function (CLF) by interacting with the chemokine receptors CXCR4 and CXCR2 to promote the recruitment of inflammatory cells. MIF triggered Gα-i-and integrin-dependent arrest and chemotaxis of monocytes and T cells, by interacting with the chemokine receptors, CXCR2 and CXCR4, to promote rapid integrin activation and calcium influx [37].

MIF acts as a chemokine, promoting the adhesion of monocytes to the vessel wall and their transendothelial migration, where every step of recruitment of these cells is carefully controlled. This immobilization of monocytes to the endothelial surface is mediated by the action of chemokines that prevents bearing these cells, where the CXCR2 chemokine receptor plays an important role in this process. The CXCR2 and their ligands CXCL1 and CXCL8 play a critical role in mobilizing and arresting monocytes to the vessel wall. However, the CXCR2 receptor is also able to interact with many binders of the CXC subfamily and with MIF, which structurally does not belong to this sub-family, but functions as a non-cognate binder to CXCR2, acting as a chemokine playing a critical role in recruiting and arresting monocytes to the vessel wall [10].

Hormone Activity

The hypothesis that MIF might be a hormone produced in stress situations has been validated in an experimental study conducted by Nishino et al., (1995) [38]. Using animal models, these authors have detected the presence of MIF within of granules found exclusively in pituitary gland cells that secrete both adrenocorticotropic hormone (ACTH) and thyroid-stimulating hormone (TSH). It was found a subset of granules containing MIF and ACTH, or MIF and TSH. The amount of MIF-pituitary present within the granules decreased significantly after endotoxemia, showing that under stress conditions, the contents of the granules are released for circulation [38]. Thus, MIF appears to be a pituitary mediator to act as an anti-glucocorticoid natural hormone, exercising its regulatory action within the immune system. MIF seems to act on the inflammatory site to neutralize the inhibitory effects of the steroid hormones on the primary immune response to be mounted to eliminate the source of infection or tissue invasion [33]. Thus, MIF is considered a pluripotent pro-inflammatory cytokine with pleiotropic functions including inhibition of migration, anchoring of the macrophages, and counteraction of the anti-inflammatory and immunosuppressive activity of glucocorticoids [39].

The traumatic spinal cord injury activates the hypothalamic-pituitary-adrenal axis, a potent neuroendocrine regulator that in conditions of stress causes a deep, systemic and sustained intraspinal inflammatory response. Together, stress hormones and inflammatory mediators affect the growth and survival of neural and non-neural cells and the neurologic recovery. Glucocorticoids are endogenous anti-inflammatory steroids, produced in response to stress or injury, partly to regulate inflammation. In this context, acting as a pituitary hormone, MIF negatively regulates steroid production, suppressing the anti-inflammatory action of these hormones produced by the adrenal glands, resulting in the worsening of the traumatic spinal cord lesions. Thus, the use of inhibitors of MIF may provide a therapeutic advantage in the treatment of these lesions [4].

Enzymatic Activity

Interestingly, it has been demonstrated that MIF has at least two distinct catalytic activities, keto-enol tautomerase and thiol-protein oxidoreductase; therefore, it has been termed a "cytokine with enzymatic properties, or cytozyme" [30, 40].

The first hypothesis about possible MIF enzyme activity emerged when Suzuki et al. (1994) [41] found the structural similarity of this molecule to the bacterial isomerase enzyme, specifically 5-carboxymethyl-2-hydroxymuconate (CHMI). However, the enzymatic activity of MIF was first described when Rosengren et al. (1996) [42] reported the tautomerase-D-dopachrome (DOPD) activity. They found that MIF has the ability to convert D-dopachrome in 5,6-dihydroxy-2-carboxylic acid (DHICA). Other studies have shown that MIF can also act as a phenylpyruvate tautomerase, using phenylpyruvate and p-hydroxyphenylpyruvate as substrates [43] and as thiol-protein oxidoreductase [44]. Furthermore, it was found that MIF is capable of catalyzing the conversion of 3,4-hydroxyphenylaminechrome and norepinefrinecromo, toxic quinine products of the neurotransmitter catecholamine

3,4-dihydroxyphenylamine and norepinephrine, to indoledihydroxy derivatives that may serve as precursors to neuromelanin [45].

In addition, it was postulated that MIF has a stake in the detoxification process of degradation products of catecholamine and may play a role in protection of nerve tissue. However, the exact role of this enzymatic activity of MIF in clinical disease has not been clearly defined, since many of the substrates defined for this enzyme do not naturally exist in vivo or do not exist in concentrations required for biological activity [46]. However, because of the great importance of MIF activity in diseases of an inflammatory nature, there is an increasing interest in the development of low molecular weight inhibitors that target this MIF enzymatic activity for use in treating inflammatory diseases [47].

Interference with the Cell Cycle

The p53 protein is the product of the TP53 tumor suppressor gene and acts as a transcription factor, regulating the expression of numerous genes, and plays a crucial role in controlling the cell cycle [48]. In normal cells, p53 remains bound to its Mdm2 inhibitor that tightly represses the p53 function, by inducing its degradation. When the incorrect base pairing occurs during the synthesis of DNA, p53 is phosphorylated and separated from Mdm2 and carries out its function, which is to stop the cell cycle and repair the DNA error. Once the repair is done, p53 is degraded and the cycle continues, leading to cell division [23].

MIF interacts with p53 in a manner dependent on the redox status and stabilizes the linkage between p53 and Mdm2, ensuring that p53 is not phosphorylated to become free and perform its function. This condition created by MIF leads to a decrease in the expression of p21 proteins, Bax and p53 itself. This negative regulation of p53 activity leads to the prevention of cell cycle arrest and inhibits cell death by apoptosis [49]. Inactivation of the p53 function can dramatically disrupt the DNA repair mechanisms, resulting in the accumulation of mutations and generating genomic instability that increases the risk of malignant transformation of the cell [50].

Suppression of the Immune Surveillance

MIF can suppress the antitumor immunity by several mechanisms. One of the most important is the inhibition of cytotoxic T lymphocyte (CTL) and natural killer (NK) cells, contributing to the escape of tumor cells of the immune surveillance [51]. Furthermore, MIF can activate the tumor cells to acquire the ability to inhibit the production of dendritic cells and to induce apoptosis of these cells. As the dendritic cells have anti-tumor action, this activity is impaired [52].

MIF can also inhibit the anti-tumor immunity by activating and increasing the production of myeloid-derived suppressor cells (MDSCs), which are highly immunosuppressive and which infiltrate the tumor [31, 32]. MDSCs use a variety of mechanisms to inhibit the function of T and NK cells, suppressing the anti-tumor immunity [53].

Moreover, MIF also promotes alternative macrophage differentiation, giving rise to tumor-associated macrophages (TAMs). As with the MDSCs, TAMs are abundant in the tumor environment and act together with MDSCs to develop immunosuppressive activity of NK and T cells [54], thus contributing to higher tumor aggressiveness [55].

Action as Growth Factor and Differentiation of Neuronal Cells

In addition to the versatile role of MIF in the immune system, it also acts as neurotrophins, a family of proteins belonging to a class of growth factors that act as regulators of survival, development, and neural cell plasticity. It has been demonstrated that MIF is widely expressed during embryonic development, particularly in the cells of the nervous system, but its role in neural development is still poorly understood [56]. However, it was found that MIF promotes the activation of proliferation and differentiation of neural stem/progenitor cells (NSPCs), which are cells with self-renewal capability and which can differentiate into multiple neuronal lineages during the development of the embryo and in the perinatal period [57]. These cells are essential for brain development and brain physiological functions. The niche where the NSPCs reside is a microenvironment that provides the conditions for the maintainability of the multipotent state of these cells, enabling their self-renewal. The components present in these niches are the source of extrinsic signals that instruct the NSPC self-renewal or differentiation and influence the decision of NSPC's fate into neuron or glia [57, 58].

MIF receptors, including CD44, CXCR2, CXCR4, and CD74, are expressed in NSPCs. This shows the potential regulatory effect of MIF on NSPCs, promoting the activation, the proliferation, and the differentiation of these neural stem/progenitor cells. It was shown that both Ki67-positive cells and neurosphere volumes were increased in a dose-dependent manner after treatment with MIF. It was also observed that, during MIF-induced NSPC differentiation, there was an increase in the activity of β-galactosidase, which responds to Wnt/β-catenin signaling, and that Wnt1 and β-catenin proteins were also up-regulated with MIF stimulation. On the other hand, doublecortin (DCX) and Tuj I, two neuronal markers, were clearly increased with MIF stimulation during NSPC differentiation. Moreover, the expression of DCX and Tuj 1 was inhibited significantly by IWR-1, the inhibitor of the Wnt/β-catenin pathway. It was also observed that the treatment with IWR-1 significantly inhibited the proliferative effect of MIF on NSPCs [57].

MIF and Cancer

Cancer is the uncontrolled proliferation of cells triggered by a suite of genetic and epigenetic events that disrupt the homeostasis of the human body. Standing out among them are the accumulation of mutations, especially of the tumor suppressor genes, conversion of proto-oncogenes to oncogenes, methylation DNA, and post-translational modifications, as well as the long-term persistent infection by certain infectious agents [14, 59]. The long-term chronic inflammation, together with disorders in immune response, has played a crucial role in process of carcinogenesis. The inflammatory milieu contributes in various stages of tumor development, including initiation, promotion, growth, and invasion, besides affecting the immune surveillance [60, 61]. Mediators such as cytokines, chemokines, PGE2, growth factors, transcription, and enzymes such as COX-2 and MAP act together to create a favorable environment for the tumor. These mediators engage in an extensive and dynamic crosstalk with cancer cells, triggering molecular events contributing to tumorigenesis [14, 61].

The association between chronic inflammation and cancer is well established, being widely accept that this condition can lead to the development and progression of tumors [27]. Studies performed since the discovery of MIF have increasingly strengthened its role in inflammation as well as in the innate and adaptive immune responses [23, 62]. In this context, because of its important role in regulation of the inflammatory and immune responses, MIF has been thought to be the link that connects inflammatory response to cancer [23].

MIF is a pro-inflammatory cytokine that is produced in the tumor environment and secreted by monocytes, macrophages, and tumor cells. Under inflammatory stimuli, cancer cells secrete growth factors and cytokines, which increase the potential for malignant transformation of cells, promote activation of tumor associated macrophages (TAMs), and interactions between stromal cells and of the tumor [63].

MIF participates in the regulation of both normal physiological and pathological conditions. Due to its pleiotropic action, MIF promotes inflammation, cell proliferation, and inhibition of cell death by apoptosis, and regulates migration, activation, differentiation and reprogramming of immune and non-immune cells. These functions are particularly important to upset homeostasis and create a microenvironment favorable to the development of cancer [64]. A remarkable overexpression of MIF was found in several types of humans cancer, including: squamous cell carcinoma of the esophagus [65], cervical cancer [66], breast [25], prostate [67], liver [68], lung [69], glioblastoma, neuroblastoma, colon and colorectal cancer [70], bladder [71], ovarian [51], endometrium [72], gastric and pancreatic [73], renal carcinomas [74], and lymphocytic leukemia B cells [75].

MIF interferes with multiple cellular signaling pathways through a complex networks of interactions. The production of MIF is activated through autocrine signaling emitted by the cancer cells, resulting in the stimulation of the production of cytokines, chemokines, and angiogenic factors, which lead to tumor growth, and the dissemination of tumor cells [16]. When binding to its receptor CD74, MIF leads to the recruitment of the hyaluronate receptor CD44, and this complex (CD74/CD44) that have been implicated in tumourigenic MIF signaling processes [76].

Currently, there is a general consensus that MIF promotes tumor growth by several mechanisms: it stimulates tumor cell proliferation by activating the MAPK/PI3K/Akt pathways, inhibits p53-dependent apoptosis, increases vascular endothelial growth factor (VEGF) production, and inhibits the antitumor immune response [27, 28, 51, 77]. Moreover, it modulates metastatic behavior of tumor cells and affects stromal tumor cells [78].

Angiogenesis is a complex process involving a series of cellular factors for the formation of new blood vessels [9]. Among the mediators involved in this process, the following stand out: the basic fibroblast growth factor (bFGF), VEGF, hypoxia inducible factor 1 (HIF-1), and angiopoetin, which are necessary for the formation of new blood vessels [9, 79]. Under conditions of stress and hypoxia, endothelial precursor cells secrete bFGF, VEGF, and other pro-angiogenic factors necessary for the formation of blood vessels [80]. The condition of hypoxia causes upregulation of HIF-1, which leads to increased expression of VEGF, bFGF, and angiopoetin. Furthermore, HIF-1 also induces the production of MIF, which, in turn, plays a key role in tumor angiogenesis [79]. It has been shown that MIF induces dose-dependent secretion of bFGF, VEGF, and IL-8 [81].

The overexpression of MIF also reduces the expression of e-cadherin [82], which is responsible for the formation of focal adhesion complex, maintaining the cells contact with each other and with the basal membrane. The decreasing of e-cadherin expression weakens the focal adhesion complex, leading to epithelial mesenchymal transition [23]. In the tumor environment are found high levels of MIF expression and other angiogenic factors, which result in an increase in expression of matrix metalloproteases (MMPs). These enzymes degrade the basement membrane, leading tumor cells to enter the bloodstream, and when they receive appropriate homing factors, they establish secondary tumors in different organs [23].

In cervical cancer a correlation was observed between the levels of MIF expression and histological grading of precursor lesions of cervical cancer of the invasive form, supporting the idea that MIF has effects in promoting tumor [24]. Also observed was a trend of increased MIF expression and of its receptor CD74 in normal cervical epithelium, cervical intraepithelial neoplasia (CIN), and squamous cell carcinoma (SCC). Besides, the expression MIF was correlated with microvessel density, inducing a dose-dependent increase in the VEGF secretion in cervical cancer cells. This suggests that over-expression of MIF and CD74 may be associated with

pathogenesis and angiogenesis in cervical cancer [66]. In prostate cancer, high expression of MIF and low expression of CD74 were detected [83]. Detected in cancers of lung and breast were high expression levels of MIF and a smaller and less uniform expression of CD74, mainly in the stromal compartment [84, 85]. In esophageal cancer and in the hepatocellular carcinoma (HCC), the over-expression of MIF has been correlated with a loss of cell differentiation and lymph node metastases. It is believed that by acting as an autocrine factor, MIF increases VEGF secretion, which promotes angiogenesis, tumor growth, and migration of tumor cells [65, 68].

Evidence indicates that MIF has a dual role in breast cancer. When it is found within the tumor cells, it may be indicative of a favorable prognosis. However, when found in an extracellular location in the tissue derived from the breast cancer, MIF may be pro-inflammatory and probably constitutes an unfavorable prognostic marker [63]. The presence of a significant increase in mean serum MIF levels has been reported in patients with breast cancer, compared to healthy women. In view of its autocrine and paracrine effects on cancer cells, MIF may contribute to shaping the microenvironment, leading to immunomodulation and angiogenesis [85].

The highly aggressive tumors attract cells of innate and adaptive immune responses to suppress anti-tumor immunity mediated by lymphocytes. Most of this immunosuppressive activity in patients in the final stage of melanoma is due to the action of a subpopulation of derived myeloid cells (MDSCs) of the monocytic subset, whose production is MIF-induced. These cells are producers of nitric oxide [86], prostaglandin, and express receptors for these lipid mediators [87], and are able to suppress both Ag-specific and nonspecific T cell proliferation [88]. An in vitro study on circulating MDSCs, isolated from melanoma patients in late-stage, showed that the immunosuppressive activity of these cells is MIF-dependent for suppression of antigen-independent T-cell activation and that MIF is required for maximum production of reactive oxygen species by these cells. Furthermore, inhibition of MIF resulted in functional reversal of T lymphocytes from the neutralization of the immunosuppressive activity of MDSCs, by action of an immunostimulatory dendritic cell (DC)-like phenotype that is, at least partly, due to reduced production of prostaglandin E2 (PGE2) by MDSC. These results indicate that MIF is directly involved in the induction of the immunosuppressive function of monocytic MDSCs in humans and that the therapeutic approach having MIF as the target may provide a novel means of inducing DC-mediated antitumor responses in late-stage melanoma patients [32].

The ability of NK and TCD8+ cells to eliminate malignant cells depends on the recognition of stress- or transformation-induced molecules that bind to receptor NK group 2D (NKG2D; 4) to activate NK and TCD8+ cells [89, 90]. Standing out among these molecules are the class I MHC components, MICA/B, and 1–4 ULBP, which are induced by DNA damage [89] and are found in cells infected by viruses and tumor cells [91]. When such molecules bind to the NKG2D receptor, this leads to the activation of the adaptor protein DAP10, which signals and initiates a perforin-mediated cytolytic response, which can lead to NK cell-mediated tumor clearance, without prior activation or Ag-specific tumor cell recognition [91]. It has been shown in studies in vitro and in vivo, that MIF contributes functionally to the immune escape of the ovarian carcinoma and malignant gliomas, through down-regulation of expression of NKG2D, which reduces the cytotoxic activity of NK and T-cells, suppressing the cellular immune response against the tumor cells [51, 90]. Additionally, it was reported that MIF increases the amount of MDSCs in the circulating blood of patients with a variety of tumors and acts by a variety of mechanisms to prevent the functions of NK and T-cells, suppressing the anti-tumor immunity [31]. It was further shown that in prostate cancer, the cancerous cells activated by MIF acquire the ability to kill dendritic cells by apoptosis and inhibits their production, thus avoiding the antitumor activity of these cells [52].

A study by Tanese et al. (2015) [92] showed that in cell lines derived from melanoma, MIF can reverse the IFN-γ role in immune surveillance against tumors, since IFN-γ increases the expression of the MIF receptor, the CD74 protein, in cell lines melanoma-derived. MIF interacts with its CD74 receptor on the surface of these cells, which results in signaling pathway activation of the P13K / AKT pathway and promotes the survival of tumor cells. IFN-γ promotes the phosphorylation of AKT Ser473, resulting in increased expression of protumorigenic factors such as IL-6, IL-8, and BCL2 in cell lines derived from human melanoma. The correlation between plasma levels of IFN-γ and MIF receptor expression in tumor cells has been found in samples from patients with melanoma. Furthermore, inhibition of MIF-CD74 interaction significantly suppressed tumor growth in the presence of IFN-γ in the mouse model [92].

A case-control study conducted by Wu et al. (2011) [93], involving Chinese women of the Shanxi province with and without cervical cancer, demonstrated a functional association between the single nucleotide polymorphism in the MIF gene (MIF-173) allele 173G/C and metastasis in the early stage of cervical cancer. These authors reported that women with the C variant of the MIF-173 allele had a significantly higher risk for cervical cancer, compared to carriers of the wild-type allele GG, and that the GC and CC genotypes behaved as risk factors for cervical cancer in the studied population. Individuals with the GC + CC genotype and C allele at the MIF-173G/C site were at a significantly higher risk of cervical cancer and lymphatic metastasis. The risk of lymph node metastases in the early stages of cervical cancer has increased by more than 1.6 times in patients with GC or CC genotype compared to those with the GG genotype. Also, a positive association was observed between high serum concentrations of MIF and

occurrence of early metastasis. In addition, patients with the CC genotype had higher MIF serum levels, indicating that this genotype increases the risk of lymphatic metastasis in women with early-stage cervical cancer. These results suggest that the MIF-173 polymorphism may be associated with increased risk of cervical cancer in women and that the quantification of MIF serum levels and genotyping of patients could be used as biomarkers of prognosis and for early treatment of the cervical cancer [93]. On the other hand, in a meta-analysis study, it was found that the polymorphism of the MIF gene -173G / C can increase the risk of cancer among Asians but not among Caucasians. The heterozygous mutational genotype CG could increase the risk of gastrointestinal cancer and hematological malignancy, while the homozygote genotype CC might increase susceptibility to gynecological cancer, as compared with the genotype wild type GG [19].

Several studies also show that MIF plays an important role in cancer development, in virtue of its ability to act in conjunction with other mediators to interfere in many cellular signaling pathways, creating a favorable environment for the tumor. Those conditions include the inflammation, cell proliferation, deregulation of the cell cycle, inhibition of apoptosis, suppression of immune surveillance against tumors, angiogenesis, and metastasis [23, 51].

In conclusion, MIF is a protein with pleiotropic action produced by virtually all cell types, presenting a variety of biological effects on the human body, participating in a complex chain of events that, together, favors the process of carcinogenesis. Experimental and clinical studies suggest that MIF could have a multifunctional role in the development of several human cancer types. Evidence shows that MIF exercises autocrine and paracrine effects on cancer cells, promoting the proliferation and migration of these cells, and inhibits apoptosis and autophagy. It also contributes to shaping a tumor microenvironment by acting on immune and non-immune cells, leading to immunomodulation. Thus, the necessary conditions are created for proliferation of cancer cells, resulting in growth, promotion, and tumor invasion. Additionally, MIF acts systemically to influence a complex network of cellular signaling pathways, leading to an imbalance of homeostasis and causing metabolic disorders such as metabolic syndrome and its potential negative implications on the immune system, which contribute to tumor growth and the development of metastases.

References

1. Bloom BR, Bennett B (1966) Mechanism of a reaction in vitro associated with delayed-type hypersensitivity. Science 153(731): 80–82
2. Takahashi N, Nishihira J, Sato Y et al (1998) Involvement of macrophage migration inhibitory factor (MIF) in the mechanism of tumor cell growth. Mol Med 4(11):707–714
3. Onodera S, Nishihira J, Koyama Y et al (2004) Macrophage migration inhibitory factor up-regulates the expression of interleukin-8 messenger RNA in synovial fibroblasts of rheumatoid arthritis patients: common transcriptional regulatory mechanism between interleukin-8 and interleukin-1beta. Arthritis Rheum 50(5):1437–1447
4. Lerch JK, Puga DA, Bloom O, Popovich PG (2014) Glucocorticoids and macrophage migration inhibitory factor (MIF) are neuroendocrine modulators of inflammation and neuropathic pain after spinal cord injury. Semin Immunol 26(5):409–414
5. Bernhagen J, Calandra T, Bucala R (1998) Regulation of the immune response by macrophage migration inhibitory factor: biological and structural features. J Mol Med 76(3–4):151–161
6. Benigni F, Atsumi T, Calandra T et al (2000) The proinflammatory mediator macrophage migration inhibitory factor induces glucose catabolism in muscle. J Clin Invest 106(10):1291–1300
7. Lolis E, Bucala R (2003) Macrophage migration inhibitory factor. Expert Opin Ther Targets 7:153–164
8. Shi X, Leng L, Wang T et al (2006) CD44 is the signaling component of the macrophage migration inhibitory factor-CD74 receptor complex. Immunity 25(4):595–606
9. Bifulco C, McDaniel K, Leng L, Bucala R (2008) Tumor growth-promoting properties of macrophage migration inhibitory factor. Curr Pharm Des 14(36):3790–3801
10. Tillmann S, Bernhagen J, Noels H (2013) Arrest functions of the MIF ligand/ receptor axes in atherogenesis. Front Immunol 4:115. doi:10.3389/fimmu.2013.00115
11. Lue H, Thiele M, Franz J et al (2007) Macrophage migration inhibitory factor (MIF) promotes cell survival by activation of the Akt pathway and role for CSN5/JAB1 in the control of autocrine MIF activity. Oncogene 26(35):5046–5059
12. Binsky I, Haran M, Starlets D et al (2007) IL-8 secreted in a macrophage migration-inhibitory factor- and CD74-dependent manner regulates B cell chronic lymphocytic leukemia survival. Proc Natl Acad Sci U S A 104(33):13408–13413
13. Hoi AY, Iskander MN, Morand EF (2007) Macrophage migration inhibitory factor: a therapeutic target across inflammatory diseases. Inflamm Allergy Drug Targets 6(3):183–190
14. Elinav E, Nowarski R, Thaiss CA, Hu B, Jin C, Flavell RA (2013) Inflammation-induced cancer: crosstalk between tumours, immune cells and microorganisms. Nat Rev Cancer 13(11):759–771
15. Bernhagen J, Calandra T, Mitchell RA et al (1993) MIF is a pituitary-derived cytokine that potentiates lethal endotoxaemia. Nature 365(6448):756–759
16. Hagemann T, Robinson SC, Thompson RG, Charles K, Kulbe H, Balkwill FR (2007) Ovarian cancer cell-derived migration inhibitory factor enhances tumor growth, progression, and angiogenesis. Mol Cancer Ther 6(7):1993–2002
17. Wu S-P, Leng L, Feng Z et al (2006) Macrophage migration inhibitory factor promoter polymorphisms and the clinical expression of scleroderma. Arthritis Rheum 54(11):3661–3669
18. Dambacher J, Staudinger T, Seiderer J et al (2007) Macrophage migration inhibitory factor (MIF) −173G/C promoter polymorphism influences upper gastrointestinal tract involvement and disease activity in patients with Crohn's disease. Inflamm Bowel Dis 13(1):71–82
19. Tong X, Zheng B, Tong Q et al (2015) The MIF -173G/C gene polymorphism increase gastrointestinal cancer and hematological malignancy risk : evidence from a meta-analysis and FPRP test. Int J Clin Exp Med 8(9):15949–15957
20. Meyer-Siegler KL, Vera PL et al (2007) Macrophage migration inhibitory factor (MIF) gene polymorphisms are associated with increased prostate cancer incidence. Genes Immun 8(8):646–652
21. Arisawa T, Tahara T, Shibata T et al (2008) Functional promoter polymorphisms of the macrophage migration inhibitory factor gene in gastric carcinogenesis. Oncol Rep 19(1):223–228

22. Grieb G, Merk M, Berhagen J, Bucala R (2010) Macrophage migration inhibitory factor (MIF): a promising biomarker. Drug News Perspect 23(4):257–264
23. Babu SN, Chetal G, Kumar S (2012) Macrophage migration inhibitory factor: a potential marker for cancer diagnosis and therapy. Asian Pac J Cancer Prev 13(5):1737–1744
24. Krockenberger M, Engel JB, Kolb J et al (2010) Macrophage migration inhibitory factor expression in cervical cancer. J Cancer Res Clin Oncol 136(5):651–657
25. Richard V, Kindt N, Saussez S (2015) Macrophage migration inhibitory factor involvement in breast cancer (review). Int J Oncol 47(5):1627–1633
26. Fingerle-Rowson GR, Bucala R (2001) Neuroendocrine properties of macrophage migration inhibitory factor (MIF). Immunol Cell Biol 79(4):368–375
27. Conroy H, Mawhinney L, Donnelly SC (2010) Inflammation and cancer: macrophage migration inhibitory factor (MIF)–the potential missing link. QJM 103(11):831–836
28. Rendon BE, Willer SS, Zundel W, Mitchell RA (2009) Mechanisms of macrophage migration inhibitory factor (MIF)-dependent tumor microenvironmental adaptation. Exp Mol Pathol 86(3):180–185
29. Rosado JDD, Rodriguez-Sosa M (2011) Macrophage migration inhibitory factor (MIF): a key player in protozoan infections. Int J Biol Sci 7(9):1239–1256
30. Lehmann LE, Weber SU, Fuchs D et al (2008) Oxidoreductase macrophage migration inhibitory factor is simultaneously increased in leukocyte subsets of patients with severe sepsis. Biofactors 33(4): 281–291
31. Simpson KD, Templeton DJ, Cross JV (2012) Macrophage migration inhibitory factor promotes tumor growth and metastasis by inducing myeloid-derived suppressor cells in the tumor microenvironment. J Immunol 189(12):5533–5540
32. Yaddanapudi K, Rendon BE, Lamont G et al (2016) MIF is necessary for late-stage melanoma patient MDSC immune suppression and differentiation. Cancer Immunol Res 4(2):101–112
33. Bucala R (1996) MIF rediscovered : cytokine, pituitary hormone, and glucocorticoid-induced regulator of the immune response. FASEB J 10(14):1607–1613
34. Fingerle-Rowson G, Koch P, Bikoff R et al (2003) Regulation of macrophage migration inhibitory factor expression by glucocorticoids in vivo. Am J Pathol 162(1):47–56
35. Mawhinney L, Armstrong ME, O′ Reilly C, et al (2015) Macrophage migration inhibitory factor (MIF) enzymatic activity and lung cancer. Mol Med 20:729–735.
36. Gregory JL, Leech MT, David JR, Yang YH, Dacumos A, Hickey MJ (2004) Reduced leukocyte-endothelial cell interactions in the inflamed microcirculation of macrophage migration inhibitory factor-deficient mice. Arthritis Rheum 50(9):3023–3034
37. Bernhagen J, Krohn R, Lue H et al (2007) MIF is a noncognate ligand of CXC chemokine receptors in inflammatory and atherogenic cell recruitment. Nat Med 13(5):587–596
38. Nishino T, Bernhagen J, Shiiki H, Calandra T, Dohi K, Bucala R (1995) Localization of macrophage migration inhibitory factor (MIF) to secretory granules within the corticotrophic and thyrotrophic cells of the pituitary gland. Mol Med 1(7):781–788
39. Bando H, Matsumoto G, Bando M et al (2002) Expression of macrophage migration inhibitory factor in human breast cancer: association with nodal spread. Jpn J Cancer Res 93(4):389–396
40. Lue H, Kleemann R, Calandra T et al (2002) Macrophage migration inhibitory factor (MIF): mechanisms of action and role in disease. Microbes Infect 4(4):449–460
41. Suzuki M, Murata K, Tanaka E, Nishihira J, Sakai M (1994) Crystallization and a preliminar X-ray diffraction study of macrophage migration inhibitory factor from human lymphocytes. J Mol Biol 235(3):1141–1143
42. Rosengren E, Bucala R, Aman P et al (1996) The immunoregulatory mediator macrophage migration inhibitory factor (MIF) catalyzes a tautomerization reaction. Mol Med 2(1):143–149
43. Rosengren E, Åman P, Thelin S et al (1997) The macrophage migration inhibitory factor MIF is a phenylpyruvate tautomerase. FEBS Lett 417(1):85–88
44. Kleemann R, Kapurniotu A, Frank RW et al (1998) Disulfide analysis reveals a role for macrophage migration inhibitory factor (MIF) as thiol-protein oxidoreductase. J Mol Biol 280(1):85–102
45. Matsunaga J, Sinha D, Solano F, Santis C, Wistow G, Hearing V et al (1999) Macrophage migration inhibitory factor (MIF)–its role in catecholamine metabolism. Cell Mol Biol (Noisy-le-grand) 45(7):1035–1040
46. El-turk F, Cascella M, Ouertatani-sakouhi H et al (2008) The conformational flexibility of the carboxy terminal residues 105 − 114 is a key modulator of the catalytic activity and stability of macrophage migration inhibitory factor. Biochemistry 47(40):10740–10756
47. Cooke G, Armstrong ME, Donnelly SC (2009) Macrophage migration inhibitory factor (MIF), enzymatic activity and the inflammatory response. Biofactors 35(2):165–168
48. Vousden KH, Lane DP (2007) P53 in health and disease. Nat Rev Mol Cell Biol 8(4):275–283
49. Jung H, Seong HA, Ha H (2008) Critical role of cysteine residue 81 of macrophage migration inhibitory factor (MIF) in MIF-induced inhibition of p53 activity. J Biol Chem 283(29):20383–20396
50. Hanel W, Moll UM (2012) Links between mutant p53 and genomic instability. J Cell Biochem 113(2):433–439
51. Krockenberger M, Dombrowski Y, Weidler C et al (2008) Macrophage migration inhibitory factor contributes to the immune escape of ovarian cancer by down-regulating NKG2D. J Immunol 180(11):7338–7348
52. Nakaya K, Nabata Y, Ichiyanagi T, An WW (2012) Stimulation of dendritic cell maturation and induction of apoptosis in leukemia cells by a heat-stable extract from azuki bean (*Vigna angularis*), a promising immunopotentiating food and dietary supplement for cancer prevention. Asian Pac J Cancer Prev 13(2):607–611
53. Youn JI, Nagaraj S, Collazo M, Gabrilovich DI (2008) Subsets of myeloid-derived suppressor cells in tumor-bearing mice. J Immunol 181(8):5791–5802
54. Yaddanapudi K, Putty K, Rendon BE, et al (2013) Control of tumor-associated macrophage alternative activation by macrophage migration inhibitory factor. J Immunol190(6):2984–2993.
55. Guo C, Buranych A, Sarkar D, Fisher PB, Wang XY (2013) The role of tumor-associated macrophages in tumor vascularization. Vasc Cell 5:20. doi:10.1186/2045-824X-5-20
56. Shen YC, Thompson DL, Kuah MK et al (2012) The cytokine macrophage migration inhibitory factor (MIF) acts as a neurotrophin in the developing inner ear of the zebrafish, *Danio rerio*. Dev Biol 363(1):84–94
57. Zhang X, Chen L, Wang Y et al (2013) Macrophage migration inhibitory factor promotes proliferation and neuronal differentiation of neural stem/precursor cells through Wnt/β-catenin signal pathway. Int J Biol Sci 9(10):1108–1120
58. Massirer KB, Carromeu C, Griesi-Oliveira K, Muotri AR (2011) Maintenance and differentiation of neural stem cells. Wiley Interdiscip Rev Syst Biol Med 3(1):107–114
59. Fernandes JV, Fernandes TAAM, Azevedo JCV et al (2015) Link between chronic inflammation and human papillomavirus-induced carcinogenesis (review). Oncol Lett 9(3):1015–1026
60. Landskron G, De La Fuente M, Thuwajit P et al (2014) Chronic inflammation and cytokines in the tumor microenvironment. J Immunol Res 2014:149185. doi:10.1155/2014/149185
61. Fernandes JV, Cobucci RNO, Jatoba CAN, Fernandes TA, Azevedo JW, Araújo JM (2015) The role of the mediators of inflammation in cancer development. Pathol Oncol Res 21(3):527–534

62. Santos LL, Morand EF (2006) The role of macrophage migration inhibitory factor in the inflammatory immune response and rheumatoid arthritis. Wien Med Wochenschr 156(1–2):11–18
63. Verjans E, Noetzel E, Bektas N et al (2009) Dual role of macrophage migration inhibitory factor (MIF) in human breast cancer. BMC Cancer 9:230. doi:10.1186/1471-2407-9-230
64. Gordon-Weeks AN, Lim SY, Yuzhalin AE, Jones K, Muschel R (2015) Macrophage migration inhibitory factor : a key cytokine and therapeutic target in colon cancer. Cytokine Growth Factor Rev 26(4):451–461
65. Ren Y, Law S, Huang X, Lee PY, Bacher M, Srivastava G, Wong J (2005) Macrophage migration inhibitory factor stimulates angiogenic factor expression and correlates with differentiation and lymph node status in patients with esophageal squamous cell carcinoma. Ann Surg 242(1):55–63
66. Cheng RJ, Deng WG, Niu CB, Li YY, Fu Y (2011) Expression of macrophage migration inhibitory factor and CD74 in cervical squamous cell carcinoma. Int J Gynecol Cancer 21(6):1004–1012
67. Tang W, Gou X, Liu Q (2011) Expression of macrophage migration inhibition factor (MIF) in serum of patients with prostate cancer and its clinical significance. Xi Bao Yu Fen Zi Mian Yi Xue Za Zhi 27(1):97–98
68. Ren Y, Tsui HT, Poon RT et al (2003) Macrophage migration inhibitory fator – roles in regulating tumor cell migration and expression. Of angiogenic factors in hepatocellular carcinoma. Int J Cancer 107(1):22–29
69. White ES, Flaherty KR, Carskadon S et al (2003) Macrophage migration inhibitory factor and CXC chemokine expression in non-small cell lung cancer: role in angiogenesis and prognosis. Clin Cancer Res 9(2):853–860
70. Ren Y, Chan HM, Fan J et al (2006) Inhibition of tumor growth and metastasis in vitro and in vivo by targeting macrophage migration inhibitory factor in human neuroblastoma. Oncogene 25(25):3501–3508
71. Guo YS, Dai YP, Li W et al (2011) Expression and significance of macrophage migration inhibitory factor in bladder urothelial cell carcinoma. Zhonghua Zhong Liu Za Zhi 33(1):28–31
72. Bondza PK, Metz CN, Akoum A (2008) Macrophage migration inhibitory factor up-regulates alpha(v)beta(3) integrin and vascular endothelial growth factor expression in endometrial adenocarcinoma cell line Ishikawa. J Reprod Immunol 77(2):142–151
73. Gabitass RF, Annels NE, Stocken DD, Pandha HA, Middleton GW (2011) Elevated myeloid-derived suppressor cells in pancreatic, esophageal and gastric cancer are an independent prognostic factor and are associated with significant elevation of the Th2 cytokine interleukin-13. Cancer Immunol Immunother 60(10):1419–1430
74. Zea AH, Rodriguez PC, Atkins MB et al (2005) Arginase producing suppressor myeloid cells in renal cell carcinoma patients: a mechanism of tumor evasion. Cancer Res 65(8):3044–3048
75. Cohen NA, Stewart ML, Gavathiotis E et al (2012) A competitive stapled peptide screen identifies a selective small molecule that overcomes MCL-1-dependent leukemia cell survival. Chem Biol 19(9):1175–1186
76. Gore Y, Starlets D, Maharshak N et al (2008) Macrophage migration inhibitory factor induces B cell survival by activation of a CD74-CD44 receptor complex. J Biol Chem 283(5):2784–2792
77. Mitchell RA (2004) Mechanisms and effectors of MIF-dependent promotion of tumourigenesis. Cell Signal 16(1):13–19
78. Tarnowski M, Grymula K, Liu R et al (2011) Macrophage migration inhibitory factor is secreted by rhabdomyosarcoma cells, modulates tumor metastasis by binding to CXCR4 and CXCR7 receptors and inhibits recruitment of cancer-associated fibroblasts.Mol. Cancer Res 8(10):1328–1343
79. Oda S, Oda T, Nishi K et al (2008) Macrophage migration inhibitory factor activates hypoxia-inducible factor in a p53-dependent manner. PLoS One 3(5):e2215. doi:10.1371/journal.pone.0002215
80. Ichihara E, Kiura K, Tanimoto M (2011) Targeting angiogenesis in cancer therapy. Acta Med Okayama 65(6):353–362
81. Veillat V, Carli C, Metz CN, Al-Abed Y, Naccache PH, Akoum A (2010) Macrophage migration inhibitory factor elicits an angiogenic phenotype in human ectopic endometrial cells and triggers the production of major angiogenic factors via CD44, CD74, and MAPK signaling pathways. J Clin Endocrinol Metab 95(12):e403–e412. doi:10.1210/jc.2010-0417
82. Funamizu N, Hu C, Lacy C et al (2013) Macrophage migration inhibitory factor induces epithelial to mesenchymal transition, enhances tumor aggressiveness and predicts clinical outcome in resected pancreatic ductal adenocarcinoma. Int J Cancer 132(4):785–794
83. Meyer-Siegler KL, Iczkowski KA, Vera PL (2005) Further evidence for increased macrophage migration inhibitory factor expression in prostate cancer. BMC Cancer 5:73. doi:10.1186/1471-2407-5-73
84. McClelland M, Zhao L, Carskadon S, Arenberg D (2009) Expression of CD74, the receptor for macrophage migration inhibitory factor, in non-small cell lung cancer. Am J Pathol 174(2):638–646
85. Richard V, Kindt N, Decaestecker C et al (2014) Involvement of macrophage migration inhibitory factor and its receptor (CD74) in human breast cancer. Oncol Rep 32(2):523–529
86. Dietlin TA, Hofman FM, Lund BT, Gilmore W, Stohlman SA, van der Veen RC (2007) Mycobacteria-induced Gr-1+ subsets from distinct myeloid lineages have opposite effects on T cell expansion. J Leukoc Biol 81(5):1205–1212
87. Sinha P, Clements VK, Fulton AM, Ostrand-Rosenberg S (2007) Prostaglandin E2 promotes tumor progression by inducing myeloid-derived suppressor cells. Cancer Res 67(9):4507–4513
88. Movahedi K, Guilliams M, Van Den Bossche J et al (2008) Identification of discrete tumor-induced myeloid-derived suppressor cell subpopulations with distinct T cell suppressive activity. Blood 111(8):4233–4244
89. Gasser S, Orsulic S, Brown EJ, Raulet DH (2005) The DNA damage pathway regulates innate immune system ligands of the NKG2D receptor. Nature 436(7054):1186–1190
90. Mittelbronn M, Platten M, Zeiner P et al (2011) Macrophage migration inhibitory factor (MIF) expression in human malignant gliomas contributes to immune escape and tumour progression. Acta Neuropathol 122(3):353–365
91. Pende D, Rivera P, Marcenaro S et al (2002) Major histocompatibility complex class I-related chain a and UL16-binding protein expression on tumor cell lines of different histotypes: analysis of tumor susceptibility to NKG2D-dependent natural killer cell cytotoxicity. Cancer Res 62(21):6178–6186
92. Tanese K, Hashimoto Y, Berkova Z et al (2015) Cell surface CD74–MIF interactions drive melanoma survival in response to interferon-γ. J Invest Dermatol 135(11):2901. doi:10.1038/jid.2015.259
93. Wu S, Lian J, Tao H, Shang H, Zhang L (2011) Correlation of macrophage migration inhibitory factor gene polymorphism with the risk of early-stage cervical cancer and lymphatic metastasis. Oncol Lett 2(6):1261–1267

JACS
JOURNAL OF THE AMERICAN CHEMICAL SOCIETY
Article
pubs.acs.org/JACS

Design, Synthesis, and Protein Crystallography of Biaryltriazoles as Potent Tautomerase Inhibitors of Macrophage Migration Inhibitory Factor

Pawel Dziedzic,[†] José A. Cisneros,[†] Michael J. Robertson, Alissa A. Hare, Nadia E. Danford, Richard H. G. Baxter, and William L. Jorgensen*

Department of Chemistry, Yale University, New Haven, Connecticut 06520-8107, United States

Supporting Information

ABSTRACT: Optimization is reported for biaryltriazoles as inhibitors of the tautomerase activity of human macrophage migration inhibitory factor (MIF), a proinflammatory cytokine associated with numerous inflammatory diseases and cancer. A combined approach was taken featuring organic synthesis, enzymatic assaying, crystallography, and modeling including free-energy perturbation (FEP) calculations. X-ray crystal structures for **3a** and **3b** bound to MIF are reported and provided a basis for the modeling efforts. The accommodation of the inhibitors in the binding site is striking with multiple hydrogen bonds and aryl−aryl interactions. Additional modeling encouraged pursuit of 5-phenoxyquinolinyl analogues, which led to the very potent compound **3s**. Activity was further enhanced by addition of a fluorine atom adjacent to the phenolic hydroxyl group as in **3w**, **3z**, **3aa**, and **3bb** to strengthen a key hydrogen bond. It is also shown that physical properties of the compounds can be modulated by variation of solvent-exposed substituents. Several of the compounds are likely the most potent known MIF tautomerase inhibitors; the most active ones are more than 1000-fold more active than the well-studied (*R*)-ISO-1 and more than 200-fold more active than the chromen-4-one Orita-13.

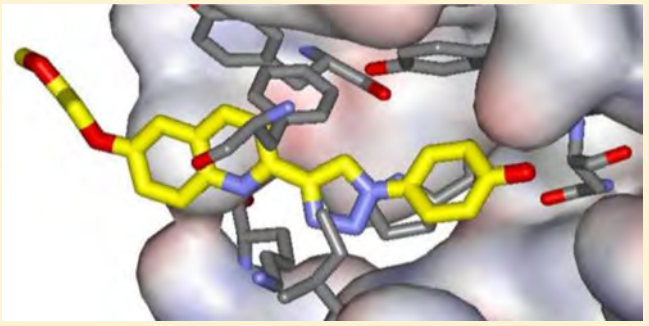

INTRODUCTION

Macrophage migration inhibitory factor (MIF) is a cytokine that plays a central role in numerous inflammatory diseases.[1−3] MIF is widely expressed in both immune and nonimmune cells including macrophages, endothelial cells, and T-cells. Upon activation, the cells release MIF, which promotes the release of other inflammatory cytokines such as TNF-α and IL-1. Excessive or chronic inflammatory response is associated with tissue damage and autoimmune diseases such as rheumatoid arthritis, Crohn's disease, and lupus erythematosus. The connection between inflammatory disease and cancer is also well-established, and MIF has been shown to enhance cell proliferation by inhibiting accumulation of the tumor suppressor p53 and by promotion of angiogenesis.[4] MIF is overexpressed in many cancer cells and can serve as a marker for disease progression. Furthermore, MIF in cancer cells is protected from degradation by Hsp90, which has led to proposed targeting of Hsp90 as an indirect way of inhibiting MIF function.[5] Disruption of the inflammatory cascade and restoration of normal p53 levels have clear implications for the potential therapeutic value of inhibitors of MIF signaling. Indeed, immunoneutralization of MIF or deletion of the MIF gene is known to suppress inflammatory response, tumor growth, and angiogenesis.[1−4] At the molecular level, what is needed is interference with the interaction between MIF and its cell-surface receptor CD74.[6]

MIF is a toroid-shaped, trimeric protein with a total of 342 amino acid residues. Besides its role as a cytokine, MIF is a keto−enol tautomerase. Though the enzymatic activity appears to be vestigial in humans, there are three tautomerase active sites at the interfaces of the monomer units opening to the outside of the toroid. Inhibition of protein−protein interactions is often challenging; however, the presence of the tautomerase sites presents an opportunity for complexation of a tautomerase inhibitor that may also interfere with MIF/CD74 binding. This notion has been supported by many studies that show correlation between the inhibition of the enzymatic and biological activities of MIF.[7] For example, this has been demonstrated through assay results for tautomerase activity, MIF/CD74 binding, and MIF-induced phosphorylation of ERK1/2 in inflamed cells, production of interleukins, glucocorticoid overriding ability, and macrophage chemotactic migration.[7−12] Nevertheless, the discovery of potent MIF tautomerase inhibitors is not well advanced as most inhibitors have arisen from screening exercises with no lead optimization.[8,11,12] In our efforts,[8−10] lead optimization has been limited by the lack of crystal structures for our tautomerase inhibitors bound to MIF, associated inconsistency between modeling results and activity data, and

Received: November 26, 2014
Published: February 20, 2015

DOI: 10.1021/ja512112j
J. Am. Chem. Soc. 2015, 137, 2996−3003

sensitivity of assay results to the substrate and protein source. As described here, these issues have been overcome for the series of biaryltriazoles, **1**−**3**. In particular, we report crystal structures for two complexes of derivatives of **3** with MIF, extensive structure−activity data that is consistent with both crystallography and modeling, and reliable assay protocols. The most active compounds are ca. 1000-fold more potent as MIF tautomerase inhibitors than the known MIF inhibitor (*R*)-ISO-1,[13,14] which has shown efficacy in rodent models as an anti-inflammatory and anticancer agent.[2,4]

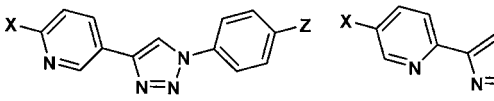

1

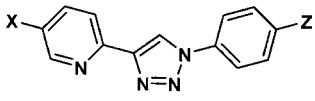

2

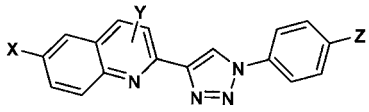

3

EXPERIMENTAL SECTION

Chemistry. In a previous report, we described the synthesis of 27 1,2,3-triazole derivatives in four motifs with a 4-hydroxyphenyl group at the 1-position and a substituted benzyl or aryl group at the 4-position or vice versa.[10] These constructs arose from de novo design using the program *BOMB*, which builds and scores libraries of compounds that it grows in a binding site.[15] Only three compounds were synthesized with a an aryl group at the 4-position, namely, the 3-pyridinyl analogue **1** (X = H, Z = OH) and the corresponding 1-naphthyl and 4-isoquinolinyl alternatives. The modeling indicated that the nitrogen atom in the 3-pyridinyl and 4-isoquinolinyl compounds would coordinate with the ammonium group of a lysine residue (Lys32A) and that this interaction would likely be lost and replaced by a repulsive interaction with the oxygen of Ile64A in 2-pyridinyl and 2-quinolinyl analogues, that is, **2** and **3**. However, **1** (X = H, Z = OH) and the isoquinolinyl analogue exhibited unexpected behavior as agonists in an assay for binding of MIF with the ectodomain of CD74.[10] They also showed inconclusive behavior in a MIF tautomerase assay; they appeared to be inactive or weak agonists lacking dose-dependent character. This eventually raised questions: (a) would the 2-pyridinyl and 2-quinolinyl isomers of the agonists be agonists, antagonists, or inactive, and (b) if an appendage were added in the 6-position of the pyridine ring in **1**, could this convert the agonist into an antagonist? As a crystal structure was not available for

Table 1. Results for Inhibition of the Tautomerase Activity of Human MIF[a]

compd	X	Y	Z	K_i (μM)[b]
1a	H		OH	37
1b	MOEO		OH	22
2a	H		OH	8.8
2b	MOEO		Cl	ND (0%)
3a	H	H	OH	0.59
3b	MOEO	H	OH	0.65
3c	AEOEO	H	OH	0.77
3d	MOEO	H	F	8.9
3e	MOEO	H	Cl	ND (3%)
3f	MOEO	H	NH_2	ND (13%)
3g	MOEO	H	OMe	ND (0%)
3h	MOEO	H	CN	ND (8%)
3i	MOEO	H	$CONH_2$	ND (0%)
3j	MOEO	H	3-Me, 4-OH	ND (15%)
3k	MOEO	H	3-OMe, 4-OH	ND (8%)
3l	H	3-Me	OH	7.3
3m	H	4-Me	OH	2.3
3n	H	8-Cl	OH	ND (16%)
3o	H	8-OMe	F	56
3p	H	8-MOEO	F	64
3q	H	8-*p*-MeOPh	OH	ND (21%)
3r	H	8-OPh	OH	2.95
3s	H	5-OPh	OH	0.37
3t	Mr$(CH_2)_3$O	H	OH	1.95
3u	Mr$(CH_2)_3$O	3-Me	OH	3.12
3v	MrEOEO	H	OH	0.41
3w	MrEOEO	H	3-F, 4-OH	0.15
3x	MrEOEO	H	F	29.6
3y	H	5-*p*-MOEO-OPh	OH	0.36
3z	H	5-*m*-MOEO-OPh	3-F, 4-OH	0.082
3aa	H	5-*p*-COOH-OPh	3-F, 4-OH	0.11
3bb	H	5-*m*-COOH-OPh	3-F, 4-OH	0.057
4a	H	H	OH	1.48
4b	H	H	Cl	ND (9%)
Orita-13				17
(*R*)-ISO-1				120

[a]MOEO = methoxyethoxy; AEOEO = aminoethoxyethoxy; Mr = *N*-morpholinyl. [b]ND = K_i not determined; % inhibition at 10 μM in parentheses.

DOI: 10.1021/ja512112j
J. Am. Chem. Soc. 2015, 137, 2996−3003

any of our compounds bound to MIF, the structural analyses and expectations for activity did not have firm footing. Thus, a scouting mission was initiated for **1** (X = methoxyethoxy, Z = OH), **2** (X = H, Z = OH), and **3** (X = H, Z = OH). As reported here, the surprising results led to lead optimization of **2** and **3** for inhibition of MIF tautomerase activity. The new compounds are listed as **1b**−**4b** in Table 1; **4** is the 1,8-naphthryidine analogue of **3**, while (*R*)-ISO-1 and 3-(3,4-dihydroxyphenyl)-7-hydroxy-4H-chromen-4-one (Orita-13) are reference compounds.[13,16]

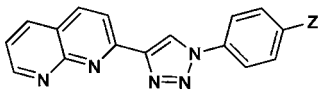

4

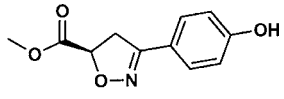

(*R*)-ISO-1

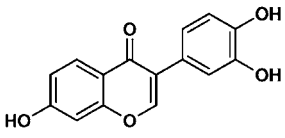

Orita-13

The synthetic approach was conceptually straightforward featuring a 1,3-dipolar cycloaddition between an azide and a substituted 2-ethynylpyridine, quinoline, or naphthyridine; however, access to the appropriately substituted heterocycles was not always easy. Though full details are provided in the Supporting Information, Schemes 1 and 2

Scheme 1. Synthesis of 3s

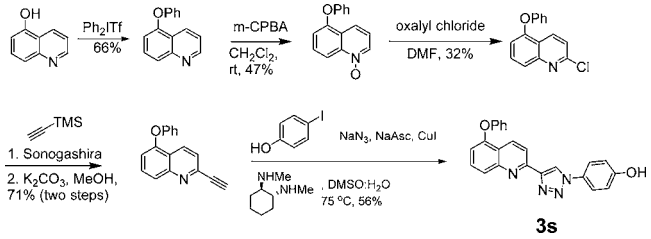

3s

Scheme 2. Synthesis of 3q

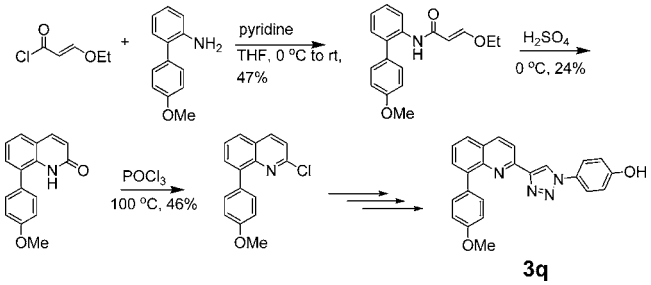

3q

illustrate the synthetic routes for two cases, **3s** and **3q**. Typically, 2-chloroquinolinols are available commercially at low cost; however, this is not the situation for 2-chloroquinolin-5-ol, which would have facilitated the synthesis of **3s**. Thus, starting with quinolin-5-ol, arylation was followed by oxidation to the *N*-oxide, which was chlorinated[17] to yield 2-chloro-5-phenoxyquinoline. A standard sequence[10] featuring Sonogashira coupling with TMS-protected acetylene followed by one-pot, Cu(I)-catalyzed reaction of the azide formed from an aryl bromide or iodide then yielded **3s**.[18]

With **3q** (Scheme 2), a substituted phenyl group was desired in the 8-position of the quinoline. This turned out to be challenging as numerous attempts at Suzuki couplings failed. For example, couplings with the triflate of 2-chloro-quinolin-8-ol gave at best 1:1 mixtures of 2- and 8-arylation, and no desired product arose from attempted couplings of either the 8-triflate or 8-pinacol boronic ester of 2-trimethylsilylethynylquinolin-8-ol. Instead, starting with commercially available 4′-methoxy-[1,1′-biphenyl]-2-amine, the desired 2-chloroquinoline was built by acylation to the acrylamide, followed by cyclization to the quinolone, and treatment with $POCl_3$ at reflux (Scheme 2). **3q** was then completed via the Sonogashira-1,3-dipolar cyclization sequence.

The identity of assayed compounds was confirmed by ^1H and ^{13}C NMR and high-resolution mass spectrometry; HPLC analyses established purity as >95%. Measurements of aqueous solubilities were carried out using a shake-flask procedure.[19] Saturated solutions were made by stirring excesses of the compounds in Britton-Robinson buffer for 48 h at 30 °C. The pH of the buffer solutions was 6.5 as measured by using a Corning General Purpose pH Combination probe (4136L21). The supernatant was collected using a Pall Life Sciences Acrodisc syringe filter with a 0.2 μm pore size, and analyzed by UV−vis spectrophotometry (Agilent 8453). Piroxicam was used as a control; our values of 7−9 μg/mL are consistent with the literature value of 5.9 μg/mL.[19]

Computer Modeling. All structure building was carried out using the *BOMB* program starting from a previously reported crystal structure of human MIF with 4-hydroxyphenylpyruvate (PDB code: 1CA7)[20] or from our structure of the complex with **3b**. Subsequent calculations included energy minimizations and free-energy perturbation (FEP) calculations with the *MCPRO* program.[21] Details of the calculations are described elsewhere.[22] Briefly, the OPLS-AA force field is used for the protein, OPLS/CM1A for the ligands, and TIP4P for water molecules.[23] For the FEP calculations, the unbound ligands and complexes were solvated in water caps with a 25 Å radius, amounting to ca. 2000 and 1250 water molecules, respectively. The 218 amino acid residues nearest to the ligand were included in the model for the complexes. A residue-based cutoff for nonbonded interactions was invoked at 10 Å. After short conjugate-gradient optimizations, the backbone atoms of the protein were fixed. The ligand and side chains with any atom within ca. 15 Å of the ligand were fully sampled. All water molecules were sampled using translations and rigid rotations. The FEP calculations used 11 or 21 windows of simple overlap sampling. Each window covered at least 10 million configurations of equilibration and 10 million configurations of averaging for the complexes and 30 million configurations of averaging for the unbound inhibitors.

Biology. *Protein Expression and Purification.* Recombinant human MIF (rhMIF) was expressed as described previously.[24] *Escherichia coli* cells were pelleted by centrifugation and stored at −80 °C. The purification followed published protocols[24,25] with slight modifications. Cell pellets were resuspended in a lysis buffer containing 20 mM Tris-HCl pH 7.5, 20 mM sodium chloride, 10% glycerol, 2 mM magnesium chloride, and 0.2× *cOmplete* EDTA-free protease inhibitor cocktail (Roche), lysed by sonication and centrifuged at 27 000*g* for 30 min. The supernatant was filtered through a 0.22 μm syringe filter and applied to Hi-Trap SP HP and Hi-Trap Q SP columns (GE Healthcare) in tandem. As rhMIF did not bind to either ion-exchange resin, the flow-through was collected, being sufficiently pure (~90%) for crystallography. Higher purity was achieved by size-exclusion chromatography on a Superdex 200 16/60 column (GE Healthcare). The resulting rhMIF was assessed by SDS gel electrophoresis to be of sufficiently high purity (>95%) for tautomerase assays. Pure protein was concentrated to 30.6 mg/mL in 20% glycerol and stored at −80 °C.

Tautomerase Assay, K_i Determination. Inhibition of the tautomerase activity of MIF was measured using 4-hydroxyphenyl pyruvic acid (HPP) as substrate, largely following previously reported protocols.[26] HPP was dissolved in 0.5 M acetate buffer, pH 6.0 to a final concentration of 10 mM and incubated overnight at room temperature to allow equilibration of the keto and enol forms. MIF (6 μL) was premixed in 500 mM boric acid, pH 6.2 (142 μL) and transferred to a transparent U bottom 96-well plate to a final concentration of 200 nM MIF. It was important to optimize the protein concentration; this was performed by analysis of progress curves for enol production at protein concentrations of 50−800 nM. High signal-to-noise and linearity were observed for 200 and 400 nM MIF; below these levels, weaker signal limited accuracy of the results. Inhibitors were dissolved in DMSO to 10 mM and an initial screen was performed. For compounds that showed

DOI: 10.1021/ja512112j
J. Am. Chem. Soc. 2015, 137, 2996−3003

ca. 25% or greater inhibition at 10 μM, an inhibition constant, K_i, was measured. Compounds were placed into wells (2 μL) at six different concentrations and incubated for 30 min until the assay was started by addition of HPP (50 μL) at two concentrations (1.0 and 2.5 mM). The negative control was MIF incubated with DMSO vehicle, which in all assays was 1% and did not influence tautomerase activity. MIF activity was monitored at 305 nm for formation of the borate−enol complex using an Infinite F500 plate reader (TECAN, Morrisville, NC) for 175 s. Calculation of initial velocities and the nonlinear regression analyses for the enzyme kinetics were repeated three times with the program Prism6 (GraphPad, La Jolla, CA). The results always fit better to the competitive inhibition mode rather than the noncompetitive one, which is consistent with the crystallographic results.

Previously, we had attempted assays using rhMIF purchased from external vendors. This proved unsatisfactory as different vials of protein showed great variation in activity, including totally inactive. Even different vials received at the same time from the same vendor showed different activities. The present assay results were all obtained with protein prepared on only two occasions; when more protein was needed, another aliquot was thawed, and never refrozen. Also, Orita-13 and/or **3b** were used as control compounds when new rounds of assays were conducted. The K_i results all fell in the range 13−22 μM for Orita-13, and nine independent measurements for **3b** yielded results of 0.55−0.85 μM. Samples of Orita-13 and (*R*)-ISO-1 were purchased both from Alfa Aesar and Santa Cruz Biotechnology; consistent spectra and K_i results were obtained.

We also investigated use of L-dopachrome methyl ester (DOPA) rather than HPP as the substrate in the manner of Orita et al.[16] An advantage in principle is that the absorbance is evaluated at 492 nm, which may experience less interference from the inhibitors than the 305 nm detection with HPP. However, DOPA is photosensitive, which limits the data collection to 25 s versus 175 s with HPP. The shorter linear range for calculation of the initial velocities results in poorer fits for the results at different concentrations and much less reliable K_i values.

Protein Crystallography. To obtain cocrystals of MIF in complex with **3a**, 100 μM **3a** in DMSO was added to rhMIF (24 μg/mL) to achieve a 3:1 molar ratio and incubated for 1 h at 5 °C. The solution was centrifuged at 13 000*g* to remove precipitated compound and used to set up hanging-drop crystallization experiments. A reservoir of 2.0 M ammonium sulfate, 0.1 M Tris pH 7, and 3% isopropanol was added to the protein solution in a 1:1 ratio and stored at 20 °C. Diffraction-quality crystals with a rod morphology grew within 2 weeks. The crystals were cryo-protected in 25% glycerol, 2.0 M ammonium sulfate, 0.1 M Tris pH 7, and 3% isopropanol and shipped to the Advanced Photon Source for remote data collection on the NE-CAT 24-ID-E beamline.

Cocrystals of MIF in complex with **3b** were obtained by soaking crystals of apo MIF. Crystals were obtained by the hanging-drop method at 20 °C. A reservoir of 2.2 M ammonium sulfate, 0.1 M Tris pH 7, and 3% isopropanol mixed in a 1:1 ratio with rhMIF (16 mg/mL) was used to produce 2 μL drops. Once crystals formed, 0.5 μL of a suspension of 10 mM **3b** in 10% DMSO, 2.0 M ammonium sulfate, 90 mM Tris pH 7, and 2.7% isopropanol was added to the drop and allowed to incubate for 14 days. Crystals were cryo-protected with 25% glycerol, 2.2 M ammonium sulfate, 0.1 M Tris pH 7, and 3% isopropanol and diffracted on a Rigaku 007 HF+ X-ray source equipped with a Saturn 944+ CCD detector at Yale. Full details of the data collection and refinement for **3a** and **3b** are provided in the Supporting Information.

RESULTS AND DISCUSSION

In presenting the results, a sense of the progression of events will be given. The previous report was for work through mid-2010 and included **1a**.[10] The triazole series were not pursued again until early 2012, when **1b**, **2a**, and **3a** were synthesized. However, the assay issues and protein access discussed above, which were needed to allow report of the carefully controlled results in Table 1, were not fully worked out until 2013.

With the present assay protocols, the parent compounds **1a**, **2a**, and **3a** are all MIF tautomerase inhibitors. Progression from the 3-pyridinyl (**1a**) to 2-pyridinyl (**2a**) to 2-quinolinyl (**3a**) derivatives shows strong enhancement in activity from 37 to 8.8 to 0.59 μM. For comparison, (*R*)-ISO-1, which is reported[14] to have an IC_{50} of 7 μM in a MIF tautomerase assay with DOPA as the substrate, has a K_i of 120 μM in our assay. Issues with IC_{50} measurements are well-known; they depend on the concentration and Michaelis constant (K_m) of the substrate, while K_i is an intrinsic measure of the binding of the protein and inhibitor.[27] In an independent assay of ISO-1 using DOPA, an IC_{50} of >100 μM was reported; the discrepancy with the 7 μM value was suggested to arise from use of different concentrations of rhMIF.[28] We also find Orita-13 with a K_i averaging 17 μM to be much less active than from the previously reported K_i of 0.038 μM, again in a dopachrome assay.[16] Orita-13 would seem to be the most potent MIF inhibitor in the journal literature.[11] It arose from a screening study that reported K_i values for 14 compounds with the next most potent compound at 0.28 μM.[16] There have been no follow-up reports with the compound except for a crystal structure[29] that found it rotated 180° in the binding site from the original X-ray study,[16] and it appears not to have been assayed again until now. Though we find Orita-13 to be 7-fold more active than ISO-1, it is 30-fold less active than **3a**.

Crystallography. To progress from this point, a recurrent conformational issue complicated modeling efforts.[10] For **3a**, as an example, four principal geometries could be constructed in the binding site, which can be labeled **3a-ud**, **3a-dd**, **3a-du**, and **3a-uu**. These represent two conformers that can both be rotated 180° about the long axis in the binding site. The structure building and energy minimizations with *BOMB* and *MCPRO* could rule out **3a-ud** and **3a-uu**, but the preference between **3a-dd** and **3a-du** was uncertain. **3a-dd** is the higher-energy conformer in the gas-phase than **3a-du**, by 6 kcal/mol according to OPLS/CM1A calculations, owing to the added quinoline N−triazole N3 repulsion; however, **3a-dd** appeared to make better hydrogen-bonding interactions in the binding site.

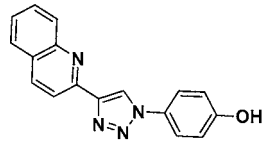

3a-ud

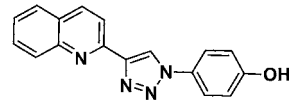

3a-dd

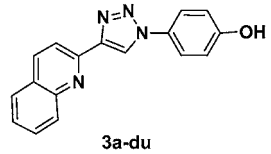

3a-du

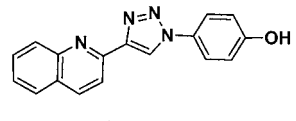

3a-uu

This issue was resolved by obtaining the crystal structures for **3a** and **3b** in complex with MIF at resolutions of 2.60 and 1.81 Å, respectively. As illustrated in Figure 1 for **3b**, the crystal structures of both complexes showed that **3a-dd** is the preferred geometry. The inhibitor is inserted such that the phenolic hydroxyl group is hydrogen-bonded with Asn97C (r(OO) = 2.52 Å); there is also a hydrogen bond between N2 of the triazole and the backbone NH of Ile64A (r(NN) = 2.90 Å), and there is the striking complexation of the ammonium group of Lys32A by the quinoline N, triazole N3, and O of Ile64A (r(NN) = 3.33, 2.95; r(NO) = 2.81 Å), which requires the higher-energy **3a-dd** geometry. There are also aryl−aryl interactions between the phenolic and quinolinyl fragments of the inhibitor and Tyr95C

DOI: 10.1021/ja512112j
J. Am. Chem. Soc. 2015, 137, 2996−3003

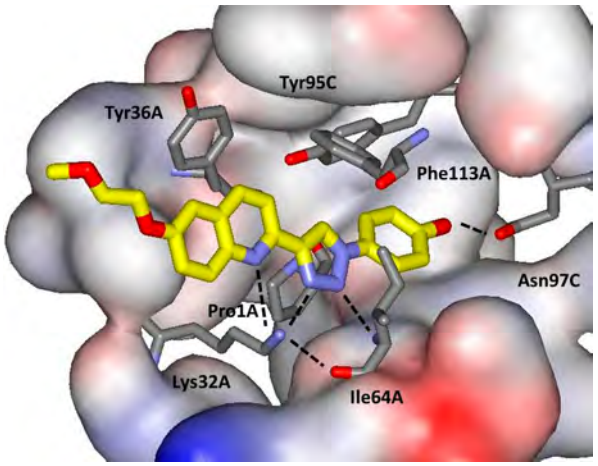

Figure 1. Rendering of **3b** bound to human MIF from the 1.81 Å crystal structure (PDP ID: 4WRB). Carbon atoms of **3b** are shown in yellow; some residues have been removed for clarity. Hydrogen bonds are highlighted with dashed lines.

and Tyr36A, respectively, and Phe113A has contacts at the junction of the quinoline and triazole. The structure appears very well packed with a large number of favorable intermolecular features given the size of the inhibitor. The crystal structures for **3a** and **3b** are essentially the same, and it was pleasing that the methoxyethoxy substituent of **3b** was well-resolved (Figure S2). Though the substituent would be solvent-exposed in dilute solution, in the crystal it is in contact with an adjacent MIF trimer. The fact that **3a** and **3b** show the same activity (Table 1) is fully consistent with the crystal structures. It may also be noted that both crystal structures only have one of the three tautomerase sites occupied by **3a** or **3b**, the remaining sites being occupied by solvent and/or glycerol.

In previously reported crystal structures, hydrogen bonding interactions for an inhibitor with the side chains of Asn97 and Lys32 and with the backbone NH of Ile64 have frequently been observed along with aryl−aryl contacts involving Tyr95 and Phe113.[16,20,29] The interactions with Lys32 have typically come from a carbonyl or carboxylate group of the inhibitor. For example, in the 3L5R structure for Orita-13, the hydroxyl group of the chromen-4-one is hydrogen bonded with Asn97, and the carbonyl oxygen atom is hydrogen-bonded to both Lys32 and the NH of Ile64.[29] The present structures are particularly striking because the triazolylquinoline substructure provides three separate hydrogen bonds with Lys32A and Ile64A as well as an additional aryl−aryl interaction with Tyr36A (Figure 1). It may also be noted that, in the present structures Pro1A, the catalytic base for the tautomerase reaction and nucleophile for formation of covalent inhibitors[11] is probably protonated. One hydrogen atom on the nitrogen is likely pointing toward the carbonyl oxygen atom of Tyr36A with an N−O distance of 3.22 Å, while there is a clear hydrogen bond between this carbonyl oxygen atom and the hydroxyl group of Tyr95C at an O−O distance of 2.51 Å. If there is a second hydrogen atom on the Pro1A nitrogen atom, it would be pointing toward N1 of the triazole (r(NN) = 3.25 Å), and there would be favorable cation−π interactions with the electron-rich ring.

Phenyl and Quinolinyl Substituents. Having resolved the structural issue, FEP calculations were performed to seek substituent modifications in the phenyl and quinolinyl fragments that could improve potency. The results are summarized in Table 2. It should be noted that Clx and Brx refer to modeling the

Table 2. MC/FEP Results for Changes in Free Energy of Binding to Human MIF[a]

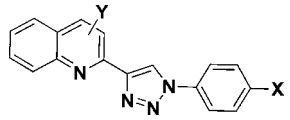

H to X	$\Delta\Delta G_b$	H to Y[b]	$\Delta\Delta G_b$	H to Y[b]	$\Delta\Delta G_b$
F	−2.27	3-F	0.15	4-OMe	0.02
Cl	−1.77	3-Cl	−0.82	4-OH	1.64
Clx	−1.06	3-Clx	−0.32	8-F	−0.79
Br	−1.16	3-Me	−2.69	8-Cl	−1.49
Brx	−0.62	3-Et	−1.56	8-Clx	−2.06
Me	2.73	3-OMe	0.23	8-Me	0.61
Et	6.26	4-F	0.46	8-Et	−0.11
NH_2	1.89	4-Cl	0.32	8-OMe	−0.51
OMe	0.14	4-Clx	0.18	8-OEt	−0.16
OH	−2.70	4-Me	−1.00	8-MOM	0.27
		4-Et	−0.34	8-CH_2F	0.40

[a] $\Delta\Delta G_b$ is the computed change in free energy of binding (kcal/mol); Clx and Brx include X-sites to allow halogen bonding; the statistical uncertainty in the results ($\pm 1\sigma$) is 0.2 kcal/mol. [b] With X = OH.

halogens with an extra partial positive charge, which allows representation of halogen bonding.[30] There is little empty space in the vicinity of the phenolic hydroxyl group. The FEP results indicated that all replacements of the hydroxyl group would be unfavorable, though the penalty for switching to fluorine should not be severe. There is a trade-off between loss of hydrogen-bonding with Asn97C and a diminished dehydration penalty. An amino group is not favorable since only one of the two amino hydrogens can form a hydrogen bond to Asn97C. The activity data for **3b** and **3d**−**3i** in Table 1 are consistent with the predictions. Only the fluoro analogue **3d** showed significant activity with a K_i of 8.9 μM, ca. 15-fold higher than that for **3b**. For **3j** and **3k**, a methyl or methoxy substituent adjacent to the hydroxyl group was also considered, but as expected from the tight packing, these additions were unfavorable.

Turning to the quinoline ring, the 3-, 4-, and 8-positions were first considered for possible additions of small groups. Structure-building with *BOMB* suggested that at least a small alkyl group might be accommodated at C3 or C4 in the space near Tyr36A. However, the FEP results indicated that about the only hope would be for a methyl group at C3 (Table 2), since we have generally observed that the computed enhancement needs to be beyond −2 kcal/mol to have good confidence in an observed activity increase.[15] Indeed, the assay results for **3l** and **3m** (7.3 and 2.3 μM) showed weaker inhibition than for the parent **3a** (0.59 μM), while **3t** and its 3-methyl analogue **3u** showed essentially the same activity. In view of the FEP results for the other options, further exploration at these sites was not pursued.

Structure building at C8 then suggested that addition of an alkoxy group or substituted phenyl might provide additional coordination with Lys32A (Figure 1). Enticing images could be generated as in Figure 2 showing a possible cation−π interaction in the latter case. Such interactions require representation of explicit polarization effects in the force fields,[23] so a confident FEP result could not be obtained with OPLS/CM1A. The FEP calculations were executed for nine options at C8, as shown in Table 2 with the result that chlorine might be most promising. However, the predicted $\Delta\Delta G_b$ values of −1.49 and −2.06 kcal/mol are on the fringe of the −2 kcal/mol threshold. In fact, the 8-Cl analogue **3n** was found to have diminished activity. The

DOI: 10.1021/ja512112j
J. Am. Chem. Soc. 2015, 137, 2996−3003

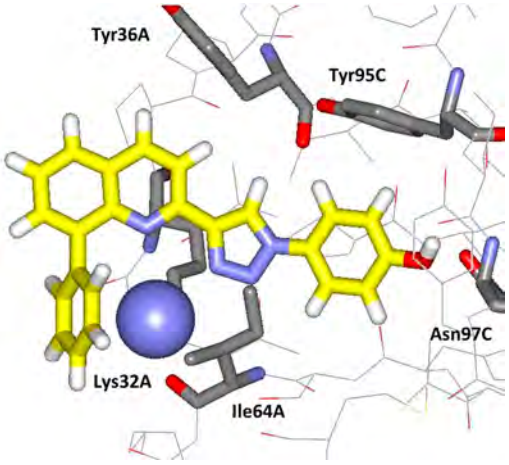

Figure 2. Computed structure for an analogue of **3a** with a phenyl substituent on C8 of the quinoline highlighting a possible cation–π interaction with Lys32A. Carbon atoms of the ligand are in yellow; the ammonium group of Lys32A is shown as a blue sphere. Some residues have been removed for clarity.

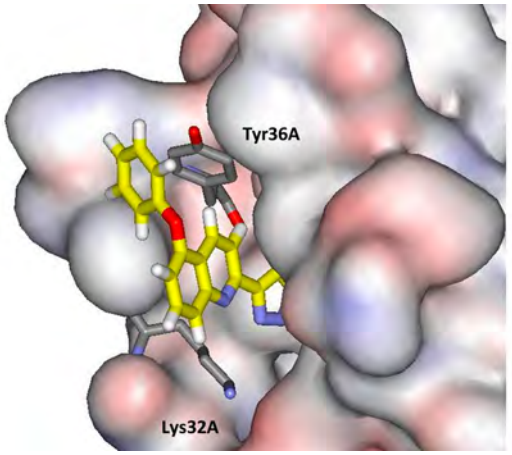

Figure 3. Computed structure for 5-phenoxy-containing **3s** bound to human MIF illustrating surface contact and a possible aryl–aryl interaction with Tyr36A. Carbon atoms of the ligand are in yellow. Some residues have been removed for clarity.

$\Delta\Delta G_b$ for an 8-methoxy group of −0.51 kcal/mol made it likely that this modification would also be unproductive. This was tested with **3o** that has a fluorine replacing the phenolic hydroxyl group; its K_i of 56 μM suggests that the phenol would be 4 or 0.8 μM, if the **3d**/**3b** or **3x**/**3v** ratio is transferable. Though the oxygen of the methoxy group of **3o** can form a hydrogen bond with the ammonium group of Lys32, it is replacing a water molecule that is fulfilling this role and it requires orientation of the oxygen toward the quinoline N, which promotes lone pair–lone pair repulsion. In the balance, consistent with the FEP prediction, the 8-methoxy group in **3o** and the methoxyethoxy (MOEO) group in **3p** did not provide a notable activity boost.

Returning to the possibility of a phenyl substituent at C8, as noted in Scheme 2, there were challenges in the synthesis of such compounds. Nevertheless, there was success with the *p*-methoxy analogue **3q**. In spite of the attractive graphics for 8-phenyl analogues (Figure 2), **3q** only showed 21% inhibition of MIF's tautomerase activity at 10 μM (Table 1). Lys32 is on the surface of MIF, and it appears difficult to substitute favorably for the water molecules on its solvent-exposed side. The possibility of additional coordination from the ligand with Lys32A via the 1,8-naphthyridine **4a** was also considered; the result was a respectable K_i of 1.48 μM, but not an improvement over **3a**.

Still not relenting, structures were built with *BOMB* with a phenoxy group at C5, C6, C7, and C8 of the quinoline ring. A conformational search on the 8-phenoxy analogue indicated that it would be better preorganized for binding and interaction with Lys32A than the 8-methoxy alternative, and perhaps the phenoxy groups might interact with other surface residues. In fact, energy minimizations showed that this could be the case for the C5 (Figure 3) and C8 phenoxy compounds. Thus, this notion was pursued yielding **3r** and **3s**. The 8-phenoxy analogue **3r** is a 3.0 μM inhibitor, while the 5-phenoxy **3s** at 0.37 μM did provide an advance over **3a** and **3b** (Table 1). The presumption is that the added intermolecular contacts illustrated in Figure 3 are beneficial for binding.

Aqueous Solubility. From the crystal structures and modeling, it was expected that physical properties of the compounds could be modulated by variation of substituents that would be solvent exposed. Attachments at the 6- or 7-positions in the quinoline ring seemed likely to be appropriate (Figures 1–3). For illustration, aqueous solubility was considered. Thus, polyether-containing groups were appended at C6 with the 6-hydroxy compounds as precursors. Aqueous solubilities were measured for a series of four compounds as summarized in Scheme 3. The solubilities of **3a** (2.2 μg/mL or 7.6 μM) and **3b** (3.6 μg/mL or 9.9 μM) are surprisingly low given the small size, percentage of heteroatoms, and the computed octanol/water partition coefficients of 3.3 to 4.0 from *ChemDraw* and *QikProp*.[31,32] When experimental data for log *S* and log $P_{o/w}$ are analyzed,[33] a rule-of-thumb is log $S = -\log P_{o/w} - 0.2$ with $r^2 = 0.70$ and rms = 1.0 for 271 compounds with log $P_{o/w} > 0$. Thus, log $S \approx 10^{-4}$ or $S \approx 100$ μM for **3a** and **3b** could be expected within a factor of 10. The observed results are at the very bottom of this range. Addition of the amino group in **3c** has the expected qualitative effect, raising the solubility to 13.9 μg/mL. A further 3–4-fold boost is obtained upon replacement of the amino group with *N*-morpholinyl, a well-known solubilizing group.[34,35] **3v** is potent with a K_i of 0.41 μM, and its solubility of 48.5 μg/mL (1.05×10^{-4} M) is well inside the range normally observed for oral drugs, 4–4000 μg/mL.[33] The ClogP appears to be high in this case; the pattern for the four compounds from *QikProp* seems more reasonable. The predicted

Scheme 3. Experimental Solubilites (*S*, μg/mL) and Computed log *P*

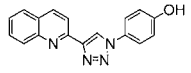

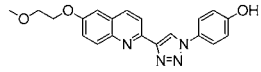

	3a	**3b**
K_i	0.59	0.65
S	2.2	3.6
ClogP	3.80	3.98
QPlogP	3.32	3.49

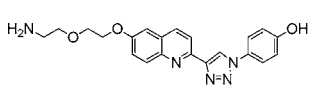

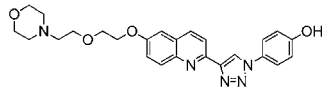

	3c	**3v**
K_i	0.77	0.41
S	13.9	48.5
ClogP	3.36	4.24
QPlogP	2.43	2.82

DOI: 10.1021/ja512112j
J. Am. Chem. Soc. 2015, 137, 2996–3003

solubility from *QikProp* of 0.2×10^{-4} M for **3v** is also within normal error bounds.[32]

Final Compounds. Given the good results for **3s** and **3v**, additional analogues were synthesized to again test the impact of replacing the phenolic hydroxyl group with fluorine (**3x**) and for addition of a fluorine adjacent to the hydroxyl group (**3w**, **3z**, **3aa**, **3bb**). Though methyl and methoxy groups could not be accommodated at the *meta* position (**3j** and **3k**), fluorine is smaller and it is expected to enhance the hydrogen-bond donor character of the hydroxyl group and strengthen the hydrogen bond with Asn97C. This idea was fruitful, as **3w** with a K_i of 0.15 μM is 3-fold more potent than **3v**. The added fluorine makes **3w** somewhat less soluble with S = 27.2 μg/mL. The same idea was then applied to the 5-phenoxy compounds. Addition of a *para*-methoxyethoxy group in **3y** did not change the potency from that of **3s**, since the added group is expected to be largely solvent-exposed (Figure 3). However, again several-fold enhancements of the potency accompanied introduction of a *meta* solubilizing group along with a fluorine adjacent to the hydroxyl group yielding the most potent compounds, **3z** and **3bb**, with K_i values of 0.082 and 0.057 μM. The solubility of **3bb** was also measured; the result of 47.2 μg/mL further supports the potential value of this compound.

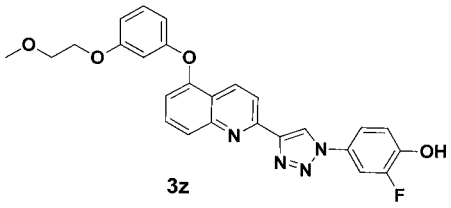

3z

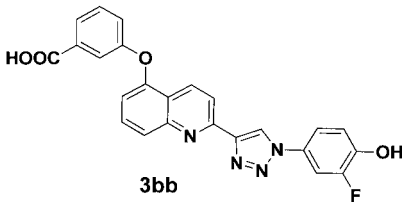

3bb

CONCLUSION

The purpose of this work was to optimize biaryltriazoles as inhibitors of the tautomerase activity of human MIF. A combined approach was taken featuring organic synthesis, enzymatic assaying, crystallography, and modeling including FEP calculations. The acquisition of the crystal structures for **3a** and **3b** bound to MIF provided important proof that the inhibitors were bound in the tautomerase active site and a firmer structural foundation for the modeling. Exploration of the structure–activity relationships using a carefully optimized and controlled tautomerase assay showed that it was challenging to improve on the activity of **3a** and **3b** owing to the limited size of the binding site and the exquisite accommodation of the inhibitors through multiple hydrogen bonds and aryl–aryl interactions (Figure 1). Some enticing possibilities such as introduction of an alkoxy or phenyl substituent at the 8-position in the quinoline ring (Figure 2) did not produce more potent compounds. Additional modeling with the *BOMB* program encouraged pursuit of 5-phenoxy analogues (Figure 3), which did deliver a gain in potency with **3s**. Consideration of appendages at the 6-position of the quinoline ring led to **3v**, which is both highly soluble and potent. Finally, addition of a *meta*-fluorine to enhance the hydrogen bonding with Asn97C yielded additional gains in potency with **3w**, **3z**, **3aa**, and **3bb**. With K_i values below 100 nM, **3z** and **3bb** are likely the most potent known inhibitors of the tautomerase activity of human MIF; they are more than 1000-fold more active than the well-studied (*R*)-ISO-1 and more than 200-fold more active than the chromen-4-one Orita-13.

ASSOCIATED CONTENT

Supporting Information

Synthetic details, NMR and HRMS spectral data for compounds in Tables 1, and crystallographic details. The crystal structure data for the complexes of **3a** and **3b** with MIF have been deposited in the RCSB Protein Data Bank with the codes 4WR8 and 4WRB. These materials are available free of charge via the Internet at http://pubs.acs.org.

AUTHOR INFORMATION

Corresponding Author

*william.jorgensen@yale.edu

Author Contributions

†P.D. and J.A.C. contributed equally to this work.

Notes

The authors declare no competing financial interest.

ACKNOWLEDGMENTS

Gratitude is expressed to the National Institutes of Health (GM32136), Yale University, and Debiopharm SA for research support, to the National Science Foundation (DGE-1122492) for a fellowship to M.J.R., to Drs. Richard Bucala and Lin Leng for the MIF expression vector and interactions on the tautomerase assay, and to Dr. Binh Le for assistance with crystallizations and X-ray data collection. The data collection for the structure of **3a** with human MIF was conducted at the Advanced Photon Source (APS) on the Northeastern Collaborative Access Team beamlines which are supported by the National Institutes of Health (P41 GM103403); the APS is operated for the U.S. Department of Energy Office of Science by Argonne National Laboratory under Contract No. DE-AC02-06CH11357.

REFERENCES

(1) Morand, E. F.; Leech, M.; Bernhagen, J. *Nat. Rev. Drug. Discovery* **2006**, *5*, 399–410.
(2) Greven, D.; Leng, L.; Bucala, R. *Expert Opin. Ther. Targets* **2010**, *14*, 253–264.
(3) Asare, Y.; Schmitt, M.; Bernhagen, J. *Thromb. Haemost.* **2013**, *109*, 391–398.
(4) Conroy, H.; Mawhinney, L.; Donnelly, S. C. *Q. J. Med.* **2010**, *103*, 831–836.
(5) Schulz, R.; Moll, U. M. *Curr. Opin. Oncol.* **2014**, *26*, 108–113.
(6) Leng, L.; Metz, C.; Fang, Y.; Xu, J.; Donnelly, S.; Baugh, J.; Delonery, T.; Chen, Y.; Mitchell, R. A.; Bucala, R. *J. Exp. Med.* **2003**, *197*, 1467–1476.
(7) Senter, P. D.; Al-Abed, Y.; Metz, C. N.; Benigni, F.; Mitchell, R. A.; Chesney, J.; Han, J.; Gartner, C. G.; Nelson, S. D.; Todaro, G. J.; Bucala, R. *Proc. Natl. Acad. Sci. U. S. A.* **2002**, *99*, 144–149.
(8) Cournia, Z.; Leng, L.; Gandavadi, S.; Du, X.; Bucala, R.; Jorgensen, W. L. *J. Med. Chem.* **2009**, *52*, 416–424.
(9) Hare, A. A.; Leng, L.; Gandavadi, S.; Du, X.; Cournia, Z.; Bucala, R.; Jorgensen, W. L. *Bioorg. Med. Chem. Lett.* **2010**, *20*, 5811–5814.
(10) Jorgensen, W. L.; Gandavadi, S.; Du, X.; Hare, A. A.; Trofimov, A.; Leng, L.; Bucala, R. *Bioorg. Med. Chem. Lett.* **2010**, *20*, 7033–7036.
(11) For reviews, see: (a) Orita, M.; Yamamoto, S.; Katayama, N.; Fujita, S. *Curr. Pharm. Des.* **2002**, *8*, 1297–1317. (b) Garai, J.; Lóránd, T.

DOI: 10.1021/ja512112j
J. Am. Chem. Soc. 2015, 137, 2996–3003

Curr. Med. Chem. **2009**, *16*, 1091−1114. (c) Xu, L.; Li, Y.; Sun, H.; Zhen, X.; Qiao, C.; Tian, S.; Hou, T. *Drug Discovery Today* **2013**, *18*, 592−600.
(12) (a) Xu, L.; Zhang, Y.; Zheng, L.; Qiao, C.; Li, Y.; Li, D.; Zhen, X.; Hou, T. *J. Med. Chem.* **2014**, *57*, 3737−3745. (b) Tsai, L.-T.; Lin, T.-H. *J. Biomol. Screening* **2014**, *19*, 1116−1123.
(13) Al-Abed, Y.; Dabideen, D.; Aljabari, B.; Valster, A.; Messmer, D.; Ochani, M.; Tanovic, M.; Ochani, K.; Bacher, M.; Nicoletti, F.; Metz, C.; Pavlov, V. A.; Miller, E. J.; Tracey, K. J. *J. Biol. Chem.* **2005**, *280*, 36541−36544.
(14) Chang, K. F.; Al-Abed, Y. *Bioorg. Med. Chem. Lett.* **2006**, *16*, 3376−3379.
(15) Jorgensen, W. L. *Acc. Chem. Res.* **2009**, *42*, 724−733.
(16) Orita, M.; Yamamoto, S.; Katayama, N.; Aoki, M.; Takayama, K.; Yamagiwa, Y.; Seki, N.; Suzuki, H.; Kurihara, H.; Sakashita, H.; Takeuchi, M.; Fujita, S.; Yamada, T.; Tanaka, A. *J. Med. Chem.* **2001**, *44*, 540−547.
(17) Georg, J. U.S. Patent Appl. 200770078155, 5 April 2007.
(18) Andersen, J.; Bolvig, S.; Liang, X. *Synlett* **2005**, 2941−2947.
(19) Baka, E.; Comer, J. E. A; Takács-Novák, K. *J. Pharm. Biomed. Anal.* **2008**, *46*, 335−341.
(20) Lubetsky, J. B.; Swope, M.; Dealwis, C.; Blake, P.; Lolis, E. *Biochemistry* **1999**, *38*, 7346−7354.
(21) Jorgensen, W. L.; Tirado-Rives, J. *J. Comput. Chem.* **2005**, *26*, 1689−1700.
(22) Jorgensen, W. L.; Bollini, M.; Thakur, V. V.; Domaoal, R. A.; Spasov, K.; Anderson, K. S. *J. Am. Chem. Soc.* **2011**, *133*, 15686−15696.
(23) Jorgensen, W. L.; Tirado-Rives, J. *Proc. Natl. Acad. Sci. U. S. A.* **2005**, *102*, 6665−6670.
(24) Bernhagen, J.; Mitchell, R. A.; Calandra, T.; Voelter, W.; Cerami, A.; Bucala, R. *Biochemistry* **1994**, *33*, 14144−14155.
(25) Sun, H.-W.; Bernhagen, J.; Bucala, R.; Lolis, E. *Proc. Natl. Acad. Sci. U. S. A.* **1996**, *93*, 5191−5196.
(26) Taylor, A. B.; Johnson, W. H.; Czerwinski, R. M.; Li, H. S.; Hackert, M. L.; Whitman, C. P. *Biochemistry* **1999**, *38*, 7444−7452.
(27) Cheng, Y.-C.; Prusoff, W. H. *Biochem. Pharmacol.* **1973**, *22*, 3099−3108.
(28) Balachandran, S.; Rodge, A.; Gadekar, P. K.; Yadav, V. N.; Kamath, D.; Chetrapal-Kunwar, A.; Bhatt, P.; Srinivasan, S.; Sharma, S.; Vishwakarma, R. A. *Bioorg. Med. Chem. Lett.* **2009**, *19*, 4773−4776.
(29) McLean, L. R.; Zhang, Y.; Li, H.; Choi, Y.-M.; Hon, Z.; Vaz, R. J.; Li, Y. *Bioorg. Med. Chem. Lett.* **2010**, *20*, 1821−1824.
(30) (a) Jorgensen, W. L.; Schyman, P. *J. Chem. Theory Comput.* **2012**, *8*, 3895−3901. (b) Yan, X. C.; Schyman, P.; Jorgensen, W. L. *J. Phys. Chem. A* **2014**, *118*, 2820−2826.
(31) *ChemBioDraw*, ver. 12.0.2; CambridgeSoft Inc.: Cambridge, MA, 2014.
(32) *QikProp*, ver. 4.0; Schrödinger Inc.: New York, 2014.
(33) Jorgensen, W. L.; Duffy, E. M. *Adv. Drug Delivery Rev.* **2002**, *54*, 355−366.
(34) Roughley, S. D.; Jordan, A. M. *J. Med. Chem.* **2011**, *54*, 3451−3479.
(35) Bollini, M.; Cisneros, J. A.; Spasov, K. A.; Anderson, K. S.; Jorgensen, W. L. *Bioorg. Med. Chem. Lett.* **2013**, *23*, 5213−5216.

DOI: 10.1021/ja512112j
J. Am. Chem. Soc. 2015, 137, 2996−3003

ACS Medicinal Chemistry Letters

Letter

pubs.acs.org/acsmedchemlett

Systematic Study of Effects of Structural Modifications on the Aqueous Solubility of Drug-like Molecules

José A. Cisneros, Michael J. Robertson, Brandon Q. Mercado, and William L. Jorgensen*

Department of Chemistry, Yale University, New Haven, Connecticut 06520-8107, United States

Supporting Information

ABSTRACT: Aqueous solubilities and activities have been measured for 17 members of the quinolinyltriazole series of inhibitors of human macrophage migration inhibitory factor (MIF). Systematic variation of a solvent-exposed substituent provided increases in solubility from 2 μg/mL for the parent compound **3a** up to 867 μg/mL. The low solubility of **3a** results from its near-planar structure and an intermolecular hydrogen bond, as revealed in a small-molecule X-ray structure. Removal of the hydrogen bond yields a 3-fold increase in solubility, but a 7-fold drop in activity. **5b** emerges as the most potent MIF inhibitor with a K_i of 14 nM and good solubility, 47 μg/mL, while **4e** has both high potency and solubility.

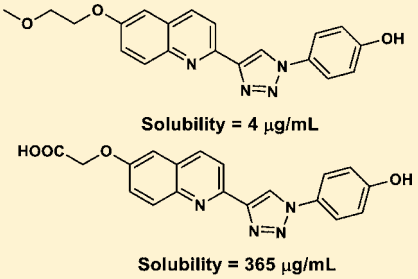

KEYWORDS: *Aqueous solubility, MIF inhibitors, crystallography*

Aqueous solubility is well-known as a critical property in the development of drugs.[1−5] Poor solubility is associated with difficulties in the reliable performance of assays, in obtaining oral formulations for *in vivo* administration, and in bioavailability. On the other hand, high solubility may lead to poor cell permeability and rapid excretion. The optimal range for the aqueous solubility S of drugs intended for oral delivery is ca. 10 μM to 10 mM or, equivalently, 4−4000 μg/mL for a compound with a molecular weight of 400.[2] Oral drugs with solubilities below 1 μM are very rare.

Poor solubility is a common issue in drug discovery efforts, since hydrophobic compounds bind well to target proteins for the same reasons that proteins fold to shield their hydrophobic groups from the aqueous environment. The problems may arise early from poorly soluble compounds that are obtained as hits in high-throughput screening. They often become aggravated during lead optimization, since the most reliable way to increase potency is to add hydrophobic substituents that fill hydrophobic regions in the target's binding site. Consistently, target proteins with highly hydrophobic binding sites are particularly prone to inhibitor designs with poor solubility. A classic example is non-nucleoside inhibitors of HIV-1 reverse transcriptase, NNRTIs.[6] The binding site in this case features a cluster of residues with aliphatic and aromatic side chains, and poor solubility has characterized many classes of NNRTIs. This is especially true for diaminopyrimidines, including the FDA-approved drugs etravirine and rilpivirine (**1**). In comparison to **1**, we were able to increase the solubility ca. 700-fold to 14 μg/mL for the triazine analogue with a morpholinylpropoxy substituent (**2**) while retaining excellent potency in infected T-cell assays.[7] This illustrates the basic principle for improving solubility without loss of potency: add conformationally flexible substituents with polar groups to a site in the inhibitor that is solvent-exposed in the complex with the protein. The benefit of flexibility includes the entropic gain from populating more conformers in solution than in the crystal. A corollary is to reduce planarity for inhibitors with multiple aromatic rings, which also leads to less tight packing in the crystalline state.[8] However, the addition of polar groups comes with uncertainties, since they may also form stabilizing hydrogen bonds in the crystal.

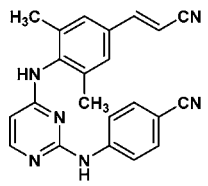

1

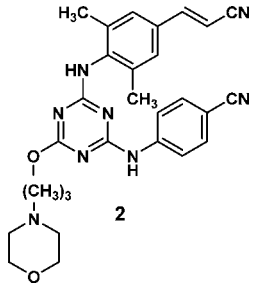

2

More recently, solubility has become an issue in our development of inhibitors of the tautomerase activity of the human macrophage migration inhibitory factor (MIF).[9] Specifically, surprisingly low solubility of 2.2 μg/mL was found for the parent quinolinyltriazole **3a** (R = H), which arose from *de novo* design. However, modeling indicated that substituents at the 6- and 7-positions of the quinoline ring should be solvent exposed. This expectation was confirmed by obtaining X-ray

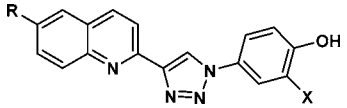

3 (X = H), **4** (X = F)

Received: November 8, 2016
Accepted: December 1, 2016
Published: December 1, 2016

DOI: 10.1021/acsmedchemlett.6b00451
ACS Med. Chem. Lett. 2017, 8, 124−127

crystal structures for **3a** and the R = methoxyethoxy (MOEO) analogue **3d** (Figure 1). The binding site is again seen to include

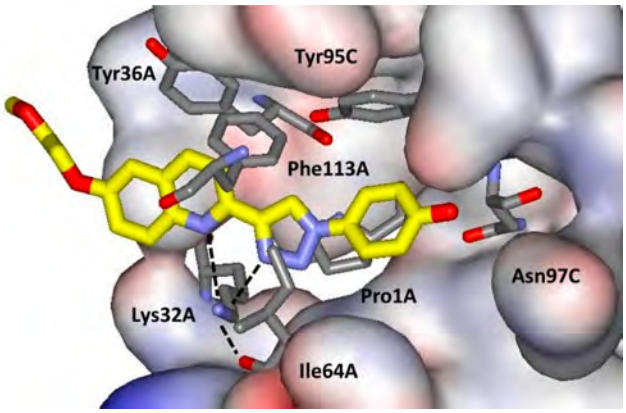

Figure 1. Rendering from the 1.8-Å crystal structure of **3d** bound to MIF (PDB ID: 4WRB).[9] Carbon atoms of **3d** are colored yellow. Some residues in front of the ligand have been removed for clarity. Coordination of Lys32A is highlighted with dashed lines; the methoxyethoxy group on C6 of the quinoline is solvent-exposed.

multiple residues with aromatic and aliphatic side chains. The poor solubility of **3a** in spite of its four nitrogen atoms and hydroxyl group can be attributed to its expected near planarity,[10] which has now been confirmed by a small molecule crystal structure.[11] As illustrated in Figure 2, the nearly planar monomers are well-stacked in the crystal structure and there are also intermolecular hydrogen bonds between the quinoline nitrogen atoms and phenolic hydroxyl groups (2.73 Å) in adjacent molecules (Figure 3). As expected, **3a** in isolation or in the crystal adopts a conformation with the quinoline nitrogen atom *anti* to N3 of the triazole ring to minimize lone-pair repulsion, while the conformation is *syn* in the complex with MIF to provide optimal coordination of the ammonium group of Lys32A (Figure 1).

Under the circumstances, it was decided to explore the solubility range that could be obtained by systematic variation of the substituent R in the 6-position of **3** and **4**. Two analogues of **5**[9] were also considered along with the deshydroxy compound **6**. Disruption of planarity by, e.g., addition of a substituent at C3 of

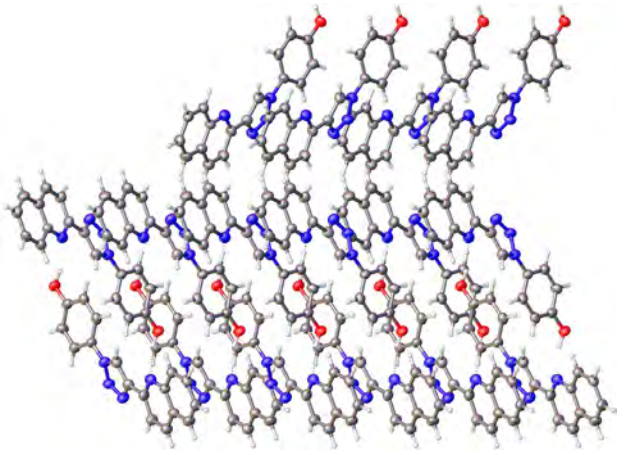

Figure 2. Illustration of the packing in the 0.84-Å crystal structure of **3a**. The space group is $Pca2_1$. The thermal ellipsoids are depicted at the 50% probability level. The CCDC ID is 1514977.

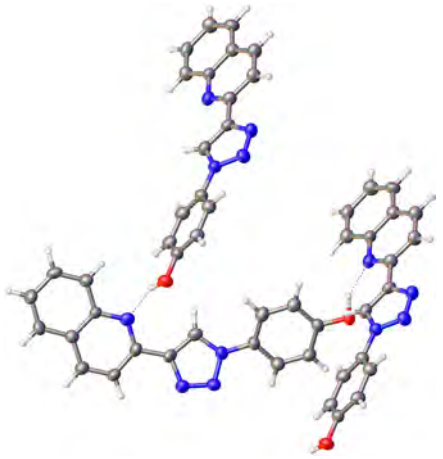

Figure 3. Close-up of the intermolecular hydrogen bonding in the crystal structure of **3a**.

the quinoline is not viable, as it is accompanied by large decreases in potency in view of the slot-like binding site (Figure 1) and coordination of Lys32.[9] In all, aqueous solubilities and inhibition constants K_i were determined for 17 analogues with 11 different substituents, as reported in Table 1. The aqueous solubilities were measured with a standard shake-flask procedure.[6,9,12] Saturated solutions are obtained by stirring for 2 days in Britton–Robinson buffer (pH 6.5), followed by filtration (Acrodisc syringe, 0.2 μm pore) and UV–vis analysis (Agilent 8453). Piroxicam has been used as a control more than 10 times, yielding $S = 6.5 \pm 1.7$ μg/mL, which is consistent with a reference value of 6.36 ± 0.04 μg/mL.[12] The inhibition constants were also determined as before using 4-hydroxyphenylpyruvic acid (HPP) as the substrate.[9,13,14] Inhibitory activity is monitored by measuring formation of the borate complex of the enol product at 305 nm using a Tecan Infinite F500 plate reader. Nine of the 17 inhibitors have been reported previously;[9,13] the synthetic and spectroscopic details for the new compounds (**3b**, **3c**, **3e**, **3f**, **3i**, **4c**, **4e**, **6**) are provided in the Supporting Information.

As reflected in Table 1, to improve solubility, we favor substituents that contain alkyleneoxy linkages with hydroxy, amino, and carboxylic acid termini. Amide and ester components are viewed as less desirable for drug prospects, owing to their potential decomposition by proteolytic enzymes. All compounds showed solubility gains over the parent **3a**. Among the smallest substituents, the benefits for the hydroxyethoxy and amino-ethoxy analogues **3b** and **3c** were modest, while the carboxymethoxy analogue **3i** provided a striking solubility boost to 365 μg/mL.

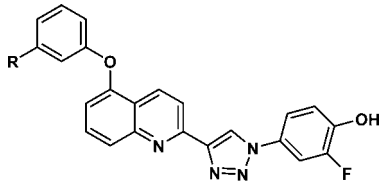

5

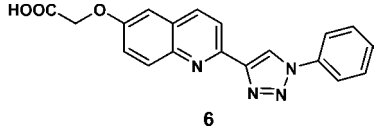

6

Though it worked well in the present cases, in general, the impact of addition of substituents with a carboxylic acid is uncertain,

DOI: 10.1021/acsmedchemlett.6b00451
ACS Med. Chem. Lett. 2017, 8, 124–127

Table 1. Computed Octanol/Water log P's, Experimental Aqueous Solubility at pH 6.5 (S in μg/mL), and K_i (μM)

Cp	R	ClogP	QP[a]	S	K_i
3a	H	3.80	3.32	2.2	0.23
3b	$HOCH_2CH_2O$	3.22	2.88	2.6	0.53
3c[b]	$H_2NCH_2CH_2O$	3.29	2.12	3.7	0.26
3d	$H_3COCH_2CH_2O$	3.98	3.49	3.6	0.20
3e	$H_3CO(CH_2CH_2O)_2$	3.85	3.81	2.4	0.147
3f	2-THP-CH_2O	4.89	4.07	3.4	0.27
3g[b]	$H_2N(CH_2CH_2O)_2$	3.36	2.43	13.9	0.36
3h[c]	4-Mr$(CH_2CH_2O)_2$	4.24	2.82	48.5	0.161
3i	$HOOCCH_2O$	3.04	2.64	365	0.20
4a[b]	$H_2N(CH_2CH_2O)_2$	3.35	2.77	9.1	0.144
4b	4-Mr$(CH_2CH_2O)_2$	4.24	3.16	27.2	0.074
4c	$HOOCCH_2O$	3.38	2.98	37.0	0.048
4d	$HOOC(CH_2)_3O$	4.06	3.90	19.2	0.039
4e	$HOOCCH_2OCH_2CH_2O$	3.63	3.30	867	0.037
5a	$H_3COCH_2CH_2O$	5.70	5.54	6.1	0.024
5b	HOOC	5.64	4.70	47.2	0.014
6[d]	$HOOCCH_2O$	2.48	3.32	1046	1.37
7[e]					27.3

[a]QPlogP. [b]TFA salt. [c]Mr = morpholinyl. [d]des-Hydroxy analogue of **3i**. [e](*R*)-ISO-1.

since carboxylic acids often form hydrogen-bonded dimers in their crystals.[4,15] The purely ether-containing substituents in **3d**, **3e**, and **3f** also just gave modest improvements for the solubility, and it is notable that addition of a second ethyleneoxy unit in going from **3d** to **3e** was not helpful. However, significant gains were found with amino-containing substituents in **3g** and **3h**.[16] It is well-known that introduction of morpholine and related heterocycles is normally successful in improving aqueous solubility.[5,7] The groups are expected to be protonated at physiological pH, which benefits hydration, and their saturated, nonplanar character eschews tight crystal packing.

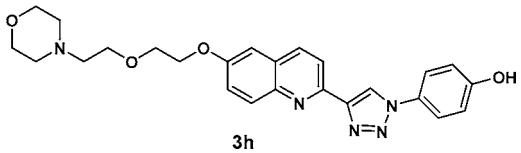

3h

Turning to **4a**–**4e**, addition of the fluorine atom adjacent to the phenolic hydroxyl group reduces solubility by factors of ca. 2–10 for the matched pairs **4a** and **3g**, **4b** and **3h**, and **4c** and **3i**. This is the typical direction in view of the increase in hydrophobicity, except in special cases where the fluorine is 2 or 3 carbon atoms removed from an oxygen.[5,17] Lengthening the linker by two methylene units in going from **4c** to **4d** reduced the solubility from 37 to 19 μg/mL; however, addition of an ethyleneoxy group in progressing to **4e** was very beneficial, yielding a 23-fold boost to 867 μg/mL. For **5a** and **5b**, the improvements with a carboxylic acid group are again apparent. Then, with **6**, removal of the intermolecular hydrogen bond in the crystal was tested; the result of 1046 μg/mL reflects a 3-fold increase over the solubility of **3i**.

In Table 1, computed octanol/water partition coefficients, ClogP and QPlogP, have been included as determined by ChemDraw and QikProp.[18,19] These are of interest as a measure of hydrophobicity and since log P and log S values are known to be correlated. The solubility equation of Yalkowsky estimates log S = 0.5 − log P − 0.01(t_m −25), where t_m is the melting point,[2,5,20] and a simpler relationship is log S = −log P − 0.2 with an rms error of 1.0 log unit.[9] Thus, log S does decrease linearly with increasing hydrophobicity, as represented by log P, but much quantitative uncertainty is associated with the crystalline state, as reflected in t_m and other terms that have been introduced to represent it in predictive methods.[2] The log P predictions with the present methods are in generally good accord with an average difference of 0.62, though the discrepancies for **3c**, **3h**, and **4b** are greater than 1 log unit. Presently, log P is not found to be a good predictor of log S. For **3a**–**3e**, the log P values would suggest solubilities in the 10^{-3} to 10^{-4} M range, while the observed values are closer to 10^{-5} M, owing presumably to the π-stacking in the crystals (Figure 2). Differences in log P are also not a good gauge of differences in log S for the present compounds. For example, **5a** might be expected to be 100-fold less soluble than **3d** based on log P, but it is more soluble; similarly, the enhanced solubility of **4e** is not reflected in its log P.

Concerning the Yalkowsky equation, routine measurement of melting points is not common today in drug discovery settings. However, we did measure the melting points of several of the compounds. They are 200–205 °C for **3d**, 268–270 °C for **4d**, and 230–235 °C for **4e**. Application of the Yalkowsky equation using the average of the two log P values in Table 1 then yields predicted log S values of −5.0, −5.9, and −5.0 for the three compounds, respectively, which translate to 3.5, 0.5, and 3.9 μg/mL. Thus, compared to the experimental solubilities in Table 1, the prediction for **3d** is accurate, but the enhanced solubilities for **4d** and **4e** are completely missed. Even differences in solubility are difficult to predict, and, if solubility is an important issue, there is no alternative but to measure it.

Finally, for the K_i results, the tautomerase assay was repeated for all of the listed compounds in this report in order to limit variations from the protein preparation, incubation times, and spectrometer.[13] For **3a**–**3i**, the activities are mostly in a narrow range of 0.2–0.4 μM, which is expected since the structural variations are only for the solvent-exposed substituent; additional modulation may come from interactions with residues on the surface of MIF. For example, the greater potency for **3e** may result from the $CH_3O(CH_2CH_2O)_2$ appendage curling back and making hydrophobic contacts with the rings of Pro33 and Pro34, which are in the gray area above Lys32 in Figure 1. The present K_i results for **3a**, **3g**, and **3h** also agree well with K_d values that we reported recently for these compounds from a fluorescence polarization assay.[14] As found previously,[9,14] addition of the fluorine in going from **3** to **4**, e.g., **3g** to **4a** or **3h** to **4b**, enhances the activities ca. 3-fold, owing to contact with Met101 and enhancement of the hydrogen bond between the phenolic hydroxyl group and Asn97. Modeling also suggested introduction of the phenoxy group at C5 of the quinoline fragment to pick up contacts with Tyr36,[9,14] which has yielded the most potent compounds, **5a** and **5b**. In addition, the importance of the hydrogen bond between the phenolic OH and Asn97 was confirmed by the increase in K_i to 1.37 μM for **6** from 0.20 μM for **3i**. As an additional control, the reference MIF inhibitor (*R*)-ISO-1 (**7**)[21] was also assayed; the observed K_i of 27.3 μM is similar to the prior average value of 24 μM from multiple measurements.[14]

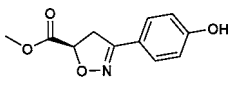

7

The principal purpose of this study was to explore systematically the effects of variations of a solvent-exposed substituent on

DOI: 10.1021/acsmedchemlett.6b00451
ACS Med. Chem. Lett. 2017, 8, 124–127

aqueous solubility in a drug-like series. The related work in the literature is largely scattered and less extensive, though the matched pair study of Zhang et al.[4] and the study of polyether and alcohol substituents by Zhu et al.[22] are particularly notable. The sequence of substituents in Table 1 may be of use to others who are faced with a similar challenge, though the quantitative outcomes will undoubtedly be different for other molecular series. However, the present and earlier results[5,7] do point to the utility of the addition of polyether chains terminated with a morpholine ring or surrogates for improving aqueous solubility. In the present case, addition of polyether chains with a carboxylic acid was also highly effective.

■ ASSOCIATED CONTENT

Supporting Information

The Supporting Information is available free of charge on the ACS Publications website at DOI: 10.1021/acsmedchemlett.6b00451.

Synthetic procedures, NMR and HRMS spectral data for all new compounds, and crystallographic details for **3a** (PDF)

Crystallographic data for **3a** (CIF)

■ AUTHOR INFORMATION

Corresponding Author

*E-mail: william.jorgensen@yale.edu.

ORCID

William L. Jorgensen: 0000-0002-3993-9520

Notes

The authors declare no competing financial interest.

■ ACKNOWLEDGMENTS

Gratitude is expressed to the National Institutes of Health (GM32136) for research support and to the National Science Foundation for a fellowship for M.J.R. (DGE-1122492).

■ ABBREVIATIONS

DCM, dichloromethane; THP, tetrahydropyran; TFA, trifluoroacetic acid

■ REFERENCES

(1) Lipinski, C. A.; Lombardo, F.; Dominy, B. W.; Feeney, P. J. Experimental and computational approaches to estimate solubility and permeability in drug discovery and development settings. *Adv. Drug Delivery Rev.* **1997**, *23*, 3−25.

(2) Jorgensen, W. L.; Duffy, E. M. Prediction of drug solubility from structure. *Adv. Drug Delivery Rev.* **2002**, *54*, 355−366.

(3) Stegemann, S.; Leveiller, F.; Franchi, D.; de Jong, H.; Lindén, H. When poor solubility becomes an issue: From early stage to proof of concept. *Eur. J. Pharm. Sci.* **2007**, *31*, 249−261.

(4) Zhang, L.; Zhu, H.; Mathiowetz, A.; Gao, H. Deep understanding of structure-solubility relationship for a diverse set of organic compounds using matched molecular pairs. *Bioorg. Med. Chem.* **2011**, *19*, 5763−5770.

(5) Walker, M. A. Improving Solubility by Structural Modification. *Top. Med. Chem.* **2013**, *9*, 69−106.

(6) Jorgensen, W. L. Computer-aided discovery of anti-HIV agents. *Bioorg. Med. Chem.* **2016**, *24*, 4768−4778.

(7) Bollini, M.; Cisneros, J. A.; Spasov, K. A.; Anderson, K. S.; Jorgensen, W. L. Optimization of diarylazines as anti-HIV agents with dramatically enhanced solubility. *Bioorg. Med. Chem. Lett.* **2013**, *23*, 5213−5216.

(8) Ishikawa, M.; Hashimoto, Y. Improvement in Aqueous Solubility in Small Molecule Drug Discovery Programs by Disruption of Molecular Planarity and Symmetry. *J. Med. Chem.* **2011**, *54*, 1539.

(9) Dziedzic, P.; Cisneros, J. A.; Robertson, M. J.; Hare, A. A.; Danford, N. E.; Baxter, R. H.; Jorgensen, W. L. Design, Synthesis, and Protein Crystallography of Biaryltriazoles as Potent Tautomerase Inhibitors of Macrophage Migration Inhibitory Factor. *J. Am. Chem. Soc.* **2015**, *137*, 2996−3003.

(10) Dahlgren, M. K.; Schyman, P.; Tirado-Rives, J.; Jorgensen, W. L. Characterization of Biaryl Torsional Energetics and its Treatment in OPLS All-Atom Force Fields. *J. Chem. Inf. Model.* **2013**, *53*, 1191−1199.

(11) Crystals of **3a** were grown via vapor diffusion with DMSO and water. A resulting crystal was diffracted under a cold nitrogen stream on a Rigaku MicroMax 007HF+ equipped with a Saturn 944+ CCD detector with Cu Kα. The structure was solved with direct methods. Heavy atoms were refined anisotropically, and hydrogen atoms were refined using a riding model. The hydrogen atom isotropic displacement parameters were fixed to the U values of the atoms to which they are linked, multiplied by 1.2. The molecules pack well with a pseudoslipped stacked morphology. The median plane formed by the triazole ring creates angles of 8.0(3)° and 23.9(4)° with the quinoline and phenol groups, respectively.

(12) Baka, E.; Comer, J. E. A; Takács-Novák, K. Study of equilibrium solubility measurement by saturation shake-flask method using hydrochlorothiazide as model compound. *J. Pharm. Biomed. Anal.* **2008**, *46*, 335−341.

(13) Cisneros, J. A.; Robertson, M. J.; Valhondo, M.; Jorgensen, W. L. Irregularities in enzyme assays: The case of macrophage migration inhibitory factor. *Bioorg. Med. Chem. Lett.* **2016**, *26*, 2764−2767.

(14) Cisneros, J. A.; Robertson, M. J.; Valhondo, M.; Jorgensen, W. L. A Fluorescence Polarization Assay for Binding to Macrophage Migration Inhibitory Factor and Crystal Structures for Two Potent Inhibitors. *J. Am. Chem. Soc.* **2016**, *138*, 8630−8638.

(15) Etter, M. C. Encoding and decoding hydrogen-bond patterns of organic compounds. *Acc. Chem. Res.* **1990**, *23*, 120−126.

(16) The primary amines **3c**, **3g**, and **4a** were prepared as their TFA salts. This resulted from use of trityl protecting groups that are removed with TFA, yielding the salts. Attempted isolation of the free amines by treatment with $NaHCO_3$ and extraction with DCM or ethyl acetate gave poor yields, owing to low solubility of the amines.

(17) Lee, W.-G.; Chan, A. H.; Spasov, K. A.; Anderson, K. S.; Jorgensen, W. L. Design, Conformation, and Crystallography of 2-Naphthyl Phenyl Ethers as Potent Anti-HIV Agents. *ACS Med. Chem. Lett.* **2016**, *7*, 0000−0000.

(18) *ChemBioDraw 12.0.2*; CambridgeSoft Inc.: Cambridge, MA, 2014.

(19) *QikProp 4.0*; Schrödinger Inc.: New York, NY, 2014.

(20) Ran, Y.; He, Y.; Yang, G.; Johnson, J. L. H.; Laskowski, S. H. Estimation of aqueous solubility of organic compounds using the general solubility equation. *Chemosphere* **2002**, *48*, 487−509.

(21) Lubetsky, J. B.; Dios, A.; Han, J.; Aljabari, B.; Ruzsicska, B.; Mitchell, R.; Lolis, E.; Al-Abed, Y. The tautomerase active site of macrophage migration inhibitory factor is a potential target for discovery of novel anti-inflammatory agents. *J. Biol. Chem.* **2002**, *277*, 24976−24982.

(22) Zhu, G.-D.; Arendsen, D. L.; Gunawardana, I. W.; Boyd, S. A.; Stewart, A. O.; Fry, D. G.; Cool, B. L.; Kifle, L.; Schaefer, V.; Meuth, J.; Marsh, K. C.; Kempf-Grote, A. J.; Kilgannon, P.; Gallatin, W. M.; Okasinski, G. F. Selective Inhibition of ICAM-1 and E-Selectin Expression in Human Endothelial Cells. 2. Aryl Modifications of 4-(Aryloxy)thieno[2,3-c]pyridines with Fine-Tuning at C-2 Substituents. *J. Med. Chem.* **2001**, *44*, 3469−3487.

DOI: 10.1021/acsmedchemlett.6b00451
ACS Med. Chem. Lett. 2017, 8, 124−127

ChemPubSoc Europe

DOI: 10.1002/cmdc.201800158

CHEMMEDCHEM Communications

Optimization of Pyrazoles as Phenol Surrogates to Yield Potent Inhibitors of Macrophage Migration Inhibitory Factor

Vinay Trivedi-Parmar, Michael J. Robertson, José A. Cisneros, Stefan G. Krimmer, and William L. Jorgensen*[a]

Dedicated to Prof. E. J. Corey on the occasion of his 90th birthday.

Macrophage migration inhibitory factor (MIF) is a proinflammatory cytokine that is implicated in the regulation of inflammation, cell proliferation, and neurological disorders. MIF is also an enzyme that functions as a keto–enol tautomerase. Most potent MIF tautomerase inhibitors incorporate a phenol, which hydrogen bonds to Asn97 in the active site. Starting from a 113-μM docking hit, we report results of structure-based and computer-aided design that have provided substituted pyrazoles as phenol alternatives with potencies of 60–70 nM. Crystal structures of complexes of MIF with the pyrazoles highlight the contributions of hydrogen bonding with Lys32 and Asn97, and aryl–aryl interactions with Tyr36, Tyr95, and Phe113 to the binding.

Human macrophage migration inhibitory factor (MIF) is a proinflammatory cytokine that is implicated in the pathogenesis of numerous inflammatory diseases,[1] neurological disorders,[2] and cancer.[3] MIF is expressed in many cell types and its tissue distribution is wide-spread. Upon activation of cells such as macrophages, monocytes and T-cells, expression of MIF in turn activates release of inflammatory cytokines including interleukins, interferon, and TNFα. Complex signaling pathways are invoked when MIF binds to its membrane-bound receptors CD74 and CXCR4, leading to leukocyte chemotaxis, inflammatory response, and potential tissue damage.[3] Strong correlation is observed between MIF expression and the severity of many inflammatory and autoimmune diseases including asthma, sepsis, lupus, and rheumatoid arthritis.[4] For cancer, the AKT pathway may be activated by MIF binding causing suppression of apoptosis by inhibition of the normal action of BAD, BAX, and p53.[3] However, MIF's role in cancer is multifaceted with undesirable effects also on cell proliferation, angiogenesis, and metastasis;[3,4] MIF is over-expressed in most human cancer cells.[5]

Interestingly, MIF also shows enzymatic activity as a keto-enol tautomerase. MIF is a toroid-shaped, trimeric protein consisting of 342 amino acid residues with three identical active sites occurring at the interfaces of the monomer subunits.[6] The active sites are small, relatively cylindrical and open to the surface of the protein in the vicinity of Pro1, which serves as the catalytic base. The resultant strategy for interference with the binding of MIF to its receptor CD74 is then to find tautomerase inhibitors that change the surface characteristics of MIF.[6] Indeed, numerous studies have shown a correlation between inhibition of the enzymatic and biological activities of MIF by measuring tautomerase activity, and, for example, MIF/CD74 binding, protein phosphorylation in inflamed cells, production of interleukins, and glucocorticoid overriding ability.[6,7] Though many MIF tautomerase inhibitors have been discovered through screening of compound libraries,[6,8] lead optimization to give inhibitors with nanomolar potency has been limited. In fact we have tested the most promising compounds from the literature in a tautomerase inhibition assay[9] and only found compounds from one patent[10] and our biaryltriazole series[11] to have sub-micromolar K_i values. The results were confirmed by measurement of K_d values in a fluorescence polarization assay.[12] Exemplary potent compounds are **1** (NVS-2[10]) and **2**[11] with K_i values of ~0.03 μM, which are ~1000-fold lower than for well-known MIF inhibitors such as **3** ((*R*,*S*)-ISO-1[13]) and the chromen-4-one **4**[6a] (Figure 1).

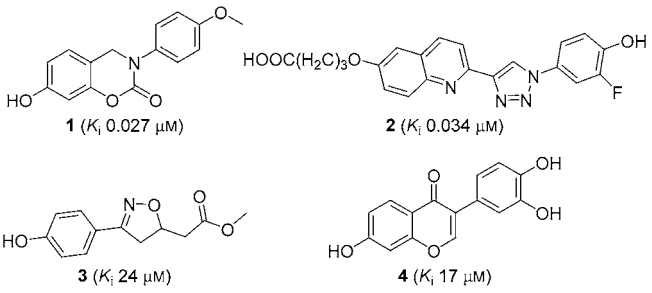

Figure 1. Examples of MIF tautomerase inhibitors with K_i data from Ref. [12].

A feature, which is addressed here, is that **1**–**4** and many other noncovalent MIF tautomerase inhibitors and substrates contain a phenol subunit, which lodges in the back of the active site and forms hydrogen bonds with the side chain of Asn97 (Figure 2).[6,11,12] Though there are more than 125 approved drugs that contain a phenolic group including, for ex-

[a] V. Trivedi-Parmar, Dr. M. J. Robertson, Dr. J. A. Cisneros, Dr. S. G. Krimmer, Prof. Dr. W. L. Jorgensen
Department of Chemistry, Yale University, New Haven, CT 06520-8107 (USA)
E-mail: william.jorgensen@yale.edu

Supporting information and the ORCID identification number(s) for the author(s) of this article can be found under https://doi.org/10.1002/cmdc.201800158.

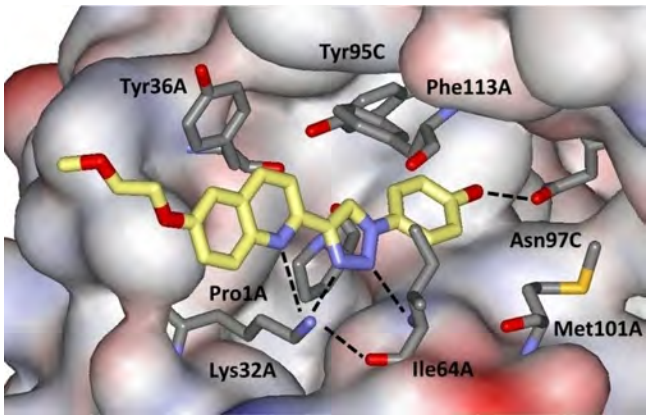

Figure 2. Rendering from a 1.8-Å crystal structure of an analogue of compound **2** bound to MIF.[11a] Carbon atoms of the inhibitor are colored yellow. Hydrogen bonds are indicated with dashed lines.

ample, acetaminophen, albuterol, amoxicillin, raloxifene, and doxycycline, the oral bioavailability of phenols is well-known to often be unacceptably low owing to metabolic glucoronidation[14] and/or sulfation.[15] Thus, we set out to find a phenol-free series of MIF tautomerase inhibitors with low-nanomolar potencies.

Success in the past has come from exchange of the phenol for a 6:5 fused heteroaromatic incorporating a pyrrole or pyrazole that retains the hydrogen-bond donating character of phenol.[16] However, the MIF active site is too constricted near Asn97 for this approach to be viable; addition of a methyl group *ortho* to the hydroxy group for the compound in Figure 2 leads to a ~100-fold loss in activity.[11a] Instead, our interest has focused on replacement of the phenol by a pyrazole. Owing to the geometrical differences, this requires exploration of new series with a pyrazole core. Fortunately, in the initial virtual screening study[8a] 11 compounds were found to be active in an assay that measured interference of binding between MIF and immobilized CD74 ectodomain; and, one contained a pyrazole with the expected hydrogen bonds to Asn97 in the docked structure. This compound, **5** (Figure 3), gave an IC_{50} of 15 μM in the binding assay; however, it showed little activity in a tautomerase assay using 4-hydroxyphenylpyruvate (HPP) as the substrate, with a maximum of 30% inhibition at 50 μM.[8a] Thus, we pursued alternative series from the virtual screening and from de novo design, which provided the biaryltriazoles including **2**.[11] However, our interest in **5** was renewed because in another phenol-containing inhibitor series[7b] rapid metabolic glucoronidation and sulfation were observed. It was decided to retest **5** in an HPP tautomerase assay using optimized protocols in our laboratory.[9] Though the K_i for **5** from this assay was only 113 μM, in view of its low molecular weight and possibilities for substitution in the phenyl ring, we were encouraged to perform structure-based, computer-aided lead optimization.[17] As detailed here, this has been successful in providing pyrazole derivatives with ~2000-fold greater potency.

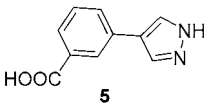

5

Figure 3. Docking hit **5**.[8a]

In working with **5**, it was noted that it had high solubility in polar media. This motivated successful pursuit of a crystal structure with MIF in spite of the modest K_i (Figure 4). There are two copies of **5** in each MIF trimer. The expected hydrogen bonds with Asn97 have average N–O and N–N lengths of 3.0 and 3.1 Å, while Lys32 has hydrogen bonds with the carboxylate group of **5** (3.0 and 2.7 Å) and the oxygen atom of Ile64 (2.7 Å). The NH of Ile64 also forms one with the carboxylate (2.9 Å), and the phenyl ring of **5** is well packed between Pro1, Tyr95, and Phe113. From this structure and model building with the BOMB program,[17b] substitution *para* to the pyrazolyl group seemed likely to yield beneficial interactions with Tyr36 and possibly Phe113. Thus, constructs **6**–**8** were pursued where R^1 was mostly an aryl group (Figure 5).

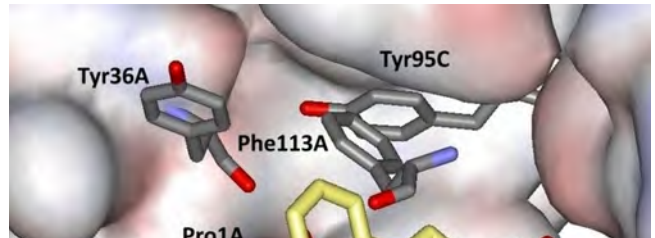

Figure 4. Rendering from the 2.0-Å crystal structure of compound **5** bound to MIF. Details as in Figure 2.

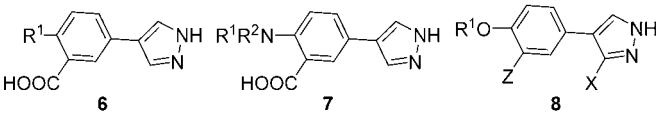

Figure 5. Designs for pyrazole-based MIF inhibitors.

The syntheses of **6**–**8** are detailed in the Supporting Information. As summarized in Scheme 1, the key steps started from the commercially available phenyl iodide **9**, which underwent Pd- or Cu-mediated coupling to yield phenylaryl, arylanilinyl, or biaryl ether derivatives **10**–**12**. Installation of the pyrazole was then achieved by a Suzuki coupling to yield esters **13**–**15**, which were hydrolyzed under mild conditions to provide the desired carboxylic acids.

The compounds reported here are listed in Table 1 along with the results from the tautomerase assay. The identity of assayed compounds was confirmed by ^1H and ^{13}C NMR and

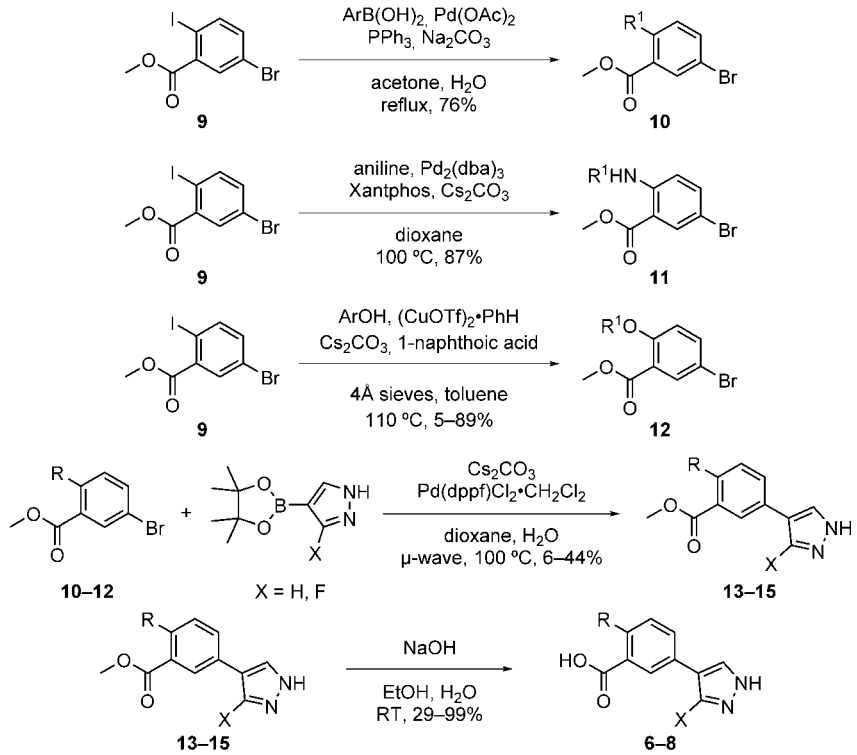

Scheme 1. Synthesis of pyrazole-based MIF inhibitors.

Table 1. Experimental inhibition constants.

Compd	R[1][a]	R[2]	Z	X	K_i [μM]
5	H	–	–	–	113
6a	Ph	–	–	–	20.6
6b	1-Np	–	–	–	19.5
6c	2-Np	–	–	–	5.4
7a	Ph	H	–	–	12.7
7b	2-Np	Me	–	–	4.2
8a	Ph	–	COOH	H	6.8
8b	*o*-MePh	–	COOH	H	4.3
8c	*m*-MePh	–	COOH	H	3.8
8d	*p*-MePh	–	COOH	H	7.0
8e	*m*-FPh	–	COOH	H	1.7
8f	*p*-FPh	–	COOH	H	4.6
8g	2-Np	–	COOH	H	4.3
8h	2-Np	–	SO_2Me	H	6.4
8i	2-Np	–	SO_2NH_2	H	5.6
8j	9-phenanthryl	–	COOH	H	2.3
8k	2-adamantyl	–	COOH	H	2.6
8l	4-Acen	–	COOH	H	1.1
8m	1-Np	–	COOH	F	0.48
8n	2-Np	–	COOH	F	0.51
8o	4-Et-2-Np	–	COOH	F	0.15
8p	5-Et-2-Np	–	COOH	F	0.17
8q	7-Et-2-Np	–	COOH	F	0.14
8r	4-*c*Pr-2-Np	–	COOH	F	0.11
8s	4-*c*Pr,7-Et-2-Np	–	COOH	F	0.066
8t	*p*-Bp	–	COOH	F	0.35
8u	*m*-Bp	–	COOH	F	0.13
8v	3,5-diMe-*m*-Bp	–	COOH	F	0.24
8w	4-OEt-*m*-Bp	–	COOH	F	0.075
8x	4-MrPrO-*m*-Bp	–	COOH	F	0.067

[a] Np = naphthyl; Acen = 1,2-dihydroacenaphthyl; *c*Pr = cyclopropyl; Bp = biphenyl; MrPrO = *N*-morpholinylpropoxy.

high-resolution mass spectrometry; HPLC analyses established purity as >95%. As in prior studies, the inhibition constants K_i were determined using HPP as the substrate.[9,11] Inhibitory activity is measured from formation of the borate complex of the enol product at 305 nm using a plate reader. Absorbance is measured in triplicate on two occasions. The average K_i results are reported; the standard error is typically 10–20% of the K_i value. In addition, the aqueous solubilities of several compounds were determined with a shake-flask procedure.[11,12,18] Saturated solutions are filtered and analyzed by UV-vis spectroscopy.

Consistent with the modeling, addition of an aryl group in **6** did provide a significant boost over **5**, bringing the K_i values down to ~20 μM for a phenyl or 1-naphthyl group and to 5 μM for 2-naphthyl (**6c**). The analogous anilinyl and phenoxy compounds, **7a** and **8a**, were prepared, and the greater activity and pharmacological desirability of diaryl ethers placed the subsequent focus on the latter series. A 2.3-Å crystal structure for the complex of **8a** with MIF was also obtained (Figure 6), which does show aryl–aryl contacts between the phenoxy phenyl group and both Tyr36 and Phe113. A basic SAR (structure–activity relationship) study was then carried out with **8b**–**8f**, which revealed a small activity range for addition of a methyl or fluoro substituent, with *para*-substitution the least favored. Consistent with this guidance, the 2-naphthyl analogue **8g** was found to show good activity at 4.3 μM; the BOMB modeling indicated increased contact with Phe113 projecting to the right in Figure 6. Modeling further indicated that still larger hydrophobic groups could be accommodated in this region at the entrance of the MIF active site. This was

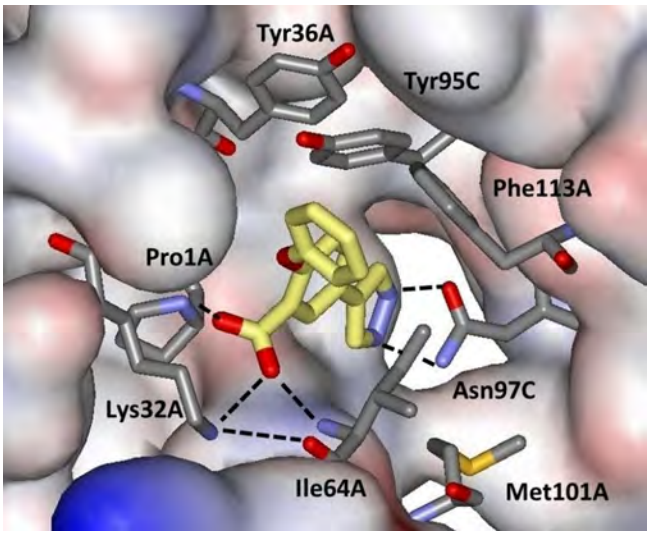

Figure 6. Rendering from the 2.3-Å crystal structure of compound **8a** bound to MIF. Details as in Figure 2.

borne out by K_i values of 1–3 μM obtained for phenanthryl, adamantyl, and acenaphthyl analogues, **8j**–**8l** (Figure 7). However, the project seemed stalled at this point without reaching the desired low-nanomolar range and with increasing concerns about solubility.

For the biaryltriazoles series, it was recalled that placement of a fluorine adjacent to the hydroxy group in compounds like **2** provided a ~3-fold increase in activity.[11] The effect was attributed to enhancing the acidity of the phenol, which increases the strength of the hydrogen bond with Asn97, and also to hydrophobic contact of the fluorine with the side chain of Met 101 (Figure 2). For the pyrazoles, the enhanced hydrogen bonding could be envisioned for a fluorine at the 3-position; however, the fluorine would project more toward the side chain of Ile64 rather than Met101 with uncertain outcome (Figure 4). Still, a potential additional benefit might arise from the influence of the fluorine on the tautomeric equilibrium for the pyrazole. Reliable quantum mechanical calculations (MP2/6-311++G**) show that the N1-H tautomer is favored by 3.6 kcal mol^{-1} over the N2-H tautomer with a fluorine in the 3-position (Figure 8).[19] From the present crystal structures the hydrogen bonds are expected to be more linear for the N1-H tautomer as implied by the alignment of the side-chain oxygen atom of Asn97 and N1 in Figures 4 and 6.

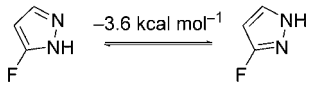

Figure 8. Shift in the tautomeric equilibrium with a fluorine atom.[19]

Preparation of the fluorinated pyrazole for the Suzuki coupling in Scheme 1 proved difficult. Multiple routes were attempted, but success was only achieved using a SEM [2-(trimethylsilyl)ethoxymethyl] protecting group; the yield was still low, but sufficient to proceed (Scheme 2).

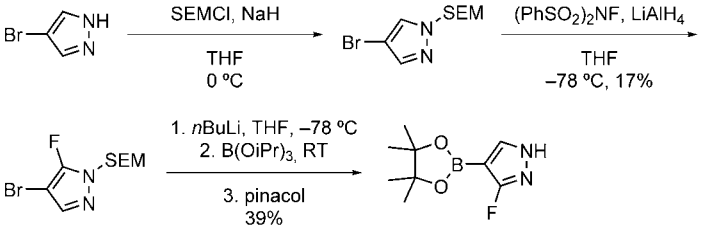

Scheme 2. Synthesis of fluorinated pyrazoles.

The effort was highly fruitful yielding a nearly 10-fold increase in potency in progressing from the parent 2-naphthyl inhibitor **8g** (4.3 μM) to its fluorinated analogue **8n** (0.51 μM). It was also possible to obtain a crystal structure for this compound in complex with MIF at 2.0-Å resolution (Figure 9). The structure confirmed the positioning of the fluorine between the side chains of Ile64 and Met101. There is one copy of the inhibitor in each MIF trimer in this case; the N–O and N–N hydrogen bond lengths with Asn97 are 2.87 and 3.12 Å. There are also close-packed aryl–aryl interactions between the naphthyl group of **8n** and Tyr36 and Phe113.

Though the exact positioning of the naphthyl group may be influenced by crystal packing, the structure and BOMB modeling indicated that additional gains in activity could arise from alkyl-substitution at the 4-, and 5-positions of the naphthyl group to achieve further contact with Phe113 or at the 7-position for contact with Ile64. This was shown to be correct with the ethyl analogues **8o**, **8p**, and **8q**, which each provided a 3-fold lowering of the K_i relative to **8n**. Addition of a cyclopropyl group at the 4-position also appeared promising for interaction with the front edge of Phe113; this was realized with **8r** bringing the K_i to 0.11 μM. Combining this with the 7-ethyl substitution provided the very potent **8s** with a K_i of 0.066 μM.

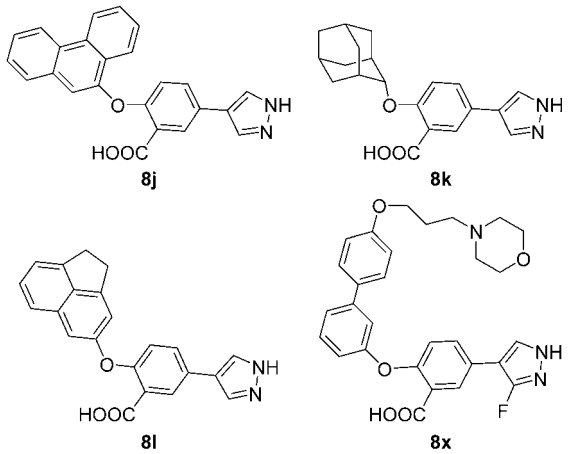

Figure 7. Some pyrazole-based MIF inhibitors reported herein.

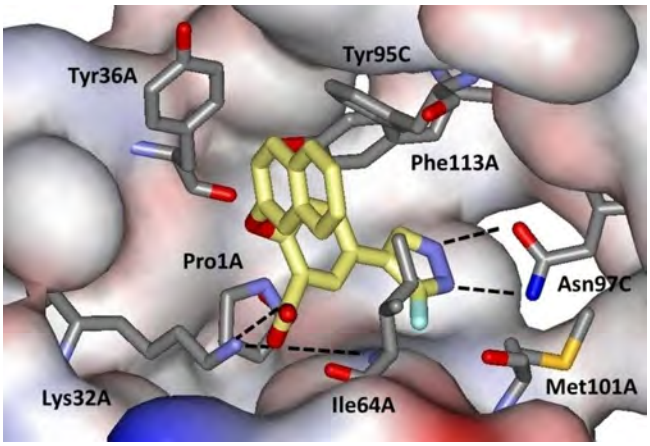

Figure 9. Rendering from the 2.0-Å crystal structure of compound **8n** bound to MIF. Details as in Figure 2.

From the structures for **8a** and **8n** (Figures 6 and 9) and modeling, it was also clear that it should be possible to expand to a biphenyl at either the *para* or *meta* position of **8a**. Thus, **8t** and **8u** were synthesized and provided significantly lower K_i values (0.35 and 0.13 μM) than the unsubstituted naphthyl analogues, **8m** and **8n**. Substantial activity gains could be expected by judicious substitution for the biphenyls; however, only a few derivatives were prepared with **8w** and **8x** (Figure 7) demonstrating ~0.07 μM potency and that large groups can be extended into the solvent from the terminal 4-position.

Two additional items are worth noting. First, the results for **8g**, **8h**, and **8i** show that the carboxylic acid group may be replaced by a methylsulfone or sulfonamide with little impact on potency. This is relevant if one wished to explore these compounds as potential neurological agents,[2] as sulfones are expected to exhibit better penetration of the blood–brain barrier than carboxylic acids or sulfonamides.[20] Secondly, it is always important to monitor aqueous solubilities for compounds of interest for oral administration.[11,17,21] Most oral drugs are observed to have aqueous solubilities of 4 to 4000 $\mu g\,mL^{-1}$, which translates to 10 μM to 10 mM for a drug with a molecular weight of 400.[21] The solubilities of several of the present compounds were measured in Britton-Robinson buffer at pH 6.5.[18] As noted, the solubility of the starting compound **5** is very high ($927 \pm 88\ \mu g\,mL^{-1}$). The solubility of the parent 2-naphthyl analogue **8g** is also high ($739 \pm 32\ \mu g\,mL^{-1}$); it is affected little by addition of the fluorine in **8n** ($681 \pm 59\ \mu g\,mL^{-1}$), while switch to the sulfonamide **8i** yields a significant decrease ($55.2 \pm 4.8\ \mu g\,mL^{-1}$). Given these results, it was surprising to find in the biphenyl series that the solubility of **8w** is only $1.7 \pm 0.7\ \mu g\,mL^{-1}$. However, this is readily remedied by attachment of solvent-exposed, solubilizing groups[11b] as in **8x** ($34.6 \pm 4.8\ \mu g\,mL^{-1}$, or 67 μM).

To facilitate further study of the in vitro and in vivo biology of MIF, series of potent MIF tautomerase inhibitors have been pursued. Starting from a 113-μM docking hit, a novel series, which features a pyrazole instead of a phenol, was optimized to yield compounds with K_i values as low as 60–70 nM. The optimization was greatly facilitated by molecular modeling and the ability to obtain multiple high-resolution crystal structures, which guided the effective selection and placement of substituents. Recognition of the potential benefit of addition of a fluorine in the pyrazole ring also provided an essential boost along with a synthetic challenge. Current efforts are being directed at testing the influence of the inhibitors on suppressing MIF-stimulated cell proliferation and at preclinical studies for off-target activity and metabolism.

Experimental Section

Recombinant expression and purification of human MIF was carried out as previously reported.[11] Crystallization of MIF in complex with **5** and **8g** was achieved by soaking with apo-MIF crystals, while for the complexes of **8a** and **8n**, co-crystallization was performed via sitting drop vapor diffusion at 20 °C. The structures were determined in-house using a Rigaku 007 HF+ diffractometer and Saturn 944+ CCD detector at $T = 100$ K. The crystal structures have been deposited in the RSCB Protein Data Bank with PDB IDs 6CBG (**5**), 6CBF (**8a**), 6CB5 (**8g**), and 6CBH (**8n**). The Supporting Information contains the synthetic procedures, NMR and HRMS spectral data for all new compounds, and details for the crystallography and solubility measurements (72 pages).

Acknowledgements

Gratitude is expressed to the US National Institutes of Health (NIH grant number GM32136) for research support, to the US National Science Foundation for a fellowship for M.J.R. (grant number DGE-1122492), and to Drs. Thomas Steitz, Michael Strickler, and Yong Xiong for assistance at the Yale Richards Center.

Conflict of interest

The authors declare no conflict of interest.

Keywords: MIF inhibitors · phenol bioisosteres · protein crystallography · pyrazoles · tautomerase

[1] a) E. Lolis, R. Bucala, *Expert Opin. Ther. Targets* **2003**, *7*, 153–164; b) J. Garai, T. Lóránd, *Curr. Med. Chem.* **2009**, *16*, 1091–1114; c) D. Greven, L. Leng, R. Bucala, *Expert Opin. Ther. Targets* **2010**, *14*, 253–264; d) Y. Asare, M. Schmitt, J. Bernhagen, *Thromb. Haemostasis* **2013**, *109*, 391–398.

[2] a) N. E. Savaskan, G. Fingerle-Rowson, M. Buchfelder, I. Y. Eyüpoglu, *Int. J. Cell Biol.* **2012**, *2012*, 139573; b) M. F. Leyton-Jaimes, J. Kahn, A. Israelson, *Exp. Neurol.* **2018**, *301B*, 83–91.

[3] a) C. Bifulco, K. McDaniel, L. Leng, R. Bucala, *Curr. Pharm. Des.* **2008**, *14*, 3790–3801; b) H. Conroy, L. Mawhinney, S. C. Donnelly, *Q. J. Med.* **2010**, *103*, 831–836; c) L. Pawig, C. Klasen, C. Weber, J. Bernhagen, H. Noels, *Front. Immunol.* **2015**, *6*, 429; d) N. Kindt, F. Journe, G. Laurent, S. Saussez, *Oncol. Lett.* **2016**, *12*, 2247–2253; e) C. C. G. Nobre, J. M. Galvão de Araújo, T. A. A. M. Fernandes, R. N. O. Cobucci, D. C. F. Lanza, V. S. Andrade, J. V. Fernandes, *Pathol. Oncol. Res.* **2017**, *23*, 235–244.

[4] C. O'Reilly, M. Doroudian, L. Mawhinney, S. C. Donnelly, *Med. Res. Rev.* **2016**, *36*, 440–460.

[5] S. N. Babu, G. Chetal, S. Kumar, *Asian Pac. J. Cancer Prev.* **2012**, *13*, 1737–1744.

[6] a) M. Orita, S. Yamamoto, N. Katayama, S. Fujita, *Curr. Pharm. Des.* **2002**, *8*, 1297–1317; b) J. Garai, T. Lóránd, *Curr. Med. Chem.* **2009**, *16*, 1091–

1114; c) J. Bloom, S. Sun, Y. Al-Abed, *Expert Opin. Ther. Targets* **2016**, *20*, 1463 – 1475.
[7] a) P. D. Senter, Y. Al-Abed, C. N. Metz, F. Benigni, R. A. Mitchell, J. Chesney, J. Han, C. G. Gartner, S. D. Nelson, G. J. Todaro, R. Bucala, *Proc. Natl. Acad. Sci. USA* **2002**, *99*, 144 – 149; b) A. A. Hare, L. Leng, S. Gandavadi, X. Du, Z. Cournia, R. Bucala, W. L. Jorgensen, *Bioorg. Med. Chem. Lett.* **2010**, *20*, 5811 – 5814.
[8] a) Z. Cournia, L. Leng, S. Gandavadi, X. Du, R. Bucala, W. L. Jorgensen, *J. Med. Chem.* **2009**, *52*, 416 – 424; b) H. Ouertatani-Sakouhi, F. El-Turk, B. Fauvet, M.-K. Cho, D. P. Karpinar, D. Le Roy, M. Dewor, T. Roger, J. Bernhagen, T. Calandra, M. Zweckstetter, H. A. Lashuel, *J. Biol. Chem.* **2010**, *285*, 26581 – 26598; c) L. Xu, Y. Zhang, L. Zheng, C. Qiao, Y. Li, D. Li, X. Zhen, T. Hou, *J. Med. Chem.* **2014**, *57*, 3737 – 3745; d) L.-T. Tsai, T.-H. Lin, *J. Biomol. Screening* **2014**, *19*, 1116 – 1123; e) M. C. Zapatero, P. Pérez, M. J. Vázquez, G. Colmenarejo, M. de los Frailes, F. Ramón, *J. Biomol. Screening* **2016**, *21*, 446 – 458.
[9] J. A. Cisneros, M. J. Robertson, M. Valhondo, W. L. Jorgensen, *Bioorg. Med. Chem. Lett.* **2016**, *26*, 2764 – 2767.
[10] A. Billich, P. Lehr, H. Gstach (Novartis AG, Novartis Pharma GmbH), Int. PCT Pub. No. WO2006045505 A1, **2006**.
[11] a) P. Dziedzic, J. A. Cisneros, M. J. Robertson, A. A. Hare, N. E. Danford, R. H. Baxter, W. L. Jorgensen, *J. Am. Chem. Soc.* **2015**, *137*, 2996 – 3003; b) J. A. Cisneros, M. J. Robertson, B. Q. Mercado, W. L. Jorgensen, *ACS Med. Chem. Lett.* **2017**, *8*, 124 – 127.
[12] J. A. Cisneros, M. J. Robertson, M. Valhondo, W. L. Jorgensen, *J. Am. Chem. Soc.* **2016**, *138*, 8630 – 8638.
[13] Y. Al-Abed, D. Dabideen, B. Aljabari, A. Valster, D. Messmer, M. Ochani, M. Tanovic, K. Ochani, M. Bacher, F. Nicoletti, C. Metz, V. A. Pavlov, E. J. Miller, K. J. Tracey, *J. Biol. Chem.* **2005**, *280*, 36541 – 36544.
[14] a) B. Wu, K. Kulkarni, S. Basu, S. Zhang, M. Hu, *J. Pharm. Sci.* **2011**, *100*, 3655 – 3681; b) A. Rowland, J. O. Miners, P. I. Mackenzie, *Int. J. Biochem. Cell Biol.* **2013**, *45*, 1121 – 1132.
[15] a) E. Chapman, M. D. Best, S. R. Hanson, C.-H. Wong, *Angew. Chem. Int. Ed.* **2004**, *43*, 3526 – 3548; *Angew. Chem.* **2004**, *116*, 3610 – 3632; b) C. Rakers, F. Schumacher, W. Meinl, H. Glatt, B. Kleuser, G. Wolber, *J. Biol. Chem.* **2016**, *291*, 58 – 71.
[16] a) J. L. Wright, T. F. Gregory, S. R. Kesten, P. A. Boxer, K. A. Serpa, L. T. Meltzer, L. D. Wise, *J. Med. Chem.* **2000**, *43*, 3408 – 3419; b) R. R. Wilkening, R. W. Ratcliffe, A. K. Fried, D. Meng, W. Sun, L. Colwell, S, Lambert, M. Greenlee, S. Nilsson, A. Thorsell, M. Mojena, C. Tudela, K. Frisch, W. Chan, E. T. Birzin, S. P. Rohrer, M. L. Hammond, *Bioorg. Med. Chem. Lett.* **2006**, *16*, 3896 – 3901.
[17] a) H. Gohlke, G. Klebe, *Angew. Chem. Int. Ed.* **2002**, *41*, 2644 – 2676; *Angew. Chem.* **2002**, *114*, 2764 – 2798; b) W. L. Jorgensen, *Acc. Chem. Res.* **2009**, *42*, 724 – 733; c) P. Schneider, G. Schneider, *J. Med. Chem.* **2016**, *59*, 4077 – 4086; d) W. L. Jorgensen, *Bioorg. Med. Chem.* **2016**, *24*, 4768 – 4778.
[18] E. Baka, J. E. A. Comer, K. Takács-Novák, *J. Pharm. Biomed. Anal.* **2008**, *46*, 335 – 341.
[19] M. Jarończyk, J. C. Dobrowolski, A. P. Maruzek, *THEOCHEM* **2004**, *673*, 17 – 28.
[20] a) S. A. Hitchcock, L. D. Pennington, *J. Med. Chem.* **2006**, *49*, 7559 – 7583; b) J. M. Meinig, S. J. Ferrara, T. Banerji, T. Banerji, H. S. Sanford-Crane, D. Bourdette, T. S. Scanlan, *ACS Chem. Neurosci.* **2017**, *8*, 2468 – 2476.
[21] W. L. Jorgensen, E. M. Duffy, *Adv. Drug Delivery Rev.* **2002**, *54*, 355 – 366.

Manuscript received: March 11, 2018
Accepted manuscript online: March 25, 2018
Version of record online: April 23, 2018